VYSOKÉ UČENÍ TECHNICKÉ V BRNĚ

BRNO UNIVERSITY OF TECHNOLOGY

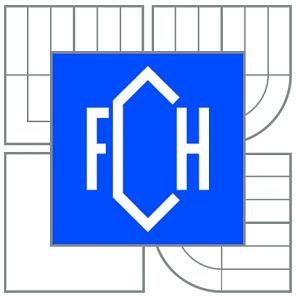

FAKULTA CHEMICKÁ

ÚSTAV CHEMIE MATERIÁLŮ

FACULTY OF CHEMISTRY

INSTITUTE OF MATERIALS SCIENCE

POROUS ELEMENTS BASED ON GRANULAR MATERIALS AND INORGANIC BINDERS

POREZNÍ PŘEPÁŽKY NA BÁZI PARTIKULÁRNÍCH MATERIÁLŮ A ANORGANICKÝCH POJIV

DIPLOMOVÁ PRÁCE

MASTER'S THESIS

AUTOR PRÁCE — Bc. PAVEL BULEJKO

AUTHOR

VEDOUCÍ PRÁCE — doc. Ing. TOMÁŠ SVĚRÁK, CSc.

SUPERVISOR

BRNO 2013

Brno University of Technology
Faculty of Chemistry
Purkyňova 464/118, 61200 Brno 12

Master's thesis Assignment

Number of master's thesis:	**FCH-DIP0666/2012**	Academic year: **2012/2013**
Institute:	Institute of Materials Science	
Student:	**Bc. Pavel Bulejko**	
Study programme:	Chemistry, Technology and Properties of Materials (N2820)	
Study field:	Chemistry, Technology and Properties of Materials (2808T016)	
Head of thesis:	**doc. Ing. Tomáš Svěrák, CSc.**	
Supervisors:		

Title of master's thesis:

Porous elements based on granular materials and inorganic binders

Master's thesis assignment:

1. Literature review;
2. Preparation of porous structures without sintering;
3. Monitoring of the influence of input material grain-size distributions on the porous structure formation;
4. Characterization of porous elements mechanical properties.

Deadline for master's thesis delivery: 3.5.2013

Master's thesis is necessary to deliver to a secreatry of institute in three copies and in an electronic way to a head of master's thesis. This assignment is enclosure of master's thesis.

Bc. Pavel Bulejko Student	doc. Ing. Tomáš Svěrák, CSc. Head of thesis	prof. RNDr. Josef Jančář, CSc. Head of institute

In Brno, 31.1.2013

prof. Ing. Jaromír Havlica, DrSc.
Dean

ABSTRAKT

Tato diplomová práce zkoumá možnosti tvorby porézních struktur za použití partikulárních materiálů pojených anorganickými pojivy bez dodatečné tepelné úpravy vypalováním. Jako základní pojiva byly použity portlandský a hlinitanový cement a pojiva na bázi alkalicky aktivovaného metakaolinu (geopolymeru). Jako základní kamenivo byl použit karbid křemíku v různých frakcích podle velikosti částic. Byly taktéž použity další zrnité materiály, např. křemenný písek anebo odpadních materiálů (mleté sklo a porcelán) roztříděných do frakcí podle velikosti částic.

Byl sledován vliv složení a množství kameniva na vytváření porézní struktury a tím i na mechanické vlastnosti, které byly testovány pomocí mechanických zkoušek. Pevnostní zkoušky byly provedeny na trámečcích 20 × 20 × 100 mm připravených z testovacích směsí. Granulometrické a fázové složení vstupních surovin bylo studováno metodou laserové granulometrie resp. RTG difrakce.

Porézní struktura byla studována metodami rtuťové porozimetrie, dále pomocí světelné a rastrovací elektronové mikroskopie a taktéž pyknometrickou metodou. V rámci charakterizace přepážek (terčíky o průměru 90 mm) připravených z jednotlivých materiálů bylo provedeno stanovení efektivní permeability průtokem vzduchu. Dále byly provedeny testy vzlínavosti kapaliny v připravených materiálech. V závěru práce byly provedeny pokusy o filtraci jemných suspenzí přes uvedené přepážky.

ABSTRACT

This master thesis aims at the possibilities of porous structures formation using granular materials cemented with inorganic binders without additional heat treatment by firing. As the basic binders were used Portland and aluminate cement and agglutinates on alkali-activated metakaoline (geopolymer) basis. Silicon carbide classified according to particle sizes was used as main aggregates, the next materials were quartz sand and some secondary material were used as well (milled glass and porcelain), which were also divided into particle size fractions.

The influence of composition and aggregates quantity upon the porous structure generation was pursued and mechanical properties were characterized by mechanical strength testing of columns with proportions of 20 × 20 × 100 mm prepared of testing mortars. Grain size measurement and characterization of phase composition of input materials were performed by means of laser granulometry and X-ray diffraction, respectively.

Porous structure was investigated using methods of mercury porosimetry, light and scanning electron microscopy and pycnometric measurement. The barriers in the form of disks with 90 mm in diameter prepared of individual materials were tested by air flux to determine effective permeability. Furthermore, the capillarity testing of the materials were carried out. Lastly, experiments to try to clarify suspensions of fine particles were accomplished.

KLÍČOVÁ SLOVA

Porézní materiál, porosita, anorganické pojivo, filtrační přepážka, filtrace, permeabilita

KEYWORDS

Porous material, porosity, inorganic binder, filtration barrier, filtration, permeability

BULEJKO, P.: *Porous elements based on granular materials and inorganic binders.* Brno: Brno University of Technology, Faculty of chemistry, 2013. 98 p. Diploma thesis. Supervisor doc. Ing. Tomáš Svěrák, CSc.

DECLARATION

I declare that I have worked out the diploma thesis by myself and that all the quotations from the used literary sources are accurate and complete. The content of the diploma thesis is the property of the Faculty of Chemistry of Brno University of Technology and all commercial uses are allowed only if approved by both the supervisor and the dean of the Faculty of Chemistry, BUT.

……..……

Student's signature

Acknowledgement

I would like to sincerely thank to doc. Ing. Tomáš Svěrák, CSc. for his help and advices for this thesis, Ing. Tomáš Opravil, Ph.D. and Mr. Lubomír Mikšík for their help with works on experimental part. Furthermore, I would like to thank to the project of Heat Transfer and Fluid Flow Laboratory of Faculty of Mechanical Engineering BUT HEATEAM CZ.1.07/2.3.00/20.0188 and Material Research Center of Faculty of Chemistry BUT CZ.1.05/2.1.00/01.0012 for their support for this work.

CONTENT

1 INTRODUCTION

Pores in materials are considered to be defects many times. It is related to materials which are used for construction purposes (by construction purposes are meant massive structures such as bridges, multistoried buildings, skyscrapers and other uniques of civil engineering). For example, in concrete resp. cement paste, there are remaining droplets of water (in principle, pores fulfilled with water), even after setting and hardening. The critical defect size for cement paste is in range of 10 μm, so if there is large defect than 10 μm, the brittle fracture will be observed. The water droplets diameter can be much bigger (range of millimeters).So in concrete, there is large amount of supercritical defects and that is the reason why concrete is so weak in tension. Even capillary pores larger than only 50 nm are assumed to be detrimental to strength and durability of cement [1]. In the places of these pores, the stress is concentrated and right from these places, the crack will start to propagate. So pore is structural defect, principally void or impurity in the material continuum.

Generally, any consideration of the material strength has to take into account a distribution of defects as an inevitable consequence of the way it was manufactured. Hence, only a small fraction of cohesive bonds at any cross-section in the solid is loaded simultaneously to their limiting strength. After the failure of the most overloaded bonds, neighboring bonds have to carry the load redistributed from the fractured bonds resulting in overloading of these bonds. This leads to their fracture and the cracking process repeat itself until crack plane expands throughout the whole cross-section [2].

So from the building applications point of view, pores are something which can be a thorn in engineers' side. But if we look at the other branches of industry and science, we will find many applications and scientists that are engaged in porous materials. Among others (catalysis, adsorption), one of the main applications of porous materials is filtration.

Generally, porous materials have been known for a very long time. Some of these materials are naturally occurring such as pumice, sand, cork, as well as some biological materials such as bone. Others are synthetized. Porous materials have attracted the attention of chemists, material scientists, and physicists alike due to their technological importance in a variety of areas, as well as the challenges posed in their synthesis, processing, and characterization. In addition, porous solids are of scientific interest because of their ability to interact with atoms, ions and molecules not only at their surfaces, but throughout their bulk. The ability of offering a large surface area makes porous materials prime candidates for catalysis. Furthermore, porous barriers have been used to change the monomer to dimer ratio of reactive gas mixtures under steady-state conditions. Micro-porous materials such as zeolite are employed as molecular sieves, and porous membranes are used in osmosis. In addition, in recent years porous materials have been used in variety of new applications ranging from adsorption and storage of gases such as hydrogen to wastewater treatment or water defluoridation. Porosity also plays an important role in the manufacturing of various materials which involve sintering, such as ceramic magnets. In some cases, however, pores are a negative factor. For example, molten metal can penetrate the pores of refractory materials and cause corrosion. Low porosity materials are generally stronger than those with high porosity. In addition, in the past few decades various porous materials have been used from a theoretical standpoint to study the fractal dimension of pores [3–9].

The production of porous supports for membranes as well as macroporous elements for filtration involves firing [10–12]. Firing is a process which belongs to basic processes in ceramic technology and which involves sintering to form strong bond (ceramic bond) between

the particles of raw material and formation of a new structure [13–15]. The structure of final product is mainly influenced by firing temperature which usually attains 1100 °C for inorganic membrane fabrication. With the increase of temperature, the porosity is reduced and flexural strength is increased [10]. Although the firing process itself can take several hours, it is very expensive [14]. So the main effort on the field of membrane processes is to reduce the cost of the membrane units and hence to reduce the cost of the overall process. One of the possibilities is to avoid heat treatment which makes the final products more expensive. And that is something which is dealt with in this thesis.

2 OBJECTIVES OF THE WORK

This master's thesis focuses on the possibilities of preparation and characterization of porous materials for filtration of fluids and related applications without additional treatment of the material by high temperatures. For the master's thesis was demarcated these objectives:

1. Literature review aimed at porous materials, their properties and main applications;
2. Preparation of porous structure without additional heat treatment by firing and sintering;
3. Monitoring of the influence of input material grain-size distribution on the generation of porous structure;
4. Characterization of mechanical properties of the prepared materials.

3 GENERAL DEFINITIONS AND TERMINOLOGY

In this section, basic terms are demarcated (according to IUPAC [16]) for better comprehension to the thesis and to avoid some misunderstandings. Some of them are introduced in a more detailed manner in the following sections.

Aggregate: loose, unconsolidated assemblage of particles.

Agglomerate: rigid, consolidated assemblage of particles.

Density:
true density – density of the material *excluding* pores and inter-particle voids,

apparent density – density of the material *including* closed and inaccessible pores,

bulk density – density of the material *including* pores *and* inter-particle voids.

Divided solid: solid made of more or less independent particles which may be in the form of a powder, aggregate or agglomerate.

Hydraulic radius: mean value for a porous solid, obtained through the relationship:

$$r_{\mathrm{h}} = V_{\mathrm{p}} \Big/ A_s \tag{1}$$

(r_{h} – hydraulic radius, V_{p} – pore volume determined at saturation, A_{s} – surface area, e.g. determined by the BET[1] method).

Porous solid: a solid with pores, i.e. cavities, channels or interstices, which are deeper than they are wide.

Pore volume V_{p}: volume of the pores, as measured by a given method which must be stated (together, for instance, with the nature of the probe-molecule, the wavelength of the radiation used or the ultimate intrusion pressure etc.).

Pore size (generally pore width): the distance between two opposite walls of the pore (diameter of cylindrical pores, width of slit-shape pores).

Pore size distribution: represented by the derivatives $\frac{\mathrm{d}A_{\mathrm{p}}}{\mathrm{d}r_{\mathrm{p}}}$ or $\frac{\mathrm{d}V_{\mathrm{p}}}{\mathrm{d}r_{\mathrm{p}}}$ as a function of r_{p}, where A_{p}, V_{p} and r_{p} are the wall area, pore volume and pore radius, respectively. The size in question is here the radius, which implies that the pores are known to be, or assumed to be, cylindrical. In other cases r_{p} should be replaced by the width.

Porosity ε: ratio of total pore volume V_{p} to the apparent volume V of the particle or powder (excluding inter-particle voids). In some cases one may distinguish between *open porosity* (i.e. the volume of pores accessible to a given probe molecule) and *closed porosity*. The methods used to measure pore volume and apparent volume should be stated.

Roughness (or rugosity) factor: ratio of the external surface area to the area of the geometrical envelope of the particles.

[1] A method based on Brunauer-Emmett-Teller isotherm

Surface area: extent of the total surface determined by a given method under stated conditions. It is essential to state the method used. External and internal surface area can be distinguished:

- ***external surface area of a powder*** **–** area of the external surface of the particles, taking into account their roughness, i.e. cavities which are wider than deep, but not the surface of the pore walls,
- ***internal surface area of a powder*** **–** area of the pore walls, excluding the external surface area [16].

4 THEORETICAL PART

This part of the thesis is going to deal with porous materials and their main applications. Some history and definitions will be introduced and properties of this very specific type of materials, as well. Then the thesis will focus on porous membranes and their utilization in filtration applications. As this work aims partially at inorganic binders as well as particular materials, next part of the thesis belongs to these fields.

4.1 Definition of porous medium

By a porous medium is meant a material consisting of a solid matrix with an interconnected void. It is supposed that the solid matrix is either rigid (the usual situation) or it undergoes small deformation. The interconnectedness of the void (the pores) allows the flow of one or more fluids through the material. In the simplest situation (single-phase flow), the void is saturated by a single fluid. In two-phase flow a liquid and a gas share the void space.

In a natural porous medium the distribution of pores with respect to shape and size is irregular. Examples of natural porous media are beach sand, sandstone, limestone, rye bread, wood, and human lung. On the pore scale (the microscopic scale) the flow quantities (velocity, pressure etc.) will be clearly irregular. But in typical experiments the quantities of interest are measured over areas that cross many pores, and such space-averaged (macroscopic) quantities change in a regular manner with respect to space and time, and hence are amenable to theoretical treatment [17].

The presence of pores (holes) in a material can render all sorts of useful properties that corresponding bulk material would not have. Generally, porous materials have porosity between 0.20 – 0.95. Pores are classified into two types – open pores which are connected to the surface of the material and closed pores which are isolated from the outside. In functional application such as adsorption, catalysis etc., closed pores are not of any use. In separation, catalysis, filtration or membranes, penetrating open pores are required most frequently. Materials with closed pores are useful in sonic and thermal insulation or lightweight structural applications. Pores have various shapes and morphology such as cylindrical, spherical and slit types. There are also pores taking more complex shape such as hexagonal shape. Pores can be straight or curved or with many turns and twists, thus having a high tortuosity [18].

4.2. Categories of pores in solid matrices

Classification of pores based on pores origin, structure, size and accessibility to surroundings was published e.g. by Kaneko [19]. In relation to their origin and structure, pores can be divided into two main categories – intra-particle and inter-particle (Fig. 1).

4.2.1 Location in particle

Intra-particle pores are standard type of pores. They are located inside the single particles and from structural point of view can be considered to be intrinsic pores. During some processes (gas evolution, extraction, topological reactions), a new porous material can form. In this case, the new pores can be regarded as “add-on intrinsic pores”, so called extrinsic pores which are formed when original matrix is impregnated with an additive which is removed subsequently by aforementioned methods. Another type of add-on intrinsic pores is so called columnar type that is caused by using of hydroxides of metals which form a layer on

particles surface. In certain cases, the add-on intrinsic pores can be considered as inter-particle pores.

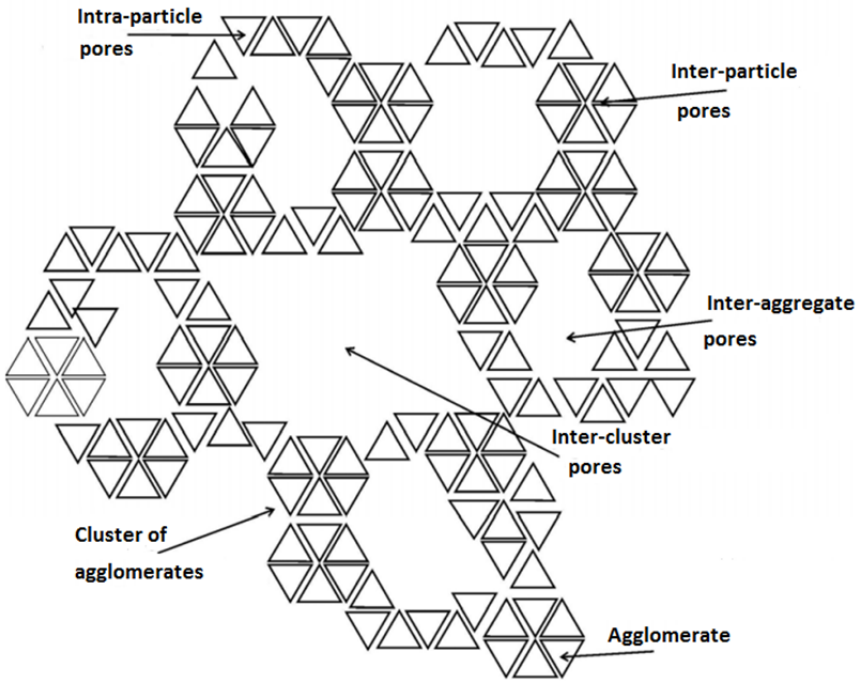

Fig. 1: *Structure elements and types of pores (modified by Kaneko)*

4.2.2 Agglomerate

If the material is consolidated, tough and size of porous matrix is many orders of magnitude bigger than size of pores, it can be termed as agglomerate. As aggregates are termed types of porous materials which are unconsolidated – those are sets of single particles. Particles themselves can be non-porous so they are surrounded by a network of inter-particle pores. Properties of these pores depend on their size, shape and arrangement. On the contrary, in other cases, e.g. catalysts which are dried by spraying, the particles can be markedly porous. That is the reason why distinction between intra- and inter-particle pores is purposeful. Generally speaking, intra-particle pores are smaller compared to inter-particle pores; however, their contribution to the specific surface area of the solid is the most important.

4.2.3 Pore accessibility

Pores can be classified according to accessibility to the surroundings. Pores which are connected to the surface are called open pores (Fig. 2b – 2f). Open pores are accessible for molecules or ions from surrounding. Some pores are open only at one end (Fig. 2b and 2f), these can be called blind pores, and others are opened at both ends (penetrable pores, fig 2e). Cavities which are not in contact with surroundings are called closed pores (Fig. 2a). Closed pores do not affect adsorption and molecules penetration but have influence on mechanical properties of solid matrices.

As the term “closed” can be relative, it can be defined as a space, which is not accessible for helium molecules (d_{crit} = 0.2 nm). Another definition says that it is an open pore whose width is smaller than the probe´s molecular size (ultrapores). Such effectively closed pores and chemically closed pores should be termed as latent [20, 21].

4.2.4 Pore shape

For the sake of simplicity, the shape of pores, when known or assumed, is preferably described in terms of cylinders (which may be the case for activated oxides like alumina or magnesia), prisms (some fibrous zeolites), cavities and windows (other zeolites), slits (possible in clays and activated carbons), or spheres (although, most often, the pores are on the contrary, the voids left between solid spheres in contact with each other, as it happens with gels: silica gel, zirconia gel etc.) the real description of many real porous solids is complicated by the existence of:

- different shapes of pores in the same material,
- connections between pores, which may vary in size, shape and location,
- distribution in the size of the pores.

To describe these complexities it was necessary to introduce descriptors based upon the concepts of connectivity, percolation, tortuosity and, more recently, fractal geometry [16]. Other types of pore geometry can be e.g. cone-shape or ink-bottle (Fig. 3) [20, 21].

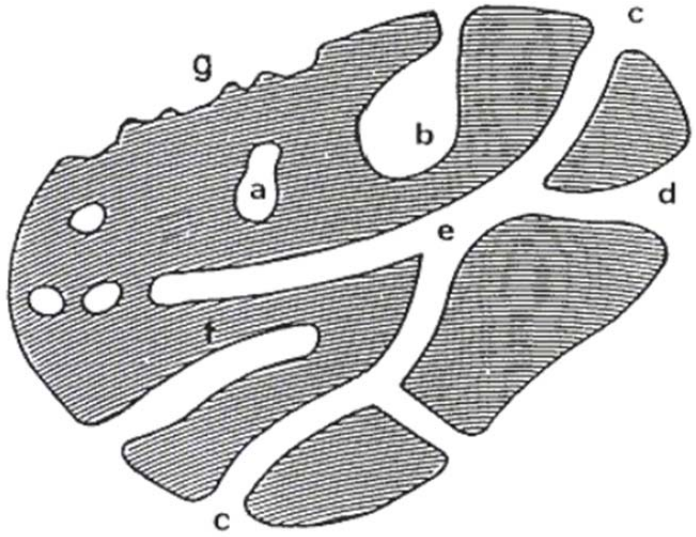

Fig. 2: *Schematic cross-section of a porous solid*

4.2.5 Pore size categories

There are various categories of pore sizes in the literature. A summary of the most frequently used pore sizes is presented in Table 1 [20].

Table 1: *Overview of pore classification by size*

Classification	**Defined types of pores d_p [nm]**					
	Macro-	Mezo-	Micro-	Supermicro-	Ultramicro-	Submicro-
IUPAC	>50	50 – 2	< 2, 2 – 0.4 resp.	2 – 0.7	< 0.7	< 0.4
Dubinin	> 400 – 200	400 – 200 >*d*> 3 – 3.2	< 1.4 – 1.2	3.2 – 3 >*d*> 1.4 – 1.2	–	–
Cheremskoj	>2000	–	2000 >*d*> 200	–	< 4 – 2	< 200
Kodikara	$10^6 – 10^4$	–	$3 \cdot 10^4 – 10^3$	$10^3 – 25$	< 4 – 3	–

Porous materials with the same apparent porosity but with pores of different size and geometry react in a different way under the same conditions. Taking these into consideration, question regarding classification of porous materials based on sizes has risen. Pore size has a precise meaning when the geometrical shape of the pores is well defined and known (e.g. cylindrical, slit-shape etc.).

4.3 Porous materials properties

4.3.1 Porosity

Porosity may be defined as the fraction ε of the apparent volume of the sample which is attributed to the pores detected by the method used:

$$\varepsilon = {}^{V_p}\!/_{V} \tag{2}$$

The value of this fraction depends on the method used to determine apparent volume V, which excludes inter-particle voids (geometrical determination, fluid displacement) and on that used to assess the pore volume V_p (adsorption, and capillary condensation, fluid displacement, ultrasonics etc.). Some methods, indeed, have only the access to open pores (i.e. the methods using a fluid), whereas others may also have access to closed pores (i.e. methods using radiation). Moreover, for a given method, the value depends on the size of the molecular probe (fluid displacement, adsorption) or of the yardstick (stereology). Thus, a recorded value of porosity can be expected to reflect not only a physical property of the material, but also the experimental method used for its determination.

The pore volume V_p used in Eq. 2 may be either of the open pores (leading to the open porosity) or that of the closed pores (leading to the closed porosity) or that of both types of pores together (leading to the total porosity) [16].

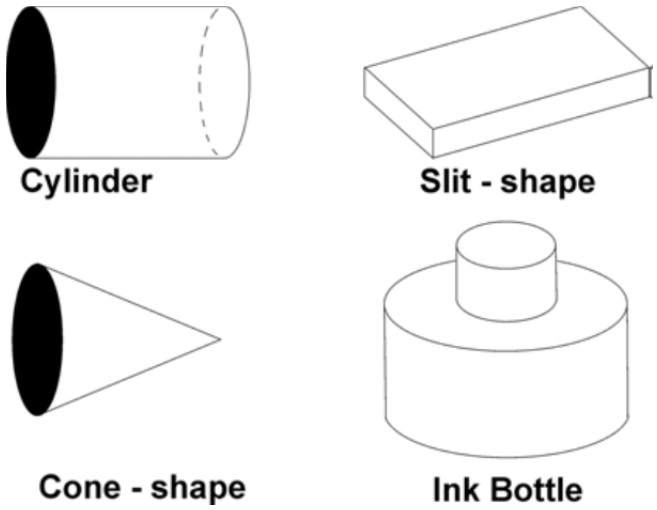

Fig. 3: *Pores geometry classification*

The pores in the fired ceramic may be either interconnected or closed. The apparent porosity (ε_a) measures the interconnected porosity and determines the permeability, or the ease with which gases and fluids seep through the ceramic component. The apparent porosity is determined by weighing the dry ceramic (m_d), then reweighing the ceramic both when it is suspended in water (m_s) and after it is removed from the water (m_w). Then

$$\varepsilon_a = \frac{m_w - m_d}{m_w - m_s} \cdot 100 \quad (3)$$

The true porosity includes both interconnected and closed pores. The true porosity (ε_t), which better correlated with properties of the ceramics, is

$$\varepsilon_t = \frac{\rho_t - \rho_b}{\rho_t} \cdot 100 \quad (4)$$

where

$$\rho_b = \frac{m_d}{m_w - m_s} \quad (5)$$

ρ_b is the bulk density and ρ_t is the true density or specific gravity of the ceramic. The bulk density is the weight of the ceramic divided by its volume [22].

For natural media, ε does not normally exceed 0.6. For beds of solid spheres of uniform diameter ε can vary between limits 0.2595 (rhombohedral packing) and 0.4764 (cubic packing). Non-uniformity of grain size tends to lead to smaller porosities than for uniform grains, because smaller grains fill the pores formed by larger grains. For man-made materials such as metallic foams ε can approach the value 1 [17].

4.3.2 Specific surface area

Specific surface area A_s is defined as the accessible (or detectable) area of solid surface per unit mass of material. It is similarly dependent on the method and experimental conditions employed, and on the size of probe used (e.g. adsorbate molecular size, wavelength of radiation etc.). However, since the interpretation of such measurements usually relies on simplified models of the processes concerned, the recorded value may further depend on the validity of the assumptions inherent to the model.

4.3.3 Pore size

The pore size is a property of major importance in practical applications of porous materials, but it is even less susceptible to precise definition. The problems already mentioned for the specific surface area are complicated by the fact that the pore shape is usually highly irregular and variable, leading to a variety of definitions of the size. Moreover, pore systems usually consist of interconnected networks, and the recorded results will often depend on the sequence in which pores are encountered within the method used (e.g. mercury intrusion). For these reasons, quantitative descriptions of pore structure are often based on model systems [16].

4.3.4 Mechanical properties

For some ceramic fabrication techniques, the precursor material is in the form of a powder. Subsequent to compaction or forming of these powder particles into desired shape, pores or void spaces will exist between the powder particles. During the ensuing heat treatment, much of this porosity will be eliminated; however, it is often the case that this pore elimination process is incomplete and some residual porosity will remain. Any residual porosity will have a deleterious influence on both the elastic properties and strength. For example, it has been observed for some ceramic materials that the magnitude of the modulus of elasticity E decreases with volume fraction porosity ε according to:

$$E = E_0\left(1 - 1.9\varepsilon + 0.9\varepsilon^2\right) \tag{6}$$

where E_0 is the modulus of elasticity of the non-porous material. The influence of volume fraction porosity on the modulus of elasticity for aluminum oxide is shown in Fig. 4.

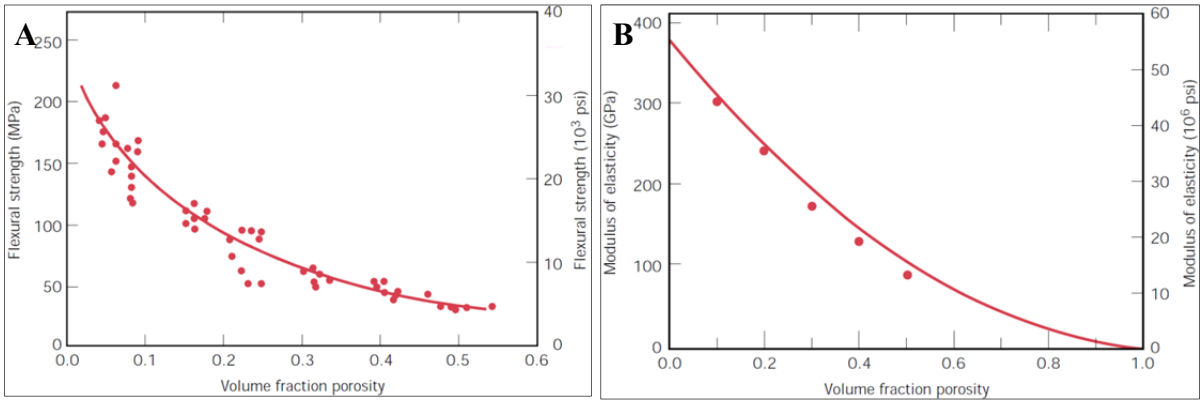

Fig. 4: *The influence of porosity on the modulus of elasticity (A) and on the flexural strength (B) for aluminum oxide at room temperature. The curves drawn are according to equation 6 and equation 7, respectively.*

Porosity is deleterious to the flexural strength for two reasons: (1) pores reduce the cross-sectional area across which a load is applied, and (2) they also act as stress concentrators – for an isolated spherical pore, an applied tensile stress is amplified by a factor of 2.The influence of porosity on strength is rather dramatic; for example, it is not uncommon that 10 % vol. porosity will decrease the flexural strength by 50 % from the measured value for the non-porous material. The degree of the influence of pore volume on flexural strength is demonstrated in figure 4, again for aluminum oxide. Experimentally it has been shown that the flexural strength decreases exponentially with volume fraction porosity ε as:

$$\sigma_{fs} = \sigma_0 \exp(-q\varepsilon) \tag{7}$$

In this expression σ_0 and n are experimental constants [23].

4.4 Methods for preparation of porous materials

4.4.1 Sol-gel method

Sol-gel technology, by which composite organic-inorganic materials are made at relatively low temperature, involves the hydrolysis of the constituent molecular precursors and subsequent polycondensation to glass-like form. Sol-gel methods enable homogeneous samples to be obtained at low temperatures and the starting cationic composition to be maintained by using metal salts as raw materials and mixing them in a liquid solution [24].

Sol-gel process can be characterized as gelation i.e. coagulation and subsequent sedimentation or polycondensation of disperse phase of micro-heterogeneous systems – sols. As colloid solutions are thermodynamically unstable, this process can take place spontaneously but it is often accelerated and affected to attain requested structure and properties of product. After formation of gel (lyogel or coagel), follows removal of dispersion medium (drying) to form xerogel. This process influences properties like porosity or mechanical properties, at most [13, 15, 25].

Methods sol-gel can be divided by precursor into:

- Alkoxide – hydrolysis and polycondensation of $X(OR)_4$ molecules are used, where X = Si, Ti, Zr,… and R = $-CH_3$, $-C_2H_5$,…,
- Semialkoxide – alkoxides and salts are used as reactants,
- Pechini and modified Pechini synthesis –chelating reagent (citric acid, EDTA etc.) are used as reactants, this method is used for preparation of highly pure reactive powders.

Alkoxide and semialkoxide precursors can be divided by obtained product structure into:

- I. type – inorganic networks based on Si-O-Si bond, e.g. tetramethoxysilane (TMOS),
- II. type – inorganic networks based on the other bonds than Si-O-Si, e.g. Zr-O-Zr, Al-O-Al, Ti-O-Ti etc., e.g. tetraethylorthotitanate (TEOT),
- III. type – inorganic networks modified by organic groups, e.g. fenyltriethoxysilane,
- IV. type – molecules have functional groups able to react with oxide network, e.g. (3-mercaptopropyl)triethoxysilane.

The main applications of sol-gel method are:

- Overlays and protective, abrasion resistant coatings, hydrophobization of surfaces,
- Organic-inorganic composites, reactive powders, low-density xerogels,
- Porous glasses, membranes, aerogels, specific adsorbents,
- Gel electrolytes, isolation materials, substrates for biology.

Example of particular preparations and materials:

Porous glasses – hydrolysis of alkoxide precursor (e.g. TMOS:H_2O, molar ratio 1:16, acid catalysis – HNO_3 or HF, 48 h, 60 °C), drying at 105 °C, thermal treatment 400 – 900 °C. *Vycor 7930:* 1.5 $g \cdot cm^{-3}$, 96.3 % SiO_2, 2.95 % B_2O_3, porosity 28 %, pore size 4 nm, specific surface area 200 $m^2 \cdot g^{-1}$.

Silicagel: porous glass material with almost uniform pore size.

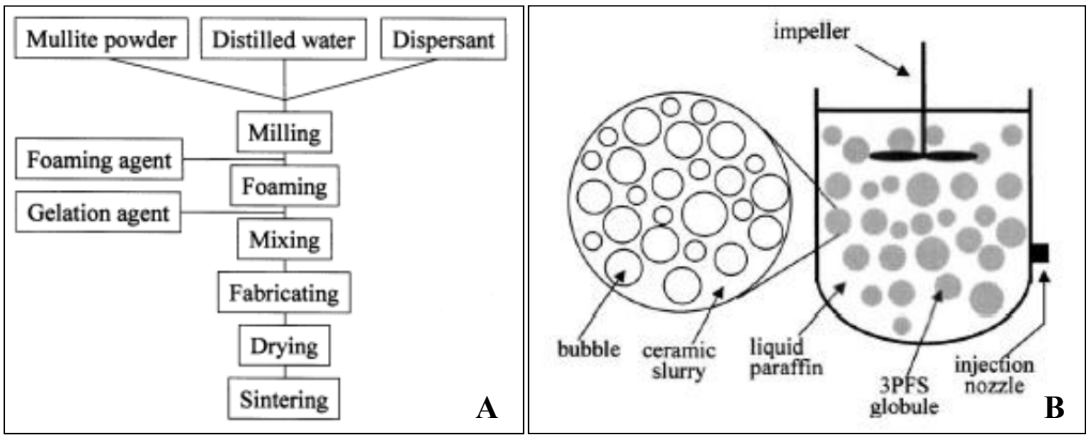

Fig. 5: *Block diagram of foaming technique process (A) and schematic picture showing emulsion preparation (B)*

The porous glass structure prepared under temperature 650 °C contains pores and cracks caused by volume contraction during drying. Over temperature of 700 °C, the presence of the cracks was not observed and over temperature of 900 °C, the pores were closing off [26].

4.4.2 Foaming

By this method, highly porous ceramic particles (Fig. 6) can be prepared, by means of double emulsion. Droplets of oil are suspended in aqueous ceramic suspension, and this system is dispersed again in paraffin. Then the emulsion is heat-treated to prepare porous ceramic particles.

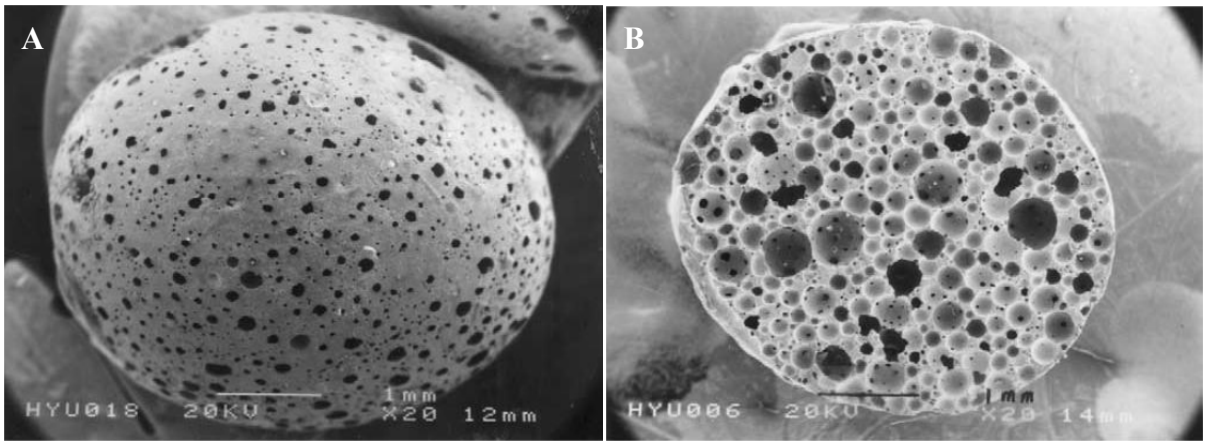

Fig. 6: *Porous particles prepared by foaming*

Ceramic foams can be prepared by using combustible matrix; this is so called sponge method. The ceramic suspension is casted into a mold of a polymer and a ceramic. Organic phase is burned out and porous layer is connected with the material the mold is filled with. Porous materials based on Al_2O_3 are being prepared by this method and used as ceramic filters (Fig. 7).

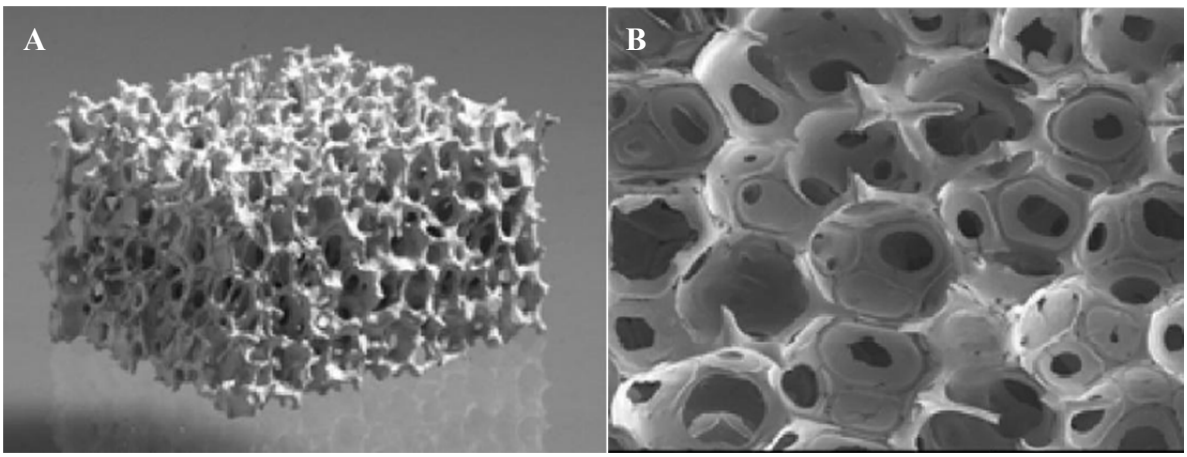

Fig. 7: *Ceramic filters – sponge method* [27]

4.4.3 Freeze –drying

The technique of ceramic powders preparation by freeze-drying (also lyophilization or cryodesiccation) consist of fast cooling of small droplets of intensively stirred aqueous emulsion of salts solution of the requested composition in non-aqueous dispersion medium(e.g. hexane). After separation of frozen particles, water is removed by sublimation under vacuum (process is carried out under triple point of *p-T* diagram of water), so water transforms from the solid state (ice) to the vapor state directly. This process leads to porous

particles of anhydrous salts, of high specific surface area, that are heat-treated, subsequently. During calcination, the salt is decomposed to form agglomerated oxide powders.

Other modifications, increasing productivity of this method, and which are usable for preparation of layers, are spray-freeze-drying (for freeze-drying of aerosols) and sol-freeze-drying (for freeze-drying of sols) in fluidized bed. Out of ceramics this technique is utilized for drying of heat-sensitive materials in food and pharmaceutical industry.

Another alternative of freezing techniques is a method called „freeze casting“, that includes casting of suspension of finely grounded ceramic powder dispersed in appropriate organic solvent on cooled underlay and subsequent sublimation of organic phase. This technique proved itself to be used for preparation of bulk samples of highly porous ceramic materials (Fig. 8). Pore size and distribution can be influenced by suspension concentration and temperature of heat treatment.

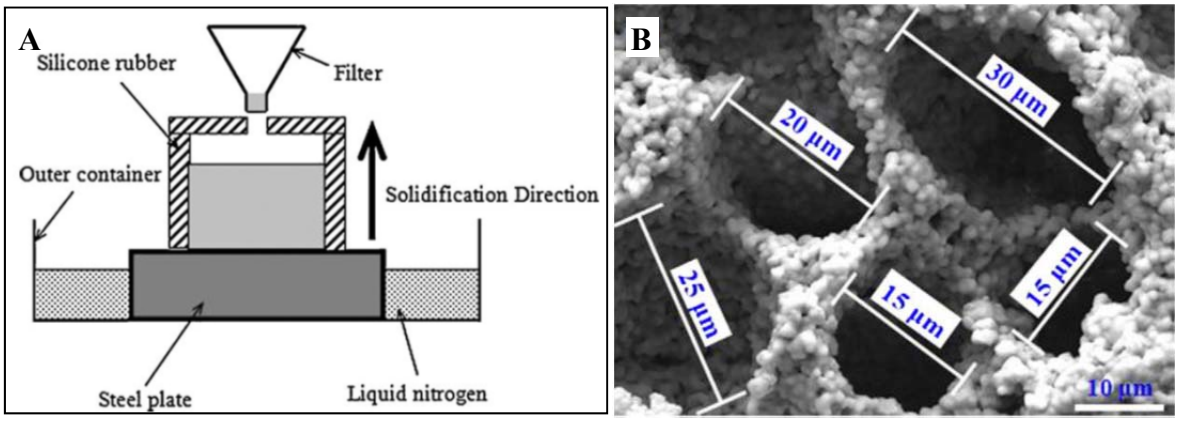

Fig. 8: *Schematic of the set for freeze casting (A) and microstructure of a product prepared by freeze casting (B)* [28]

4.4.4 Cementation

By cementation, the ceramic raw materials are joined using a binder that does not require firing or sintering. A liquid resin, such as sodium silicate, aluminum phosphate, or Portland cement, coats the ceramic particles and provides bridges (Fig. 9). A chemical reaction produces a solid that joins the particle together. Because cemented ceramic materials often have a high porosity and permeability, they may be used as ceramic filters. The binder systems are also used to make molds for metal castings. The binder produces strong, rigid bonds between sand grains, yet permits mold gases to escape through the permeable mold rather than be trapped as gas defects in the casting [22].

4.5 Flow in porous media

Fluid flow in a porous medium is a common phenomenon in nature, and in many fields of science and engineering. Important everyday flow phenomena include transport of water in, living plants and trees, and fertilizers or wastes in soil. Moreover, there is a wide variety of technical processes that involve fluid dynamics in various branches of process industry. The importance of improving our understanding of such processes arises from the high amount of energy consumed by them. In oil recovery, for example, a typical problem is the amount of unrecovered oil left in oil reservoirs by traditional recovery techniques. In many cases the porous structure of the medium and the related fluid flow are very complex, and detailed

studies of these flows pose demanding tasks even in the case of stationary single-fluid flow [29].

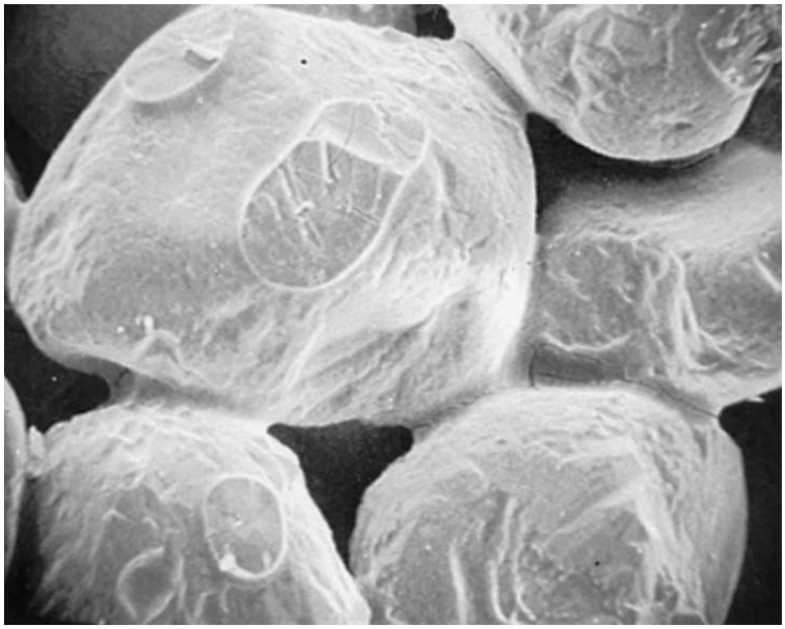

Fig. 9: *A photograph of silica sand grains bonded with sodium silicate through the cementation mechanism* [22]

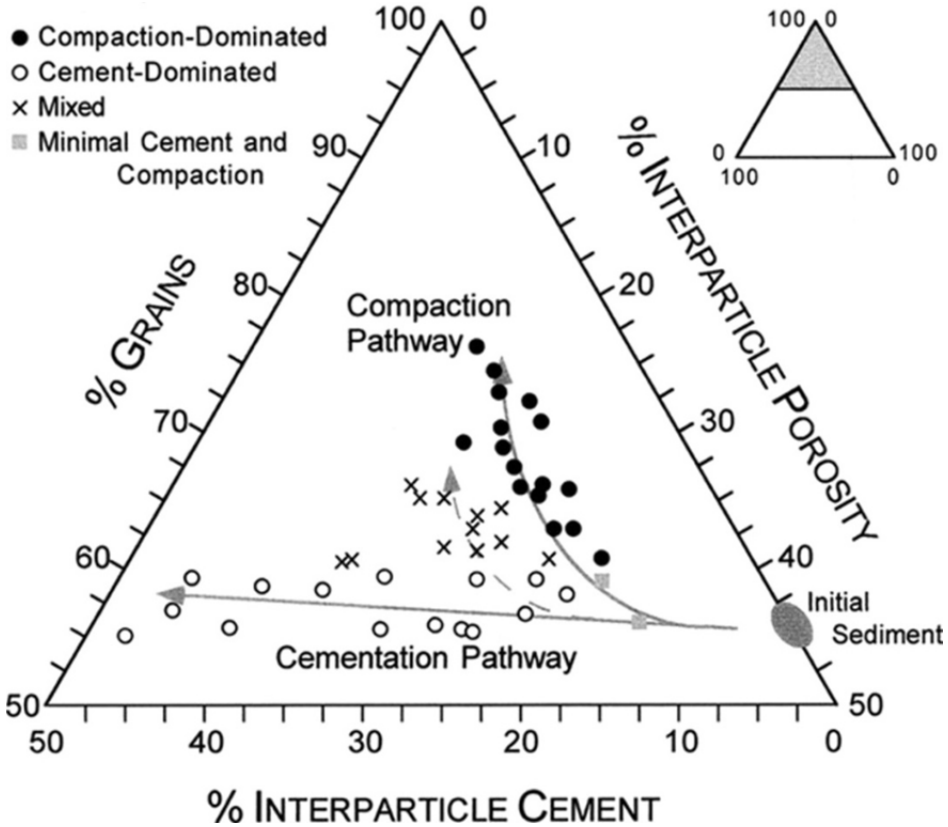

Fig. 10: *Ternary diagram defining cementation and compaction pathways from the relative abundance of inter-particle pores, grains, and inter-particle cements* [30]

In experimental and theoretical work on fluid flow in porous material it is typically relevant to find correlations between material characteristics, such as porosity and specific surface area, and flow properties. The most important phenomenological law governing the

flow properties, first discovered by Darcy, defines the permeability as conductivity to fluid flow of the porous material. Permeability is given by the coefficient of linear response of the fluid to a non-zero pressure gradient in terms of the flux induced.

Some of the material properties that affect the permeability, e.g. tortuosity, are difficult to determine accurately with experimental techniques, which have been, for a long time, the only practical way to study many fluid-dynamical problems [29].

4.5.1 Darcy's law

Henry Darcy's (1856) investigations into the hydrology of the water supply of Dijon and his experiments on steady-state unidirectional flow in a uniform medium, revealed proportionality between flow rate and the applied pressure difference. In modern notation this is expressed, in refined form, by:

$$u = -\frac{K}{\eta}\frac{\partial p}{\partial x} \tag{8}$$

Here $\partial p/\partial x$ is the pressure gradient in the flow direction and η is the dynamic viscosity of the fluid. The coefficient K is independent of the nature of the fluid but it depends on the geometry of the medium. It has dimension $(\text{length})^2$ and is called the specific permeability or intrinsic permeability of the medium. The permeabilities of common porous materials are summarized in Table 2. In three dimensions, Eq. 8 generalizes to:

$$\mathbf{u} = \eta^{-1}\mathbf{K}\nabla p \tag{9}$$

where now the permeability **K** is in general second-order tensor.

Darcy's law has been verified by the results of many experiments. Theoretical backing for it has been obtained in various ways, with the aid of either deterministic or stochastic models. It is interesting that Darcy's original data may have been affected by the variation of viscosity with temperature [17, 31].

Table 2: *Properties of common porous material*

Material	**Porosity ε**	**Permeability K [cm^2]**
Concrete	~ 0.10	-
Leather	0.56 – 0.59	$9.5\cdot10^{-6} – 1.2\cdot10^{-5}$
Limestone	0.04 – 0.10	$2\cdot10^{-11} – 4.5\cdot10^{-10}$
Sand	0.37 – 0.50	$2\cdot10^{-7} – 1.8\cdot10^{-6}$
Silica powder	0.37 – 0.49	$1.3\cdot10^{-10} – 5.1\cdot10^{-10}$
Soil	0.43 – 0.54	$2.9\cdot10^{-9} – 1.4\cdot10^{-7}$
Brick	0.12 – 0.34	$4.8\cdot10^{-11} – 2.2\cdot10^{-9}$

4.5.2 Filtration

The general problem of separating solids from liquids may be solved by a wide variety of operations depending upon the character of the solids and proportion of solid to liquid in the mixture to be separated. When the amount of solid is relatively small as compared to the liquid, the process is usually called filtration. As the percentage of solid in suspension becomes higher, the operation passes into either pressing or centrifuging. Curiously enough, the centrifuging is also used in certain separations where the amount of solid to be removed is almost infinitesimal [32].

Filtration is a process whereby solid particles present in a suspension are separated from liquid or gas employing a porous medium, which retains the solids but allows the fluid to pass through. The suspension to be filtered is known as sludge. The porous medium used to retain the solids is known as filter medium (filtration barrier). The accumulated solids on the filter are referred as filter cake and the clear liquid passing through the filter is filtrate. The pores of the filter medium are smaller than the size of particles to be separated. Filter medium like filter paper or muslin cloth is placed on a support. When feed is passed over the filter medium, the fluid flows through the filter medium by virtue of a pressure differential across the filter. Gravity is acting on the liquid column. Therefore, solids are trapped on the surface of the filter medium. After a particular point of time, the resistance offered by the filter cake is high that stops the filtration [33].

Based on the mechanism, there are two basic types of filtration (Fig. 11):

Cake filtration – the particles bigger than pore size of the barrier are captured on its surface where a layer of particles (cake) is formed.

Depth filtration – by this filtration mechanism, particles are retained not only on the surface but also inside the filtration barrier. Particle size is usually much smaller than channels diameter in the barrier.

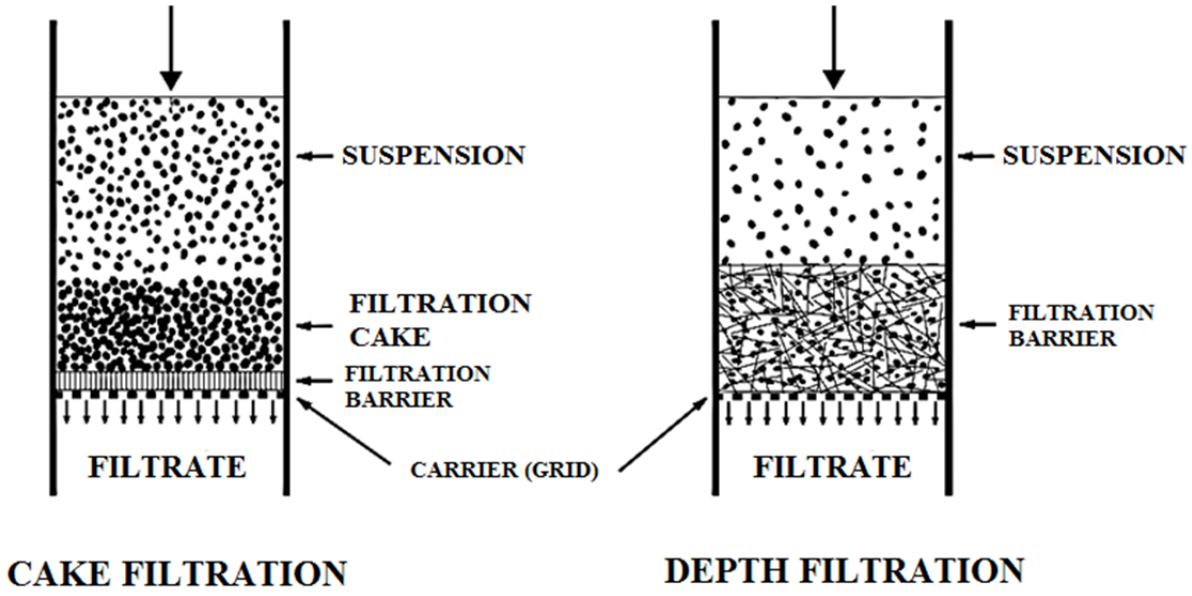

Fig. 11: *Comparison of cake and depth filtration*

The term filtration is used for processes whereby suspensions of particles bigger than $1 \cdot 10^{-5}$ m are separated. If the particles are smaller, the filtration process is termed as membrane process because it involves special micro-porous filtration materials – membranes [34].

Velocity of liquid flow through a porous barrier can be expressed in terms of column cross-section and volume flow. This is velocity of flow out of the porous layer relating to the vacant cross-section of column:

$$u = \frac{\dot{V}}{A} = \frac{4\dot{V}}{\pi D^2} \tag{10}$$

where $\dot{V}$, A and $D$are volume flow, column cross-section area and column diameter, respectively. The real velocity in channels of the porous barrier is:

$$u_\varepsilon = u \diagup \varepsilon \tag{11}$$

So fluid flows only through vacant space of the barrier and therefore the real velocity is bigger than the flow rate out of the barrier. Reynolds number for flow through porous barrier is defined as follows:

$$\mathrm{Re} = \frac{d_\mathrm{e} u_\varepsilon \rho_\mathrm{l}}{\eta} \tag{12}$$

where d_e, ρ_l are equivalent diameter and fluid density, respectively. Filtration rate is defined as follows:

$$u = \frac{1}{A}\frac{\mathrm{d}V_\mathrm{f}}{\mathrm{d}t} \tag{13}$$

where A is filtration area perpendicular to the flow direction, $\mathrm{d}V_\mathrm{f}$ is differential volume obtained in differential time interval of filtration dt. Basic equation of filtration is derived from relationship for pressure drop in porous barrier at laminar conditions:

$$\Delta p = \lambda_\mathrm{s} \frac{h_\mathrm{b}}{d_\mathrm{e}} \frac{u_\varepsilon^2}{2} \rho_\mathrm{l} \tag{14}$$

where h_b is barrier thickness, λ_s always equals to const./Re and $u_\varepsilon = u/\varepsilon$, so we get:

$$\Delta p = \frac{\mathrm{const.}}{\mathrm{Re}} \frac{h}{d_\mathrm{e}} \frac{u^2}{2\varepsilon^2} \rho_\mathrm{l} \tag{15}$$

Values characterizing barrier (d_e, ε) including constant 2 can be involved in constant K to form permeability coefficient. The relation as follows is obtained:

$$u = \frac{K\Delta p}{h\eta} \tag{16}$$

and this is Darcy's equation for filtration (compare Eq. 8). In the case of incompressible cake, the value K is constant. Now, the dependence of filtration layer thickness (filtration cake and barrier) on time or amount of flown filtrate, which is equivalent, is supposed to be derived. So the balance of solid phase in filtration cake is necessary to carry out, for this purpose.

For amount of solid phase in a cake m_sp, the following relation can be written:

$$m_\mathrm{sp} = A h_\mathrm{c} (1-\varepsilon) \rho_\mathrm{s} \tag{17}$$

where h_c and ρ_s are cake thickness and solid phase density, respectively. Amount of solid phase in the volume of liquid captured in the cake m_sl equals to:

$$m_{\mathrm{sl}} = A h_{\mathrm{c}} \varepsilon \rho_{\mathrm{l}} x_{\mathrm{s}} \tag{18}$$

where x_s is concentration of suspension (kg of solid phase/kg of liquid). This is amount of solid phase which is not captured by the barrier, so it flows through the barrier with filtrate. For amount of solid phase m_{sf} which corresponds to amount of filtrate flown V_f, can be written:

$$m_{sf} = \rho_{\mathrm{l}} V_{\mathrm{f}} x_{\mathrm{s}} \tag{19}$$

Solid phase balance:

$$m_{\mathrm{sp}} = m_{\mathrm{sl}} + m_{sf} \tag{20}$$

$$A h_{\mathrm{c}} (1-\varepsilon) \rho_{\mathrm{s}} = A h_{\mathrm{c}} \varepsilon \rho_{\mathrm{l}} x_{\mathrm{s}} + \rho_{\mathrm{l}} V_{\mathrm{f}} x_{\mathrm{s}} \tag{21}$$

Amount of solid phase in the volume of liquid captured in the cake (member m_{sl}) is usually negligible compared to the amount of solid phase in the cake (m_{sp}) so the Eq. 21 is simplified and the thickness of the cake h_k and thickness of filtration barrier h_b can be derived:

$$h_{\mathrm{k}} = \frac{V_{\mathrm{f}} \rho_{\mathrm{l}} x_{\mathrm{s}}}{A(1-\varepsilon)\rho_{\mathrm{s}}} \tag{22}$$

$$h_{\mathrm{b}} = \frac{V_{\mathrm{fb}} \rho_{\mathrm{l}} x_{\mathrm{s}}}{A(1-\varepsilon)\rho_{\mathrm{s}}} \tag{23}$$

where V_{fb} is volume of filtrate which form layer of filtration cake with the same resistance as filtration barrier has. By substitution in Eq. 16, the basic equation of filtration is obtained:

$$\Delta p = \Delta p_{\mathrm{c}} + \Delta p_{\mathrm{b}} = \frac{\eta \rho_{\mathrm{l}} x_{\mathrm{s}}}{K(1-\varepsilon)\rho_{\mathrm{s}}} \left(V_{\mathrm{f}} + V_{\mathrm{fb}}\right) \frac{1}{A^2} \frac{\mathrm{d}V_{\mathrm{f}}}{\mathrm{d}t} \tag{24}$$

where Δp_c and Δp_b are pressure drop in cake and pressure drop in barrier, respectively. So now the filtration conditions must be specified. There are principally two main proceedings of filtration:

1. Constant pressure filtration,
2. Constant rate filtration

3.5.2.1 Filtration at constant pressure

This is frequently used in practice. Constant pressure drop can be attained by keeping suspension surface level with help of spillway or by suitable pump or compressor which preserves pressure supply in the system. It is possible to maintain constant vacuum with help of air-pump placed beneath the filtration barrier (vacuum filtration).

By integration of Eq. 24 for Δp = const. the filtration equation at constant pressure is obtained:

$$V_{\mathrm{f}}^2 + 2 V_{\mathrm{f}} V_{\mathrm{fb}} = 2Ct \tag{25}$$

The constant C contains value Δp:

$$C = \frac{\Delta p A^2 K(1-\varepsilon)\rho_s}{\eta \rho_l x_s} \tag{26}$$

Constants V_{fb} and C are determined experimentally as flow of filtrate related to the unit of filter area A.

Filtration time for another area A_1 can be calculated by using of modified Eq. 25:

$$\left(\frac{V_{\mathrm{f}}}{A_1}\right)^2 + 2\left(\frac{V_{\mathrm{f}}}{A_1}\right)V_{\mathrm{fb}} = 2Ct \tag{27}$$

3.5.2.2 Filtration at constant rate

The main effort in this procedure is to preserve constant flow of filtrate in time. With growing filtration cake, this is possible only by increasing pressure difference. For constant rate is valid:

$$u = \frac{1}{A}\frac{\mathrm{d}V_{\mathrm{f}}}{\mathrm{d}t} = \frac{V_{\mathrm{f}}}{At} = const. \tag{28}$$

$$\Delta p = \Delta p_{\mathrm{c}} + \Delta p_{\mathrm{b}} = \frac{\eta \rho_1 x_{\mathrm{s}}}{K(1-\varepsilon)\rho_{\mathrm{s}}}\left(\frac{V_{\mathrm{f}}}{At}\right)^2 t + \frac{\eta \rho_1 x_{\mathrm{s}} V_{\mathrm{f}}}{K(1-\varepsilon)\rho_{\mathrm{s}} A}\left(\frac{V_{\mathrm{f}}}{At}\right) \tag{29}$$

3.5.2.2 Influence of cake compressibility

The value called specific cake resistance can be defined:

$$\alpha = \frac{1}{K(1-\varepsilon)\rho_s} \tag{30}$$

Dependence of this value on Δp was measured experimentally and a relation was found:

$$\alpha = \alpha_1 \Delta p^s \tag{31}$$

where α_1 is measured value of α at unit pressure and s is index of cake compressibility (for uncompressible cake $s = 0$, for compressible cake $0 < s < 1$) [35]

4.6 Filtration barriers

From definition of filtration is obvious that a filtration barrier is to separate particles (solid phase) of suspension from liquid and it is a support of forming filtration cake. Particles which are bigger than diameters of channels in the barrier are captured by sieve-like manner. Smaller particles can be captured, too. It mainly depends on whether other capturing mechanisms, besides the sieving, e.g. electrical effects, or surface mechanisms, take place.

Definition of filtration barrier:

Filtration barrier is a porous material in which particles are captured during filtration process.

4.6.1 Properties of filtration barriers

Filtration medium – the barrier is characterized by its filtration properties, especially by penetrability of fluid and impenetrability of solid phase (particles). The barrier can be made of natural or synthetic materials, metals, ceramics, fabric or paper. For certain type of filtration

device and suspension to be filtrated are suitable only certain types of filtration barriers. They must have unique properties from various aspects which may be divided into three categories:

1. Mechanical properties deciding on manufacturing of the barrier and its applicability in certain construction type of filter,
2. Application properties deciding on how it is usable for processing of substrates of specific chemical, biochemical and physical properties. Properties required by ecological and sanitary standards and mainly cost are important as well,
3. Process characteristics deciding on separation procedure suspension phases, e.g. permeability, resistance to flow, porosity, pore size, sludge capacity, blocking of pores, removal of filtration cake etc.

Toughness is a primary criterion of compatibility of filtration medium with specific type of filter. It is characterized by modulus of elasticity. Paper and fabrics are characterized by elongation at break in longitudinal and transverse direction. *Strength* of material in general, is a characteristic of stress-strain dependence. The main parameters are ultimate strength, yield point etc. Other properties are resistance to creep, stability of edge of filtration medium, abrasion and vibration durability, possibility of sealing at frame etc.

4.6.2 Types of filtration barriers

4.6.2.1 Ceramic, stoneware, glass barriers

These are widespread types of filtration barriers. They are chemical resistant and can be used at higher temperatures. Stoneware barriers are made of certain types of kaolin containing quartz (SiO_2), ceramic barriers are made of powders containing aluminum (e.g. Al_2O_3). Both types are being fired at temperatures about 1400 °C. They may be used as support – in this case they have holes with up to 6 mm in diameter and filtration barrier itself has various sizes of pores (from 1 to 2500 μm) and various thicknesses. Recently, they are used for filtration of liquids and gases at higher temperatures. Glass frits are being made of chemical and heat resistant enamel (Simax, Kavalier Sázava). Frits can be heated to maximal temperature of 530 °C slowly and cooled slowly, too.

4.6.2.2Barriers sintered of metal powders, fibers and sieves

They are widely applied in chemical and food industry and the other spheres of industry for filtration of liquids and gases.

Sintered metal powders – the initial material is a metal powder of spherical particles or other granular material with particle size from 0.5 to 100 μm. Powders are made by means of powder metallurgy (e.g. spraying of metal in inert atmosphere and subsequently finely grinded). Powders of stainless steels, bronze, brass, nickel, monel, titanium etc. Powder is pressed in a mold and then sintered.

Sintered metal fibers – these are made of fine fibers of various diameters. High porosity, low flow resistance and high sludge capacity are characteristic for them (mainly for types with gradient structure – increasing pore size with width).

Sintered woven sieves and composite sintered metal media are the other types of metal barriers which have high strength and are used for filtration of high viscous polymers at high pressure difference.

4.6.2.3 Plastic porous barriers

Exploitation of plastic materials is greatly widespread and new types of these barriers are persistently developed. Polyvinylchloride, polyurethane, polyethylene, polypropylene, polyamide and other polymers are used for manufacture of various porous boards, discs, pipes and many types of shaped cartridges. Materials are made by means of thermic smelting or foaming technique resulting in porous permeable material with continuous channels.

4.6.2.4 Textile fabrics and geotextiles

Woven textile fabrics are the most widely used filtration material. They are manufactured by weaving of various types of fibers either natural or most recently synthetic. Barriers made of synthetic fibers like polyester, polyamide, polypropylene etc. have better mechanical properties as well as chemical and biological resistance compared to the fibers natural such as wool, cotton, hemp, flax etc.

Nonwoven textile fabrics (felts) are being made of various fibers which can be compacted and arranged into a structure. Felts have been used for long time mainly for depth filtration. [36]

Geotextiles are flexible, textile-like fabrics of controlled permeability used to provide filtration, separation, reinforcement and drainage functions (except liquid barriers) in soil, rock and waste materials. Geotextiles act as filters between soil and drainage gravel, preventing soil particles from being carried away by the filtered water. The drainage gravel has a tendency to become clogged, and the soil has a tendency to be washed away. The role of geotextiles as a filter is to limit this phenomenon [37].

4.6.2.5 Beds of granular materials and filter paper

These types of filter material include layers of e.g. sand, diatomite, expanded perlite or activated carbon stored on suitable macroporous (perforated) support. The layer is formed by precoating of suspension of the filter material on the perforated support. These layers can be easily regenerated [34].

For complete listing, the filter paper has to be mentioned because this material is widely used in filtration techniques as well. It is basic type of filter medium for laboratory purposes but is widespread in industry as well. It is typical material for surface filtration which is made of cellulose fibers [36].

4.7 Inorganic binders

4.7.1 Cement

In the most general sense of the word, cement is a binder, a substance that sets and hardens independently, and can bind other materials together. Cement is hydraulic powder binder whose active components are CaO, SiO_2, Al_2O_3 and Fe_2O_3 or other compounds of similar type. From chemical composition point of view, the cements may be divided into three types:

1. Silicate cements – the most important in this group is Portland cement (PC),
2. Aluminate cements (AC) – with the most of calcium aluminates,
3. Other cements [14].

4.7.1.1 Portland cement

The raw materials – lime, silica, alumina, iron oxide – used in the manufacture of PC interact with one another in the kiln to form series of complex products. These combined

products referred to as clinker are specified by their oxide contents and by the proportion of four main compounds (also designated as phases) shown in Table 3 together with their abbreviated symbols [1]. PC is essential part of all modern hydraulic binders (except aluminate cement). Clinker is then grinded in ball mill. The grinded clinker itself cannot be used in practical way because as soon as it is mixed with water, it reacts rapidly and hence the concrete could not be processed. If the clinker is grinded together with appropriate amount of calcium sulfate in the form of gypsum or anhydrite, PC sets as it is supposed to be. So calcium sulfate is added as an inhibitor to prevent flash setting [39].

The reactions of PC that produce the hardened cement matrix occur in a water cement paste. In the presence of water, the silicate and aluminates (Table 3) form hydration products, which in time produce a hard mass. The products of hydration of cement have a low solubility in water and the hydrated cement adheres firmly to the aggregates and the unreacted cement.

Table 3: *Main compounds of Portland cement*

Compound	Oxide composition	Abbreviation
Tricalcium silicate	$3CaO \cdot SiO_2$	C_3S
Dicalcium silicate	$2CaO \cdot SiO_2$	C_2S
Tricalcium aluminate	$3CaO \cdot Al_2O_3$	C_3A
Tetracalcium aluminoferrite	$4CaO \cdot Al_2O_3 \cdot Fe_2O_3$	C_4AF

The main anhydrous compounds of cement react with water causing partial solubilization of the calcium compounds and calcium sulfate, and rapidly saturating the liquid phase with various ionic species. Combinations between the ions occur within a few minutes of hydration producing needle-shaped crystals of calcium sulfoaluminate hydrate (ettringite). This is followed by the appearance of large prismatic crystals of calcium hydroxide and the formation of very small fibrous crystals of calcium silicate hydrate that begin to occupy the spaces formerly held by water and the dissolving cement particles. The main hydration products formed from the different mineral components can be broadly classified as calcium silicate hydrates (CSH) and calcium aluminate hydrates (CAH) [1, 38].

4.7.1.2 Aluminate cement

AC is produced from special kind of clinker. According to chemical composition content of the main oxides is in range of 35 – 52 % Al_2O_3, 35 – 45 % CaO, 3 – 10 % SiO_2, 1 – 15 % Fe_2O_3. AC is characterized by rapid setting and hardening, high hydration enthalpy, progressed chemical resistance (SO_4^-, Cl^-). Hydrated clinker minerals are metastable, they are converted which cause porosity increase and strength loss. This process can take several years and therefore AC must not be used for construction purposes [40, 41]. Characteristic properties of AC can be summarized into these points:

1. Slow initial setting followed by rapid hardening – after 12 – 24 hours AC reaches strengths which PC has after 28 days (50 MPa),
2. High final strengths of 60 – 100 MPa, however, after a certain period of time the strengths decreasing occurs,
3. Rapid release of hydration heat, which allows processing of concrete in moderate freeze; on the contrary, this property can lead to overheating of massive constructions and hence to blemish the hydration process and setting,

4. Resistance against sulfate and carbonic solutions, especially sea water but AC does not resist to alkaline solutions,
5. Durability to higher temperatures which is as better as the content of Al_2O_3 increases.

AC is used in special applications where long term strengths are not required. The production is relatively small. It is convenient for emergency repairs of concrete constructions, reservoirs for sulfate and mineral waters and refractory concretes i.e. mixtures of AC and refractory filler. These materials are used to make refractory linings of furnaces and to repair furnaces without stopping of work [14, 40, 41].

4.7.1.3 Pores and voids

The hydrated cement paste contains a variety of voids and pores that exert an important influence on the properties of concrete. Interlayer spaces are the smallest pores within the C-S-H structure and occupy 28 % of the total volume of the hydrated paste. The actual figure is characteristic of given cement, but is largely independent of water/cement ratio (W/C) of the mixture. With the progress of hydration, total volume of paste pores increases, while the volume of capillary pores decreases. The void size of the interlayer pores is too small to have an adverse effect on strength and permeability of the cement paste. However, removal of water from these pores under certain conditions may contribute to drying shrinkage and creep.

Capillary pores represent the space originally occupied by water but partly filled by the solid hydration products. In well hydrated, low W/C ratio paste, the size of the capillary pores may range from 10 to 50 nm; in high W/C ratio pastes they may be as large as 3 to 50 μm at ages less than 28 days. Although pores vary in shape, permeability measurements show that they form an interconnected system, randomly distributed throughout the cement paste that is mainly responsible for the permeability of hardened cement paste and for its vulnerability to frost [1].

4.7.2 Geopolymers and alkali activated materials

4.7.2.1 Definition and structure

Geopolymers may be defined in a number of ways, in terms of their principal constituents (alumina and silica), their structure (tetrahedral Al-O and Si-O units in random 3D framework charge-balanced by alkali ions), their synthesis (room temperature condensation of alumina and silica resources at high pH) or their properties (moderately strong and hard, stable at least 1000 °C). As a result of the recent upsurge of interests on environmentally friendly and energy-efficient materials and processes, geopolymers, which behave as ceramic but are formed at ambient temperature, have attracted increasing attention [42].

Generally, geopolymers are amorphous three-dimensional aluminosilicate binder materials, which were first discovered by professor Glukhovsky in the former Soviet Union in the 1950s. In France, J. Davidovits also started similar studies in the 1970s and assigned geopolymer. Geopolymer binder materials can be synthetized by mixing aluminosilicate reactive materials (such as metakaolin) and strong alkaline solutions (NaOH, KOH) and then curing at room temperature. Under a strong alkaline solution, aluminosilicate reactive materials are rapidly dissolved into solution to form free SiO_4 and AlO_4 tetrahedral units. With the development of the reaction, water is gradually split out and these SiO_4 and AlO_4 tetrahedral clusters are linked alternatively to yield polymeric precursors (–SiO_4–AlO_4–) by sharing all oxygen atoms between two tetrahedral units (Fig. 7), and thereby forming amorphous geopolymer [42 – 44].

Geopolymers can be included to alkali activated cements (AAC) that refer to any system that uses an alkali activator to initiate the reaction or a series of reactions (Fig. 8) that will produce a material that possesses cementitious property. AAC, alkali activated slag (AAS) and fly ash (AAFA), and geopolymers are all considered to be alkali activated cementitious systems, however, it is expected that the structures of these materials are vastly different as result from different chemical mechanistic paths. It is commonly acknowledged that calcium silicate hydrates (CSH) is the major binding phase in PC and alkali activated slags. However, the binding property of geopolymers is generally assumed to be result of the formation of a three-dimensional amorphous aluminosilicate network.

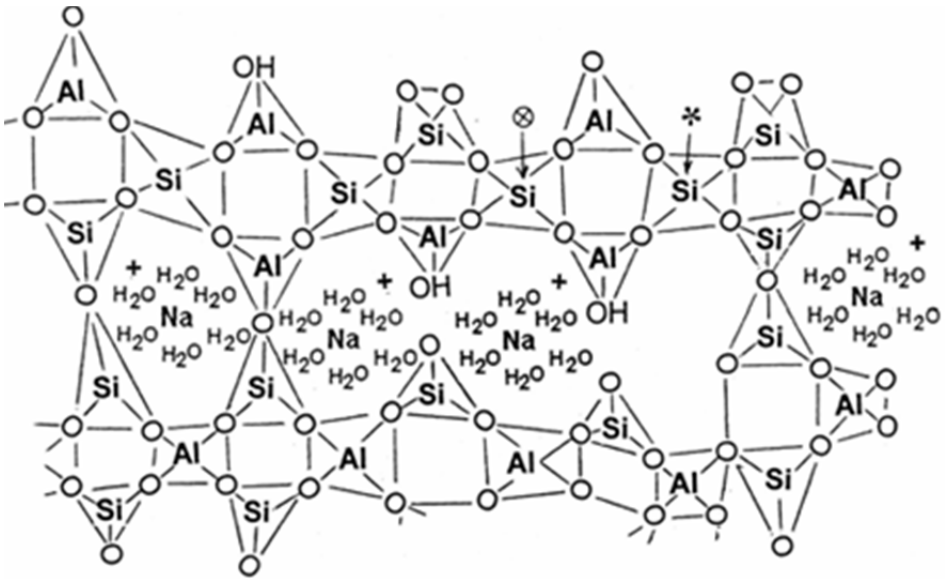

Fig. 12: *Structure of sodium geopolymer composite* [45]

In terms of chemical composition, the major difference between geopolymers and PC is in presence of calcium. It is important to note that calcium is not essential in any part of a basic geopolymeric structure. Given that CSH will be formed when soluble calcium and silicate species are present in a neutral to mild alkaline pH environment, it is thought that provided sufficient calcium is added to a geopolymeric system, a CSH based cementitious material may form instead. Thus the amorphous microstructure of alkali activated aluminosilicates containing calcium is a combination of geopolymeric and CSH based structure elements.

The most important practical property of these materials is that they are formed by condensing alumina and silica components under appropriate conditions (high pH and controlled water content) at ambient temperatures, and thus constitute a group of inorganic material with the high-temperature properties of ceramics but which, unlike the ceramics, do not require high temperature to attain their properties of durability and hardness [42].

4.7.2.2 Geopolymerization process

As stated before, the process of geopolymerization starts with the dissolution of Al and Si from Al-Si materials in alkaline solution as hydrated reaction products with NaOH or KOH, hence forming the $[M_x(AlO_2)_y(SiO_2)_z \cdot nMOH \cdot mH_2O]$ gel. Subsequently, after a short time setting proceeds, next the gel is hardening into geopolymers. Consequently, an understanding of the extent of dissolution of natural Al-Si minerals is important for study and description of geopolymerization reactions [42, 45].

4.7.2.3 Raw materials

As concerned of raw materials used for geopolymers preparation, these may be defined as compound or mixture of more components which are able to enter in reaction process with water and especially with activator. The condition concerned the negative Gibbs energy of activation process is in principle fulfilled in most events because a reaction with relatively active/aggressive electrolyte is expected. For practical purposes deciding role play kinetics of process and therefore more important is the rate of activation process.

Generally any material that contains mostly amorphous aluminosilicates is a possible source material for the manufacture of geopolymer. Several minerals and industrial by-product material have been investigated in the past, such as metakaolin, blast furnace slag (steel slag, foundry slag), fly ash, red-mud, tungsten mine mud. Typical composition of raw materials is obvious from Fig. 9, examples and their availability in Table 4 [42, 46].

$$\underset{\text{solid particle}}{\text{Al}-\text{Si}} + \text{OH}^-(\text{aq}) \Leftrightarrow \underset{\text{monomer}}{\text{Al(OH)}_4^-} + \underset{\text{monomer}}{{}^-\text{OSi(OH)}_3}$$

$${}^-\text{OSi(OH)}_3 + \text{OH}^- \Leftrightarrow {}^-\text{OSi(OH)}_2\text{O}^- + \text{H}_2\text{O}$$

$${}^-\text{OSi(OH)}_2\text{O}^- + \text{OH}^- \Leftrightarrow {}^-\text{OSi(OH)O}^- + \text{H}_2\text{O}$$

$$\text{M}^+ + \underset{\text{monomer}}{{}^-\text{OSi(OH)}_3} \Leftrightarrow \underset{\text{monomer}}{\text{MOSi(OH)}_3}$$

$$2\text{M}^+ + \underset{\text{monomer}}{{}^-\text{OSi(OH)}_2\text{O}^-} \Leftrightarrow \underset{\text{monomer}}{\text{MOSi(OH)}_2\text{OM}}$$

$$3\text{M}^+ + \underset{\text{monomer}}{{}^-\text{OSi(OH)O}^-} \Leftrightarrow \underset{\text{monomer}}{\text{MOSi(OH)OM}}$$

$$\text{M}^+ + \underset{\text{monomer}}{\text{Al(OH)}_4^-} + \text{OH}^- \Leftrightarrow \underset{\text{monomer}}{\text{MOAl(OH)}_3^-} + \text{H}_2\text{O}$$

$$\underset{\text{monomer}}{{}^-\text{OSi(OH)}_3} + \underset{\text{monomer}}{\text{MOSi(OH)}_3^-} + \text{M}^+ \Leftrightarrow \underset{\text{dimer}}{\text{MOSi(OH)}_2 - \text{O} - \text{Si(OH)}_3} + \text{MOH}$$

$$\underset{\text{monomer}}{{}^-\text{OSi(OH)}_2\text{O}^-} + \underset{\text{monomer}}{\text{MOSi(OH)}_3} + \text{M}^+ \Leftrightarrow \underset{\text{dimer}}{\text{MOSi(OH)}_2 - \text{O} - \text{Si(OH)}_2\text{O}^-} + \text{MOH}$$

$$\underset{\text{monomer}}{{}^-\text{OSi(OH)O}^-} + \underset{\text{monomer}}{\text{MOSi(OH)}_3} + \text{M}^+ \Leftrightarrow \underset{\text{dimer}}{\text{MOSi(OH)} - \text{O} - \text{Si(OH)}_2\text{O}^-} + \text{MOH}$$

Fig. 13: *Proposed mechanism of dissolution and further condensation of aluminosilicate materials* [42]

4.7.2.4 Influence of curing condition

Although low-calcium FA based geopolymer concrete can be cured in ambient conditions, heat-curing is generally recommended. Important factors that influence the properties of hardened FA based geopolymer concrete are the curing temperature and curing time. Both curing time and curing temperature influence the compressive and flexural strength. Higher curing temperature leads to the higher compressive strength. Curing temperature increase seems to affect the development of the strength more at early ages. Higher curing temperature accelerates the slag alkali-activation process, but as reaction time increases at later ages, the curing temperature increment has a negative effect and leads to decrease of final strength value. The explanation for this phenomenon is based in the formation of a large amount of reaction product at early ages in these mixes cured at higher temperature, with subsequent paste densification a microstructure modification. So, as reaction time increases, diffusion processes are more difficult to develop and the following reaction occur slowly.

4.7.2.5 Porosity of geopolymers

FA based geopolymer basic mass is of amorphous glass character, where acicular minority configurations are present only seldom. There are the rests of origin ash parts present in the geopolymer mass, where the influence of gradual dissolution is obvious on. At those geopolymers, the relatively high porosity was found out (up 50 %) without any regards to character of preparing conditions.

There are closed ball-shaped pores here, which were made by dissolving the origin fly ash parts, resp. bringing the air at preparing. The influence of preparing conditions, it means Na_2O content, resp. proportion SiO_2/Na_2O, is displayed on the approached geopolymers strength but also on pore size distribution. The geopolymer porosity is also influenced by the value of the water-to-fly ash ratio. Lower porosity is at the geopolymers prepared from mixture of fly ash and slag, where the total porosity was 2 – 10 %.

High pressure mercury porosimetry, however, gives only limited information on the character of the pores in range of nanometers. Other information is possible to get from measurement with the BET where distribution of the pore sizes of geopolymer prepared at different conditions is seen at Fig. 14 B. This picture shows that geopolymers have relatively similar character in nanometer scale which is not dependent on preparing conditions [45].

Table 4: *Potential raw materials*

Type	Origin	Approximate availability
Blast-furnace slag	Steel industry Pig iron production	Very high
Steel slag	Steel industry Steel production	High
Foundry slag	Foundry	Medium
Fluid-bed fly ash	Energetics Fluid-bed coal combustion	Very high
High-temperature fly ash	Energetics High-temp. coal combustion	Very high
Metakaolin	Artificial mineral Calcined kaolin	Low
Red mud	Alumina industry Bayer process	Medium
Mine wastes	Natural mineral and grounds	Very high

Note: Approximate availability:

- low (up to 50 000 t/year/Europe)
- medium (50 000 – 1 000 000 t/year/Europe)
- high (1 000 000 – 50 000 000 t/year/Europe)
- very high (over 50 000 000 t/year/Europe) [42]

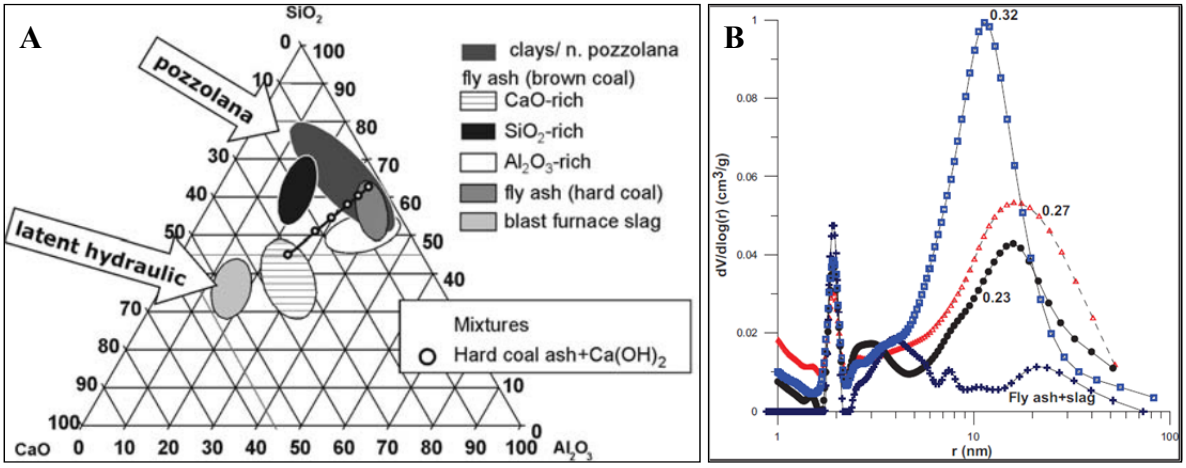

Fig. 14: *Usable raw materials and their position in the CaO-SiO_2-Al_2O_3 ternary diagram compared to the generated mixtures (A)* [47] *and pore size distribution of FA based geopolymer determined with BET (B)* [45]

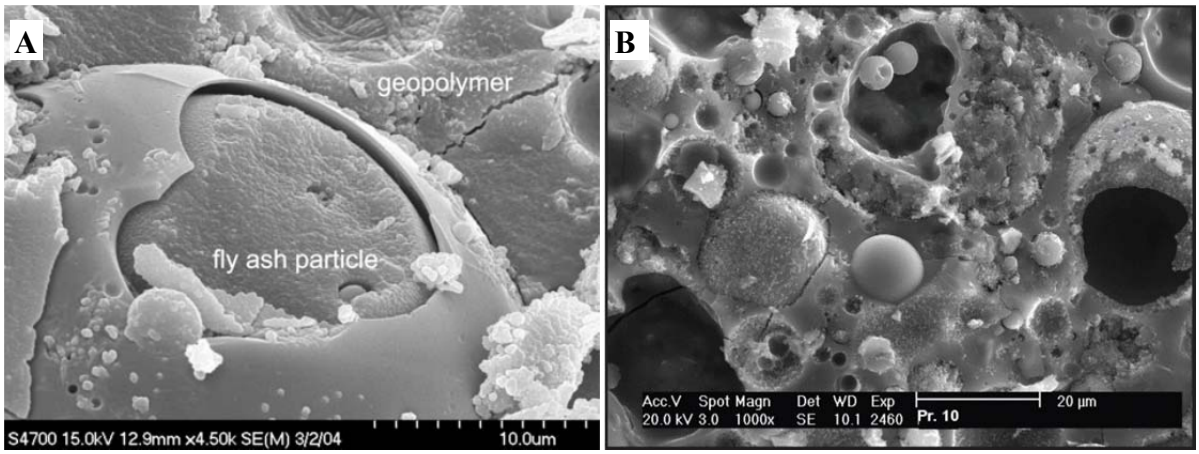

Fig. 15: *Microstructure of FA based geopolymer (A* [48]*) and porous nature of geopolymeric material (B* [45]*) (SEM)*

5 EXPERIMENTAL PART

5.1 Materials and chemicals

Materials and chemicals as follow were used in the experimental part of this thesis:

1. PC CEM I 52.5 N, CEM I 52.5 R;
2. AC Sekar 71;
3. Metakaolin Mefisto L05 and K05;
4. Silicon carbide (Table 6);
5. Grinded porcelain, grinded glass;
6. Standard sand fine – ČSN 1;
7. Finely ground quartz – FGQ;
8. Polypropylene fibers Kuralon;
9. Water glass Na (WG Na) – sodium silicate;
10. Sodium hydroxide.

5.1.1 Binder

As binding systems PC, AC and Metakaolin (MK) Mefisto L05 and K05 were used for the preparation of samples tested. To be specific PC CEM I 52.5 N and CEM I 52.5 R from manufacturer Českomoravský cement, a.s. (HEIDELBERG Cement Group) and AC Secar 71.

Table 5: *Chemical composition of cements* [49 – 51]

Content [%]	CEM I 52.5 N	CEM I 52.5 R	Secar 71
CaO	65	64	≤ 31
SiO_2	20	21	≤ 0.8
Al_2O_3	4	4	≥ 68.5
Fe_2O_3	3	4	≤ 0.4
MgO	1	1	< 0.5
SO_3	2.9	2.7	< 0.3
S^{II-}	0.05	0.03	-
Cl^-	0.056	0.053	-
K_2O	0.75	0.75	< 0.5
Na_2O	0.16	0.18	
TiO_2	-	-	< 0.4
insoluble residue	0.7	0.6	-
loss by ignition	2.9	1.7	-

5.1.2 Granular materials – aggregates and reinforcement

As main aggregates the green (highest purity) silicon carbide (Carborundum Electrite a.s., Benátky nad Jizerou) was used because it is commercially available with defined particle size distribution which enables to influence porosity and pore size of materials prepared. It typically contains 99 % or greater SiC. It is generally used in grinding wheels for particular grinding properties (9.3 on Mohs hardness scale) [52].

Some waste materials were used as well. The first secondary material was waste glass (broken bottles) which was disintegrated on laboratory grinder (Fig. 16 A) and then milled on planetary mill (Fig. 16 B) and the same was done with excluded laboratory porcelain. After grinding and milling, the sieving was done to divide particles into defined particle sizes

(Fig. 16 C). There was also used, in some mixtures, finely ground (micronized) quartz as microfiller.

The polypropylene (PP) fibers Kuralon A-8 of 6 mm length and fineness 2.0 dtex was used as reinforcement of prepared porous materials to enhance mechanical properties.

Table 6: *Particle sizes of individual SiC classes*

SiC	F40	F60	F100	F150	F220
***d* [µm]**	500 ~ 425	300 ~ 250	150 ~ 125	106 ~ 75	75 ~ 33

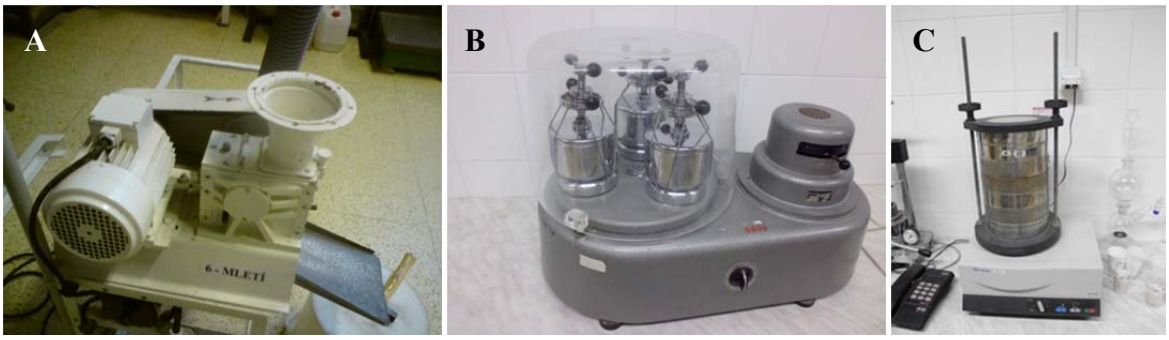

Fig. 16: *Laboratory jaw crusher (A), planetary ball mill (B) and sieving vibration analyzer AS 200 digit (C)*

5.2 Composition of mortars

To get approximate idea about specimens' composition in the whole subsequent text, without persistent peeping into table of composition, the specimen labeling nomenclature has been established. The samples are marked in the form of Binder-Aggregates-Percent of binder, all using defined abbreviations. For example, notation L05-220-24 describes a mortar which consists of metakaolin Mefisto L05/sodium silicate binder, SiC F220 and the content of binder is 24 % or PC-150-32 means Portland cement, SiC F150 with binder content of 32 %. If there is e.g. 60/40, it means there was used mixture of SiC F40 and F60 in weight ratio 1:1. If there is mark ALL, it means there were used all types of SiC in ratio 1:1. Generally, the ratio 1:1 is in all mortars with the mixture of different aggregates use.

Table 7: *Composition of mortars based on geopolymer binder (MK L05 activated by WG Na) – testing of individual SiC particle-size fractions*

Sample	**L05-220-24**	**L05-150-26**	**L05-100-29**	**L05-60-14**
WG Na[g]	100	100	100	100
MK L05 [g]	100	100	100	100
SiC F 220 [g]	500	-	-	-
SiC F 150 [g]	-	565	-	-
SiC F 100 [g]	-	-	626	-
SiC F 60 [g]	-	-	-	1200

Specimens prepared according to Table 7 were prepared and treated in two ways. At the first way, the mortars were put into the mold and slightly compacted with spattle (marked with letter U – unrammed), secondly these mortars were put into mold and then rammed (marked with letter R) with the help of hammer to form intensely compacted columns. One

set of columns was then deposited at laboratory oven at 80 °C, the other set was left to harden at laboratory conditions.

Table 8: *Composition of geopolymer mortars based on MK K05 activated by NaOH solution and WG Na*

Sample	K05-220-28	K05-150-25	K05-100-22	K05-220/150-25	K05-220/150/100-28	K05-220/ČSN1-22	K05-150/ČSN1-20
NaOH [g]	10	10	10	10	10	10	10
Water [cm^3]	16	16	16	16	16	16	16
MK K05 [g]	44	44	44	44	44	44	44
WG Na [g]	64	64	64	64	64	64	64
FGQ [g]	170	170	170	170	170	170	170
SiC F 220 [g]	179	-	-	112	60	150	-
SiC F 150 [g]	-	227	-	112	60	-	175
SiC F 100 [g]	-	-	300	-	60	-	-
ČSN 1 [g]	-	-	-	-	-	150	175

Table 9: *Composition of mortars based on aluminate cement Sekar 71*

Sample	AC-220-53	AC-150-42	AC-100-32	AC-60/40-26	AC-ALL-36	AC-G-0.24-32	AC-G-0.12-48	AC-40-19	AC-60-31
Sekar 71 [g]	100	100	100	100	100	100	100	100	100
Water [cm^3]	40	40	40	40	40	40	40	40	40
SiC F 220 [g]	123	-	-	-	50	-	-	-	-
SiC F 150 [g]	-	195	-	-	50	-	-	-	-
SiC F 100 [g]	-	-	300	-	50	-	-	-	-
SiC F 60 [g]	-	-	-	200	50	-	-	-	315
SiC F 40 [g]	-	-	-	200	50	-	-	600	-
Glass 0.24-0.40 [g]	-	-	-	-	-	300	-	-	-
Glass 0.12-0.24 [g]	-	-	-	-	-	-	150	-	-

Table 10: *Composition of mortars based on Portland cement CEM I 52.5 N*

Sample	PC-220-53	PC-150-42	PC-100-32	PC-60/40-26	PC-ALL-36	PC-G-0.24-32	PC-G-0.12-48	PC-40-19	PC-60-31
CEM I 52.5 N [g]	100	100	100	100	100	100	100	100	100
Water [cm^3]	40	40	40	40	40	40	40	40	40
SiC F 220 [g]	123	-	-	-	50	-	-	-	-
SiC F 150 [g]	-	195	-	-	50	-	-	-	-
SiC F 100 [g]	-	-	300	-	50	-	-	-	-
SiC F 60 [g]	-	-	-	200	50	-	-	-	315
SiC F 40 [g]	-	-	-	200	50	-	-	600	-
Glass 0.24-0.40 [g]	-	-	-	-	-	300	-	-	-
Glass 0.12-0.24 [g]	-	-	-	-	-	-	150	-	-

Table 11: *Composition of mortars based on Portland cement CEM I 52.5 N reinforced with 1 g of Kuralon fibers*

Sample	PC-220-53	PC-150-42	PC-100-32	PC-60/40-26	PC-ALL-36	PC-G-0.24-32	PC-G-0.12-48
CEM I 52.5 N [g]	100	100	100	100	100	100	100
Water [cm^3]	40	40	40	40	40	40	40
SiC F 220 [g]	123	-	-	-	50	-	-
SiC F 150 [g]	-	195	-	-	50	-	-
SiC F 100 [g]	-	-	300	-	50	-	-
SiC F 60 [g]	-	-	-	200	50	-	-
SiC F 40 [g]	-	-	-	200	50	-	-
Glass 0.24-0.40 [g]	-	-	-	-	-	300	-
Glass 0.12-0.24 [g]	-	-	-	-	-	-	150
Kuralon [g]	1	1	1	1	1	1	1

Table 12: *Composition of mortars based on Portland cement CEM I 52.5 N reinforced with 2 g of Kuralon fibers*

Sample	PC-220-53	PC-150-42	PC-100-32	PC-60/40-26	PC-ALL-36
CEM I 52.5 N [g]	100	100	100	100	100
Water [cm^3]	40	40	40	40	40
SiC F 220 [g]	123	-	-	-	50
SiC F 150 [g]	-	195	-	-	50
SiC F 100 [g]	-	-	300	-	50
SiC F 60 [g]	-	-	-	200	50
SiC F 40 [g]	-	-	-	200	50
Glass 0.24-0.40 [g]	-	-	-	-	-
Glass 0.12-0.24 [g]	-	-	-	-	-
Kuralon [g]	2	2	2	2	2

Table 13: *Composition of mortars based on aluminate cement Secar 71 and milled porcelain*

Sample	AC-Por-30	AC-Por-40	AC-Por-50	AC-Por-60	AC-Por-70
Secar 71 [g]	100	100	100	100	100
Water [cm^3]	40	40	40	40	40
Porcelain [g]	327	210	140	94	60

Table 14: *Composition of mortars based on Portland cement CEM I 52.5 R and milled porcelain*

Sample	PC-Por-30	PC-Por-40	PC-Por-50	PC-Por-60	PC-Por-70
CEM I 52,5 R [g]	100	100	100	100	100
Water [cm^3]	40	40	40	40	40
Porcelain [g]	327	210	140	94	60

5.3 Preparation of testing samples

5.3.1 Samples for mechanical properties testing

Columns with proportions of 100 × 20 × 20 mm were used for mechanical testing. The mixtures were prepared by mechanical mixing in laboratory mixer.

In the case of geopolymer binder, sodium silicate and metakaolin was mixed for 10 minutes and to this mixture the aggregates were added and homogenized for next 5 minutes. The proportion of aggregates was added in amount to form optimal consistence (almost dry mixture where grains of aggregates are coated by the binder).

The mortars where FGQ was used as micro-filler were prepared in this way: NaOH solution was mixed with MK K05 for 15 minutes, then sodium water glass was added and mixed for next 15 minutes, finally the FGQ and appropriate amount of aggregates and mixed 10 more minutes. The resulting mortars were filled into steal molds which were stored at temperature of 80 °C for two hours in laboratory oven (accelerated concrete setting – ACS) and after

cooling to ambient temperature were remitted to mechanical testing. Some of the geopolymer mortars were let to setting at ambient conditions (normal concrete setting – NCS).

In the case of hydraulic binder usage, water and cement were mixed for a minute, the aggregates were added, then homogenized for 3 minutes and casted in steel molds. To ensure appropriate densification of the samples, the casting occurred with the aid of vibrations or, in the case of very high aggregates content, by manual ramming with the help of hammer. Molds were enclosed in polyethylene bag (to avoid humidity outflow) for 24 hours and then demolded. After demolding the samples were cured at laboratory temperature and pressure in plastic bath with higher moisture level (Fig. 19 A). The mechanical properties were measured after 24 hours, 7 and 28 days from fabrication.

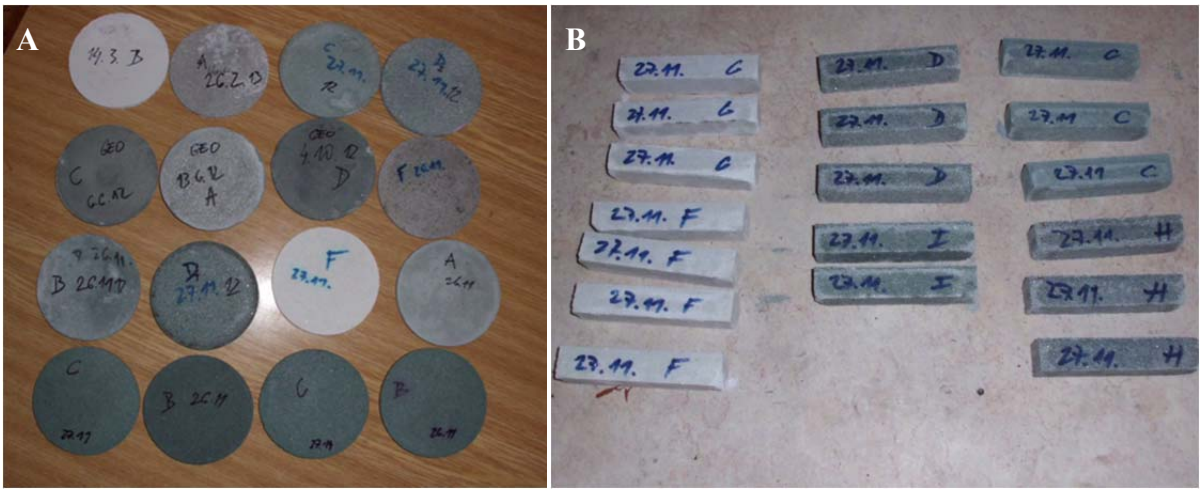

Fig. 17: *Samples for filtration testing – disks with 90 mm in diameter (A) and specimens for testing of mechanical strength – columns 20 × 20 × 100 mm (B)*

5.3.2 Samples for filtration testing

The mixing procedure was carried out in the same way as described in chapter 4.2.1 but some of the mixtures were prepared by homogenizing with planetary vacuum mixer Thinky (Fig. 17 B). The mixtures were then pressed in a mold to form a disk. Two types of disks were prepared varying in diameters (40 mm and 90 mm). The 90 mm disks (Fig. 17 A) were used for filtration and permeation measurements, the disks of 40 mm in diameter were used as samples for pycnometric determination of density and porosity as well as its assessment by mercury porosimetry.

5.4 Testing methods

5.4.1 Mechanical strength testing

Testing of compressive and flexural strength was performed involving instrument DESTTEST 4310 COMPACT A designed by company Beton System (Fig. 20 A). It is complex equipment for mechanical testing of building materials and elements which consist of several components (presses, breakers, box with hydraulic aggregate and computer with control panel). For purposes of this work, press BS-300 was used for compressive strength measurements and breaker BS-10 for flexural strengths measurements. Compressive strength can be calculated according to relation:

$$f_c = \frac{F}{a \cdot b} \tag{32}$$

Fig. 18: *Laboratory mechanical mixer (A) and vacuum mixer Thinky (B)*

Fig. 19: *Water bath for storage of samples (A) and laboratory press (B)*

where F is force acting perpendicularly to the surface area $a \cdot b$ (a – length of the support edge whereon the testing columns are placed, b – column width) which equals to 800 mm^2. For flexural strength can be written following relation:

$$f_b = \frac{3}{2} \cdot \frac{F \cdot l}{a \cdot h^2} \tag{33}$$

where F is force acting perpendicularly to the column (freely supported beam arrangement), l is distance between supports, a is column length, h is its height.

5.4.2 Laser granulometry

Grain size measurement was performed on laser analyzer Sympatec HELOS KR (Fig. 20 B). HELOS, the well proven laser diffraction sensor is the first system using one measuring principle (laser diffraction in the parallel laser beam) for the whole measuring range from 0.1 µm to 8750 µm. Two evaluation modes are offered:

1. FREE – a parameter free solution basing on Fraunhofer diffraction,
2. MIEE – basing on precision Mie theory extended to the full size range, as an option.

The combination of measuring ranges is available for both, allowing the analysis of extremely wide size distributions at highest precision.

It is classical instrument for particle size analysis of dry and wet samples, i.e. powders, suspensions, emulsions or sprays. It is entirely built to the specifications of ISO 13320 "Particle size analysis – laser diffraction methods" – and designed for absolute precision measurements to typically ± 1 % deviation with respect to the standard metre.

High resolution and guaranteed reproducibility, combined with high speed data acquisition, network interface and the standardized WINDOX software supporting all Sympatecs instruments, result in superior solutions.

The HELOS analysis system with its modular configuration and in combination with appropriate dispersing units adapts in an ideal way to the products to be analyzed [53].

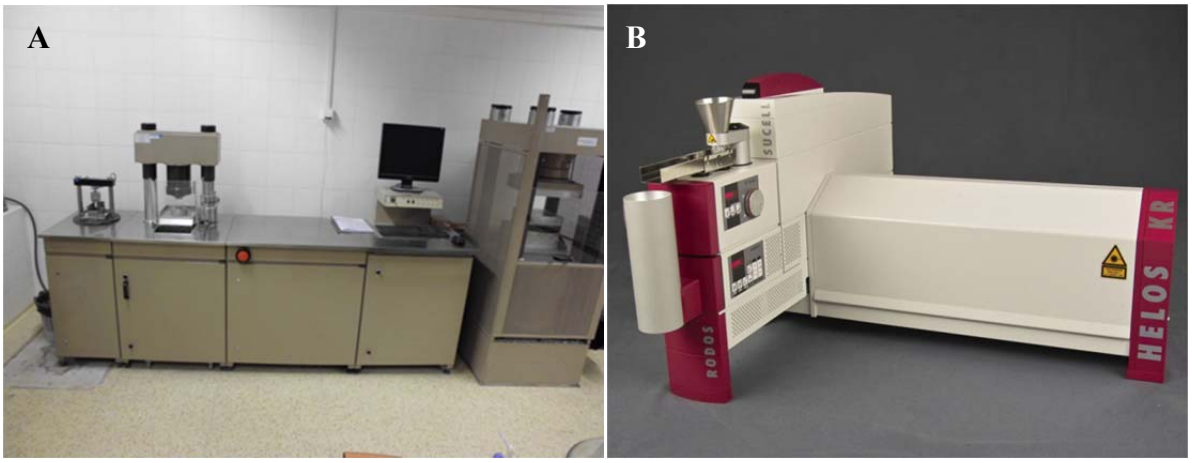

Fig. 20: *Device DESTTEST 4310 COMPACT A for mechanical properties measurements (A) and laser analyzer Sympatec HELOS KR (B)*

5.4.3 Mercury intrusion porosimetry (MIP)

Porosity measurement was carried out on Micromertitics Poresizer 9310.MIP is based on the capillary law governing liquid penetration into small pores. This law, in the case of non-wetting liquid like mercury, is expressed by the Washburn equation [54]:

$$d_{\mathrm{p}} = \frac{4\gamma \cos\varphi}{p} \tag{34}$$

where d_{p}, p, γ and φ are pore diameter, the applied pressure, the surface tension of mercury and contact angle between the mercury and the sample, respectively. The volume of mercury V penetrating the pores is measured directly as a function of applied pressure p. This p-V information serves as a unique characterization of pore structure.

The Washburn equation assumes that all pores are cylindrical. Although pores are rarely cylindrical in reality, this equation provides a practical representation of pore distribution yielding very useful results for most applications.

As pressure increases during an analysis, pore size is calculated for each pressure point, and the corresponding volume of mercury required to fill these pores is measured. These measurements taken over a range of pressures give the pore volume versus pore size distribution for the sample material.

To perform an analysis, the sample is loaded into a penetrometer, which consists of a sample cup connected to a metal-clad, precision-bore, glass capillary stem. The penetrometer is sealed and placed in a low pressure port, where the sample is evacuated to remove air and moisture – the user controls the speed of the evacuation, and there's no need for a separate preparation unit. The penetrometer's cup and capillary stem are then automatically backfilled with mercury. Excess mercury is automatically drained back into the internal reservoir; only a small amount remains in the penetrometer [55].

5.4.4 Optical (OM) and scanning electron microscopy (SEM)

Optical (also called light) microscopy is the oldest and simplest method for direct observation of microworld. Generally, it allows studying of objects and structures with magnification ranging up to 1000×. It uses visible light and system of lenses built into microscope for observing. Particular image of the objects depends on the technique used, most recently supported by digitizing and computer equipment. It is possible to observe dry samples or objects in solution, pursuable are observations at lowered or increased temperature [56].

The scanning electron microscope uses a focused beam of high-energy electrons to generate a variety of signals at the surface of solid specimens. The signals that derive from electron-sample interactions reveal information about the sample including external morphology (texture), chemical composition, and crystalline structure and orientation of making up the sample. In most applications, data are collected over a selected area of the sample surface, and a 2-dimensional image is generated that displays spatial variations in these properties. Areas ranging from approximately 1 cm to 5 μm in width can be imaged in a scanning mode using conventional SEM techniques (magnification ranging from 20× to approximately 30000×, spatial resolution of 50 to 100 nm). The SEM is also capable of performing analyses of selected point location on the sample [57].

The prepared samples of porous materials were observed on OM Zeiss Stemi 2000-C and SEM Zeiss EVO LS 10. For SEM, the samples had to be adjusted because of a non-conductive structure by depositing of Au thin layer on specimen's surface.

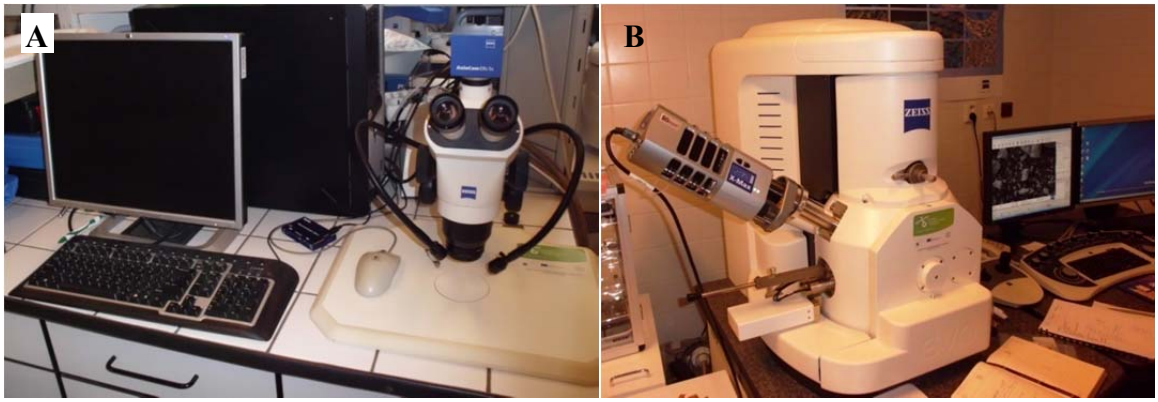

Fig. 21: *Optical microscope Zeiss Stemi 2000-C (A) and scanning electron microscope Zeiss EVO LS 10 (B)*

5.4.5 X-Ray diffraction (XRD)

X-ray powder diffraction is a rapid analytical technique primarily used for phase identification of a crystalline material and can provide information on unit cell dimensions.

The analyzed material is finely ground, homogenized, and average bulk composition is determined.

XRD is based on constructive interference of monochromatic X-rays and a crystalline sample. These X-rays are generated by a cathode ray tube, filtered to produce monochromatic radiation, collimated to concentrate, and directed toward the sample. The interaction of the incident rays with the sample produces constructive interference (and a diffracted ray) when conditions satisfy Bragg's law:

$$n\lambda = 2d\sin\theta \tag{35}$$

where n (an integer) is the order of reflection, λ is the wavelength of the incident X-rays, d is the inter-planar spacing of the crystal and θ is the angle of incidence.

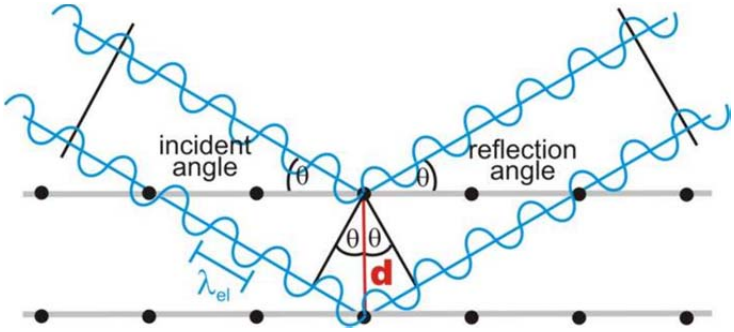

Fig. 22: *Constructive interference of reflected waves (maxima are superimposed)*

This law relates the wavelength of electromagnetic radiation to the diffraction angle and the lattice spacing in a crystalline sample. These diffracted X-rays are then detected, processed and counted. By scanning the sample through a range of 2θ angles, all possible diffraction directions of the lattice should be attained due to random orientation of the powdered material. Conversion of the diffraction peaks to d-spacings allows identification of the mineral because each mineral has a set of unique d-spacings. Typically, this is achieved by comparison of d-spacings with the standard reference patterns [58].

The XRD analyses of input materials were accomplished by means of X-ray diffraction spectrometer PANalytical Empyrean.

5.4.6 Capillarity testing

Capillary attraction is the ability of a narrow tube to draw a liquid upwards against the gravity force. This phenomenon is induced by capillary forces. The height h, which the liquid rises to, is directly proportional to surface tension γ and contact angle φ between porous material and the liquid, and inversely proportional to radius of pores r_p and liquid density ρ_l which relation as follows describes:

$$h = \frac{2\gamma\cos\varphi}{r_p g \rho_l} \tag{36}$$

In case of wettable (hydrophilic) material, the value $\cos\varphi$ approximate to one. After substitution of values for water at standard conditions (ρ_l = 998.2 kg·m^{-3} and $\gamma = 7.275\cdot10^{-2}$ N·m^{-1}) in the Eq. 36, the relationship can be simplified to:

$$h \cong \frac{1.49 \cdot 10^{-5}}{r_c} \tag{37}$$

The height h to which water can rise thus depends indirectly on tube (capillary) radius r_c – the lower the radius, the greater height water can reach in the material [59].

Fig. 23: *XRD spectrometer PANanalytical Empyrean*

After the liquid attain equilibrium height, it stops rising through the porous material because applied capillary pressure is in balance with hydrostatic pressure of the liquid column in the capillary. The dependence of height of rising liquid on time, so called capillary action curve, is parabolic:

$$h^2 = D_g t \tag{38}$$

where t is time and parameter D_g is diffusion coefficient of water in the porous material [15].

For determination of capillarity set of samples in form of columns with proportions 100 × 20 × 20 mm prepared of various mortars was used. The samples were weighed. In a suitable dish, the specimens were put onto glass rods and the dish was filled with water to reach bottom edge of the columns (Fig. 24). At the same time, the time measurement was initiated. The height of water raised in the material of specimens was measured in three-minute intervals and one set of the specimens was also weighed during the measurement. The measurement was ended after 30 minutes.

5.4.7 Determination of permeability by air flux

The permeability of prepared filtration barriers in the form of disks with 90 mm in diameter (chapter 4.3.2) were tested in the manner as described in [11]. In the air jet of compressor, with volume of 0.001 m^3, connected to filtration apparatus, the overpressure (Δp_0) in range of 120 kPa (compared to atmospheric pressure) was set up. The beginning of the experiment was defined by turning on the tap to chamber with the barrier and the time of the instantaneous overpressure (Δp) was measured until it was in equilibrium with atmospheric pressure. The results of measurement were displayed in the form of linear dependence:

$$\ln\left(\frac{\Delta p}{\Delta p_0}\right) = -\beta t \tag{39}$$

Effective permeability K_{eff} [mol·m^{-1}·s^{-1}·Pa^{-1}] of the barriers was determined using angular coefficient β [s^{-1}] of the linear dependence mentioned above, according to relation:

$$K_{\text{eff}} = \frac{\beta h_{\text{b}} V_{\text{a}}}{ART} \tag{40}$$

where V_{a} is volume of air jet, R = 8.314 J·mol^{-1}·K^{-1} and T is ambient temperature [K].

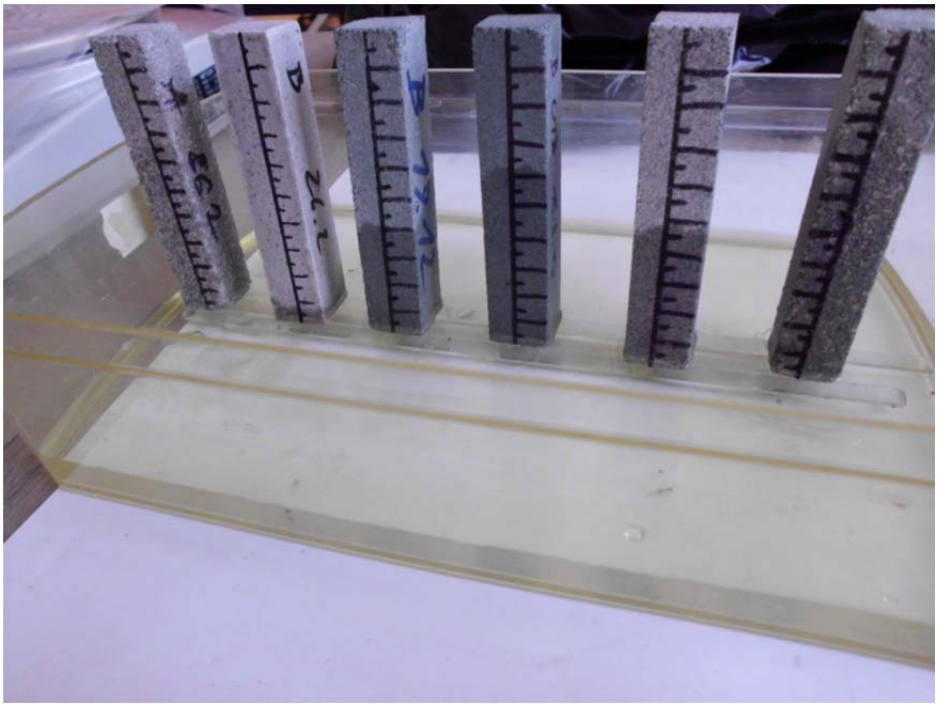

Fig. 24: *Capillarity measurement*

5.4.8 Pycnometric measurements

5.4.8.1 Determination of bulk density

The sample was dried at 105 °C to the constant weight and let to cooling in desiccator. The sample was then weighed with an accuracy of 1 mg (m_1), put into a pycnometer, filled up with distilled water and reweighed (m_2). Finally, the weight of water-filled pycnometer was evaluated. Bulk density is calculated using relation:

$$\rho_{\text{b}} = \frac{m_1}{m_3 - (m_2 - m_1)} \rho_{H_2O} \tag{41}$$

5.4.8.2 Determination of absorptive capacity (absorbability)

The samples used for determination of bulk density were subsequently put into 50 cm^3 beakers and these were filled with water to make the samples completely immersed. The beakers with the samples were put on hot plate and water was boiled for an hour. After saturation of samples by boiling water, their surfaces were wiped off the water droplets and weighed again (m_4). The absorbability is determined by relation:

$$A_C = \frac{m_4 - m_1}{m_1} 100 \tag{42}$$

Fig. 25: *Chamber with the filtration barrier (A) and panorama of the filtration station (B)*

5.4.8.3 Determination of specific weight

The saturated samples from previous measurement were put into pycnometer, filled up with distilled water and weighed. Now the procedure is analogous with bulk density determination. As the open pores are fulfilled with water after saturation (4.4.8.2), the specific weight ρ_{sw} is obtained according to Eq. 41.

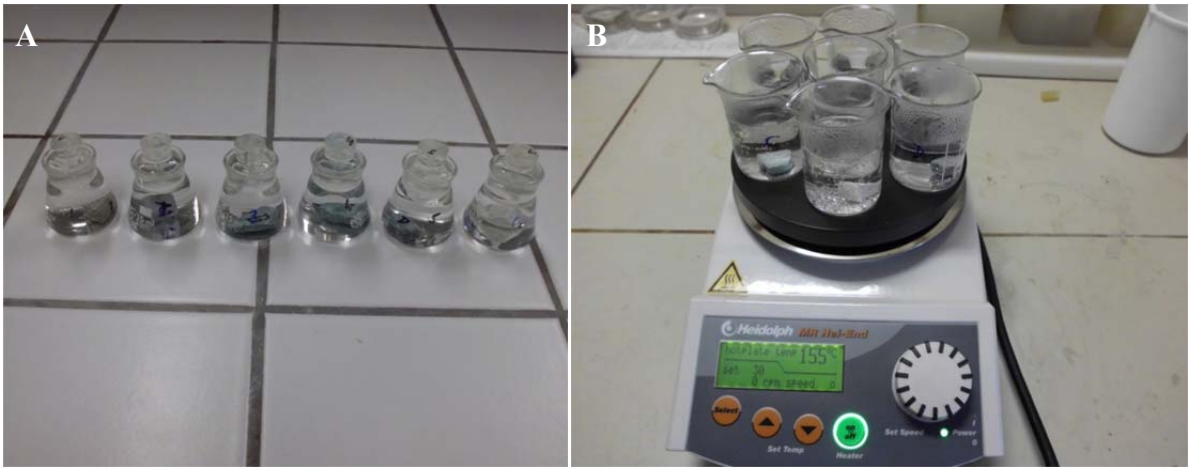

Fig. 26: *Set of pycnometers with samples inside (A) and boiling of samples to saturate pores with water (B)*

Except of values determined by methods mentioned above, from the relationships as follow were calculated apparent porosity (ε_a) and true porosity (ε_t) [15]:

$$\varepsilon_a = \rho_b A_C \tag{43}$$

$$\varepsilon_t = \left(1 - \frac{\rho_b}{\rho_{sw}}\right) 100 \tag{44}$$

5.4.9 Filtration testing

The filtration experiments were performed with the accessories as shown in Fig. 25. Water or suspension was poured into chamber and the pressure air tap turned on. The time and volume of filtrate flowed through the barrier were measured. The data measured were portrayed as linear dependence:

$$\left(\frac{A}{V_{\mathrm{f}}}\right)t = f\left(\frac{V_{\mathrm{f}}}{A}\right) \tag{45}$$

The constants of filtration equation were determined of the measured data using two different ways of calculation. The first one was calculation using particular values of filtrate volume at certain time and substituted in Eq. 27. The second one solution was carried by means of regression analysis using the regression equation of the dependence as Eq. 45 describes.

The next experiment was based on measuring of time taken for flow through the free column and column with the barrier. From this measurement were determined flow velocity in free column and then velocity in the channels of the barriers using values of porosities from pycnometric measurement according to Eq. 11.

6 RESULTS AND DISCUSSION

6.1 Resulting strengths of prepared mortars

Table 15: *Strengths of mortars based on geopolymer binder (MK L05 activated by sodium water glass), monitoring of influence of compacting and heat treatment*

Treatment	***NCS***		***ACS***	
Sample	f_b **[MPa]**	f_c **[MPa]**	f_b **[MPa]**	f_c **[MPa]**
L05-220-24U	3.82	11.66	5.78	9.55
L05-220-24R	4.84	16.94	6.22	22.02
L05-150-26U	4.73	17.42	6.99	16.18
L05-150-26R	6.37	20.96	11.65	29.81
L05-100-29U	2.96	13.38	4.17	16.45
L05-100-29R	2.92	15.93	4.80	22.56
L05-60-14U	1.52	3.20	3.18	2.25
L05-60-14R	3.50	8.55	4.60	8.85

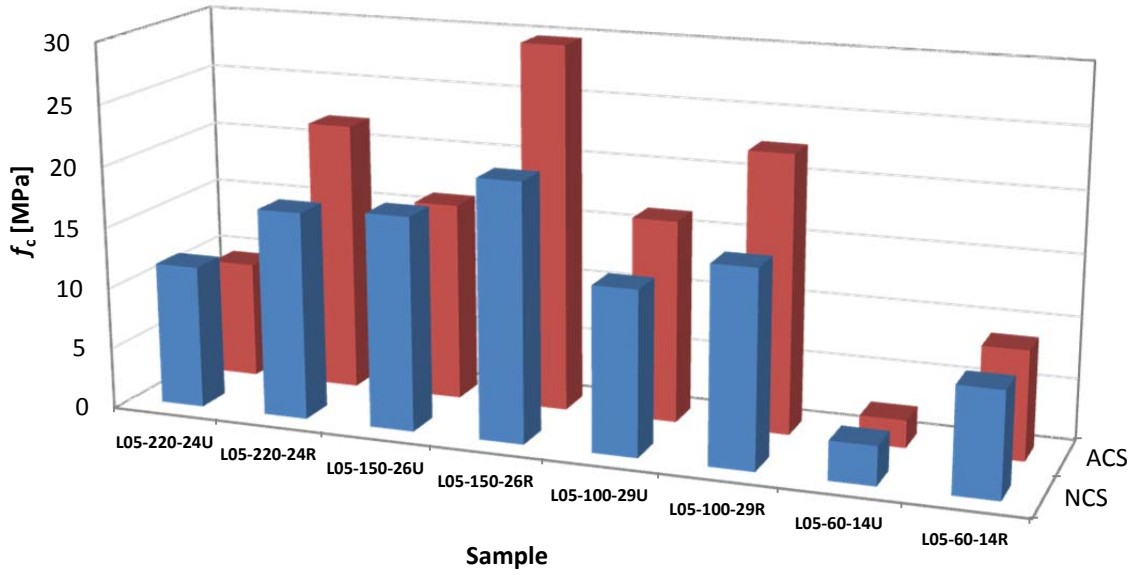

Fig. 27: *Development of compressive strengths of geopolymer mortars based on MK L05 activated with sodium water glass*

The first mortars, consisting of metakaolin Mefisto L05 activated by sodium water glass and individual fractions of SiC, were first steps made for this thesis. The specimens noted with letters R and U (rammed and unrammed) were distinguished as they have been processed in different manner. The unrammed samples were compacted in a mold slightly using a spattle to create more porous structure and to find its strength for comparison with those of higher compaction. It is obvious that with slighter ramming the more porous structure will be obtained but it leads to the strength deterioration at the same time. So to create a material which will be compact and suitable for certain application, it is necessary to compress and

solidify the mixtures to preserve certain integrity of the material. But also intensively rammed mortars together with appropriate composition lead to required porous structure. Fig. 27 and 28 represent compressive and flexural strengths of mortars prepared. Results (see Table 15) show that the strengths of rammed mortar are greater which is comprehensible but these were compared with the different treatment which one of them was at higher temperature (80 °C for 2 hours – ACS) and the other at ambient conditions (NCS). From the Fig. 27, 28 is obvious that the strengths are, with some exceptions, increasing if are heat-treated. The exceptions (specimens L05-220-24U, L05-150-26U and L05-60-14U) pertain only to compressive strengths of unrammed mixtures. The first reason of that can be unequal ramming because the procedure of compaction was carried out manually because of high content of aggregates and thus impossibility to do it with help of vibration table to preserve equivalent degree of compaction. Other reasons e.g. inhomogeneity of mortars or dissimilar period of mixing are possible, too.

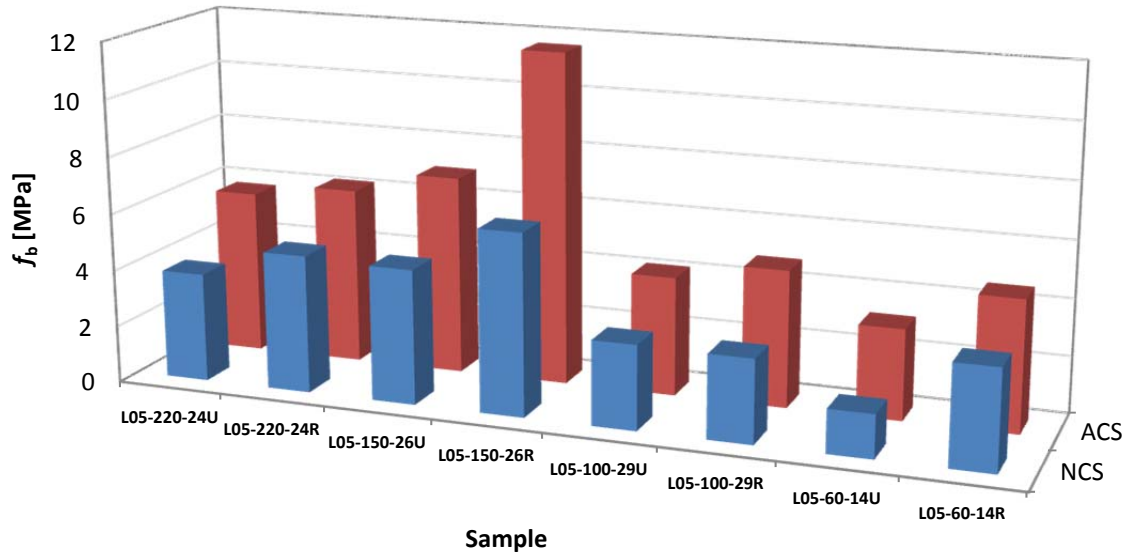

Fig. 28: *Development of flexural strengths of geopolymer mortars based on MK L05 activated with sodium water glass*

Next test was performed with pressed disks with 90 mm in diameter and it was testing of its integrity in water. The disks were immersed in water for 7 days. It was observed that only heat-treated disks remain tenacious without any loss of grains by virtue of water with exception of some samples which crumbled at the edges. This was mainly sample L05-60-14 as this sample was prepared from SiC F60 whose grains sizes (the range 250 ~ 300 μm) are too large which means lower specific surface area and necessity to add larger amount of the grains to preserve dry mixture and appropriate porous structure.

So after this first set of samples was decided to prepare only compacted specimens together with heat treatment, for better properties of those samples. Nevertheless, another problem has arisen, mainly with heat-treated specimens – shrinkage. Shrinkage does not interrupt the column specimens themselves for strength testing but it is a problem for the 90 mm disks, which are after heat treatment a bit distorted and thus ineligible for filtration

testing because when the disk is inserted to filtration chamber, it must be screwed up to provide adequate sealing and when it is screwed up too much, the disk rupture occurs.

Table 16: *Strengths of geopolymer mortars based on MK K05 activated by NaOH solution and sodium water glass*

Sample	f_b [MPa]	f_c [MPa]
K05-220/150-25	4.13	17.58
K05-220/150/100-28	4.81	17.62
K05-220-28	2.43	11.77
K05-150-25	1.96	14.44
K05-100-22	2.62	10.76
K05-220/ČSN1-22	1.80	10.01
K05-150/ČSN1-20	3.33	5.49

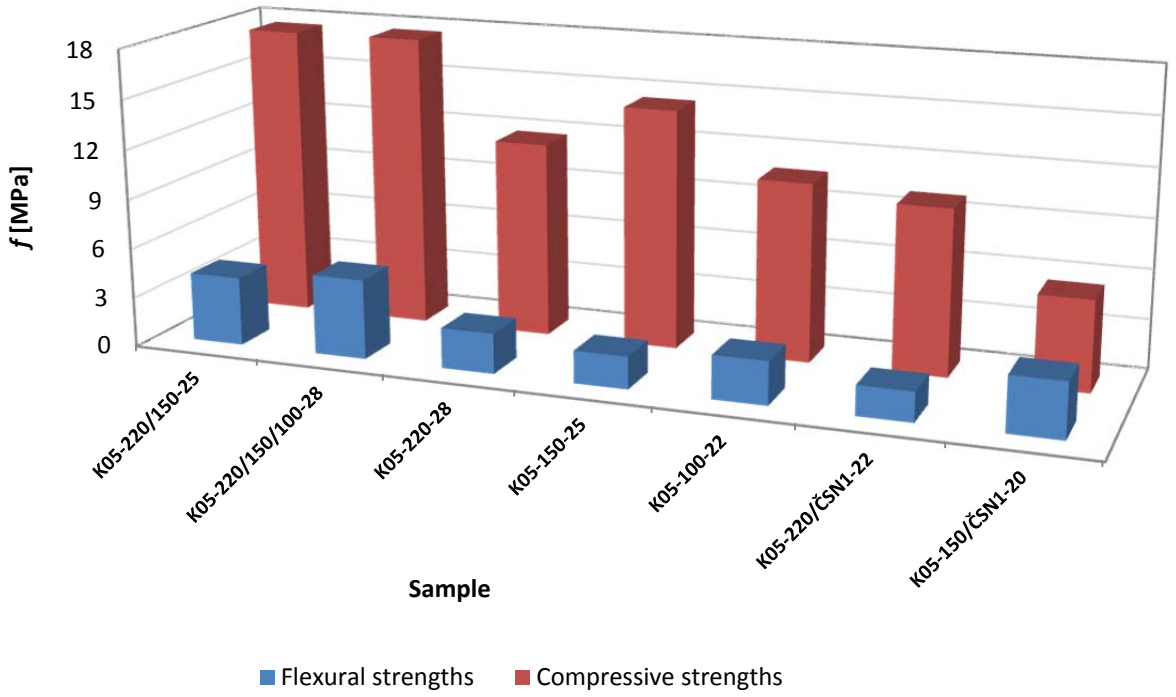

Fig. 29: *Development of flexural and compressive strengths of geopolymer mortars based on MK K05 activated with sodium water glass and NaOH solution*

The other geopolymer based mortars were prepared using metakaolin Mefisto K05 which was activated by NaOH solution and sodium water glass and as micro-filler was used finely ground quartz (for composition see Table 8, for resulting strengths see Table 16).

Compared to the previous mortars based on MK L05 and NaWG, the strengths are lower (see Fig. 29). The main problem in the mixing was large amount of FGQ added which was not appropriately homogenized and maybe therefore the strengths are lower. It can be caused by too large aggregates content which is probably larger than really needed and maybe the reason is the heat treatment which can cause formation of microcracks due to shrinkage and thus decrease the resulting strengths of the composites. However, the disks prepared of this

recipe are relatively hard and compact when immersed in water although the drying shrinkage is enormous. The aforementioned high aggregates content is probably the reason of relatively low strengths of all geopolymer mixes compared to the PC and AC mixes (see below).

Table 17: *Strengths of mortars based on aluminate cement Secar 71*

Sample	AC-220-53	AC-150-42	AC-100-32	AC-60/40-26	AC-ALL-36	AC-G-0.24-32	AC-G-0.12-48	AC-40-19	AC-60-31
f_b (24 h) [MPa]	5.29	4.04	2.96	3.89	4.81	1.76	5.68	2.53	3.47
f_c (24 h) [MPa]	38.01	22.38	19.08	24.94	43.53	9.56	31.35	16.84	16.39
f_b (7 days) [MPa]	10.50	6.76	3.84	4.94	8.92	3.34	8.36	3.29	5.72
f_c (7 days) [MPa]	61.44	40.10	21.46	32.15	56.51	14.24	55.51	22.05	30.34
f_b (28 days) [MPa]	11.39	5.73	5.12	6.26	14.52	3.45	7.90	3.88	9.65
f_c (28 days) [MPa]	99.43	45.22	21.83	31.73	80.95	16.42	55.17	16.93	26.37

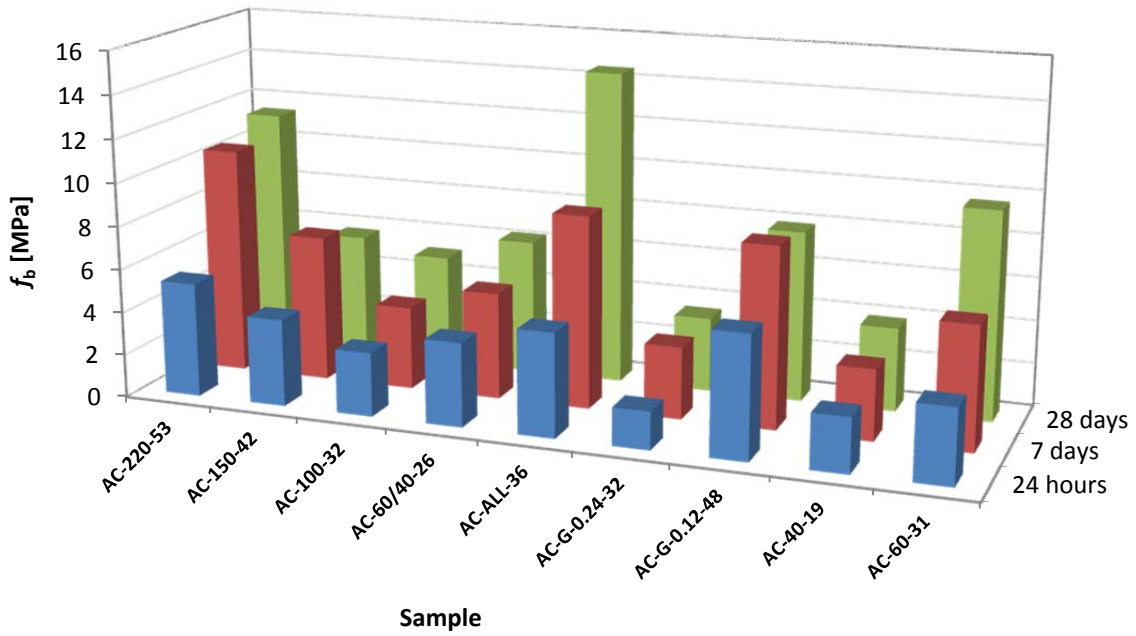

Fig. 30: *Development of flexural strengths of mortars based on aluminate cement Secar 71*

Aluminate cement Secar 71 is the other binding system used in this work. The comparison with the use of geopolymer binders cannot be realized because of different binder content. The content of geopolymer binder in the mortars mentioned above is lower than that of the mortars mixed with cement. The next difference between using of the geopolymer and cement binders is the period of mature which is, in the case of the geopolymer binder, almost immediate if the heat treatment is introduced, compared to the 28 days for "complete" hardening of AC or PC.

The resulting strengths of AC mortars are shown in Table 17, the comparison between them is demonstrated in Fig. 30 and 31. The binder content ranges from 19 to 53 %, for optimal consistence ensuring water-penetrable porous structure.

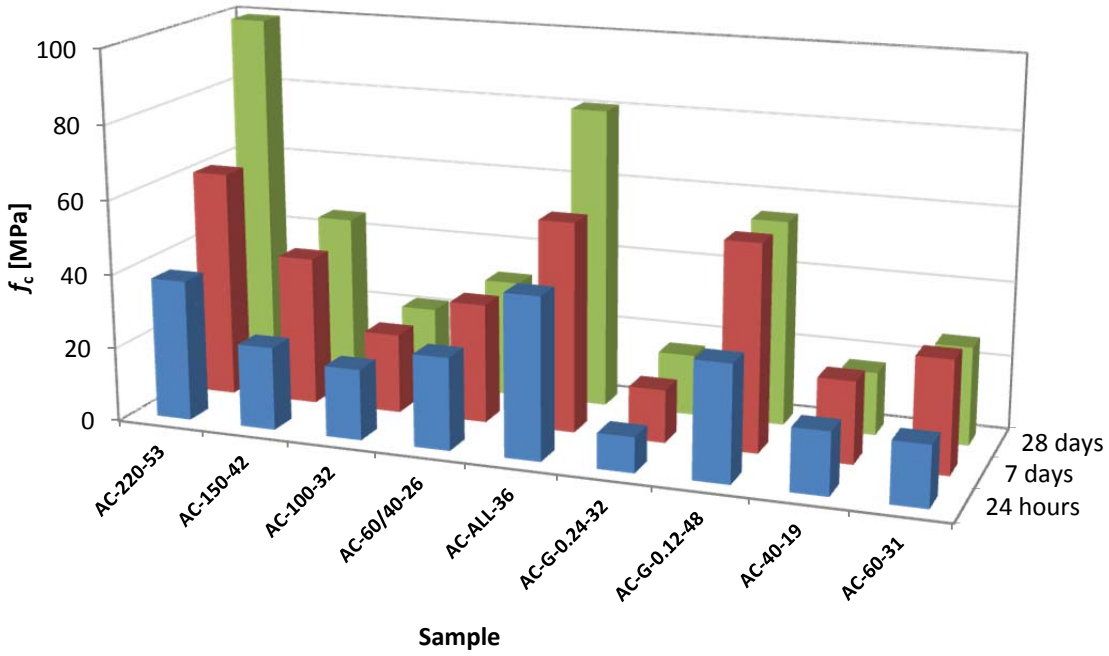

Fig. 31: *Development of compressive strengths of mortars based on aluminate cement Secar 71*

The highest value of flexural strength after 28 days is observed in the case of specimen AC-ALL-36 which consists of all fractions of SiC blended in the ratio 1:1 and 36 % of binder. The highest value of flexural strength for this sample is reasonable because of presence of various particle sizes which means that the granulometric composition can be closed to ideal grain-size curve and therefore the spaces between particles can be fulfilled with gradually diminishing particles of aggregates until the space of minimal size is occupied by a cement grain itself. So maybe that is why the high value of flexural strength. However, the grain-size pattern is mostly not perfect and never so much ideal to eliminate the pores completely. So this can be a way how to increase the flexural strengths because if there is a mortar prepared of one fraction, the spaces between the single particles are bigger and grains of cement are not enough to provide bridges sufficiently strong to retain all the material together. The truth is that, if there is an effort to substitute the particles of aggregates by cement particles, it will lead not only to the strength increase but to the higher reduction, almost elimination of the pores, at the same time, too. So to find out the suitable composition of grain sizes is necessary to make these experiments purposeful. Nevertheless, the mortars consisting of individual fractions of SiC were studied, as well and to enhance mechanical properties, the reinforcement was used (see below).

As concerns of the compressive strengths, these are on relatively high level although the sample AC-220-53 with compressive strength of 99.43 MPa is almost on the boundary between penetrable and impenetrable porous material. It is important to point out, that the

mortars are mixed with water-cement ratio 0.40 which is relatively high but necessary to ensure proper rheological properties of the mixes.

Table 18: *Strengths of mortars based on Portland cement CEM I 52.5 N*

Sample	PC-220-53	PC-150-42	PC-100-32	PC-60/40-26	PC-ALL-36	PC-G-0.24-32	PC-G-0.12-48	PC-40-19	PC-60-31
f_b (24 h) [MPa]	2.26	0.86	0.99	1.74	2.73	2.28	2.33	2.50	2.72
f_c (24 h) [MPa]	10.81	4.47	4.94	6.20	11.04	9.88	13.91	8.63	10.23
f_b (7 days) [MPa]	3.92	2.73	2.89	2.11	3.91	2.33	3.35	2.86	3.41
f_c (7 days) [MPa]	20.50	14.04	10.86	11.62	17.04	12.96	19.96	16.00	19.14
f_b (28 days) [MPa]	4.50	4.04	3.40	3.51	-	3.38	4.33	3.72	4.70
f_c (28 days) [MPa]	27.15	20.45	16.01	15.31	-	23.90	24.00	20.16	22.79

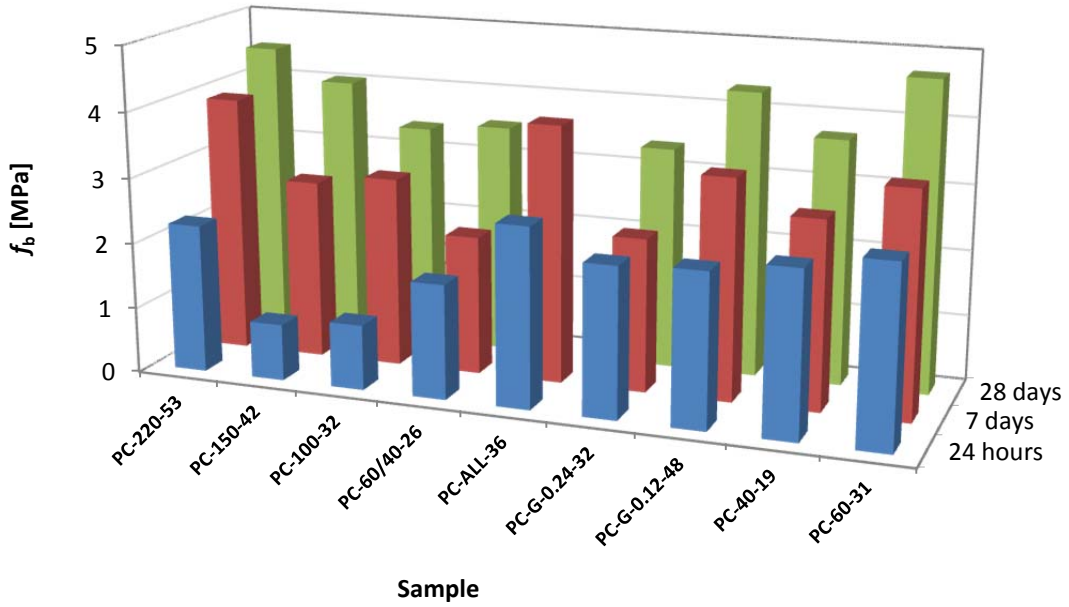

Fig. 32: *Development of flexural strengths of mortars based on Portland cement CEM I 52.5 N*

Now we get to the Portland cement which is the other binder used for grains-bonding purposes. For the used type of PC (CEM I 52.5 N) is guaranteed compressive strength of at least 52.5 MPa after 28 days (relative to cement paste). Strengths values displayed in Table 18 are of the mortars prepared of PC and these are lower than those prepared of AC, especially the flexural strengths which do not exceed even 5 MPa after 28 days. The sample PC-60-31 reaches highest value of 4.70 MPa which is paradoxical as the SiC F60 is relatively coarse wherefore the strength should be lower. But it is characteristic of the ratio between binder and aggregates. To prepare the mixtures of optimal consistence for single fraction, we can observe how the content of binder with the increasing particle size needs to be decreased. It is

characteristic because with decreasing particle size, the specific surface area increases and thus increases the reaction surface which is then more accessible to water in the mixture.

Table 19: *Strengths of mortars based on Portland cement CEM I 52.5 N reinforced with 1 g of Kuralon fibers*

Sample	PC-220-53	PC-150-42	PC-100-32	PC-60/40-26	PC-ALL-36	PC-G-0.24-32	PC-G-0.12-48
f_b (24 h) [MPa]	3.78	1.92	0.00	1.64	1.64	0.00	1.88
f_c (24 h) [MPa]	16.24	7.00	3.65	6.70	7.85	3.75	7.55
f_b (7 days) [MPa]	3.24	2.48	2.75	3.86	5.11	0.00	3.75
f_c (7 days) [MPa]	30.86	17.97	6.85	16.19	18.77	5.92	19.37
f_b (28 days) [MPa]	6.76	4.57	2.18	4.42	3.38	2.15	5.05
f_c (28 days) [MPa]	34.53	16.97	7.21	16.87	13.03	10.28	16.73

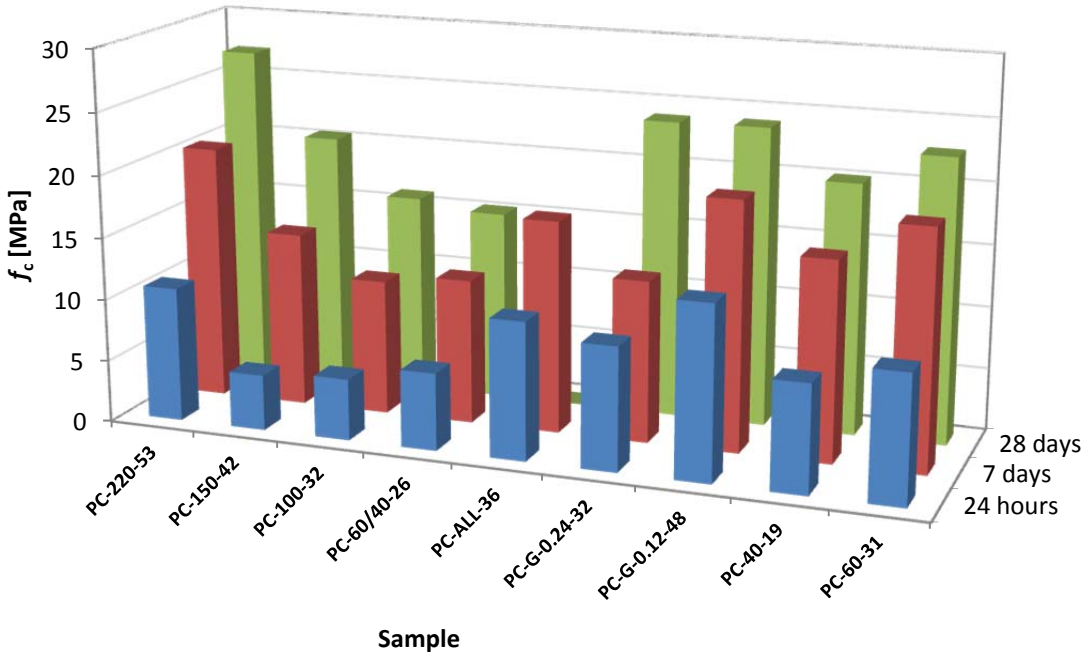

Fig. 33: *Development of compressive strengths of mortars based on Portland cement CEM I 52.5 N*

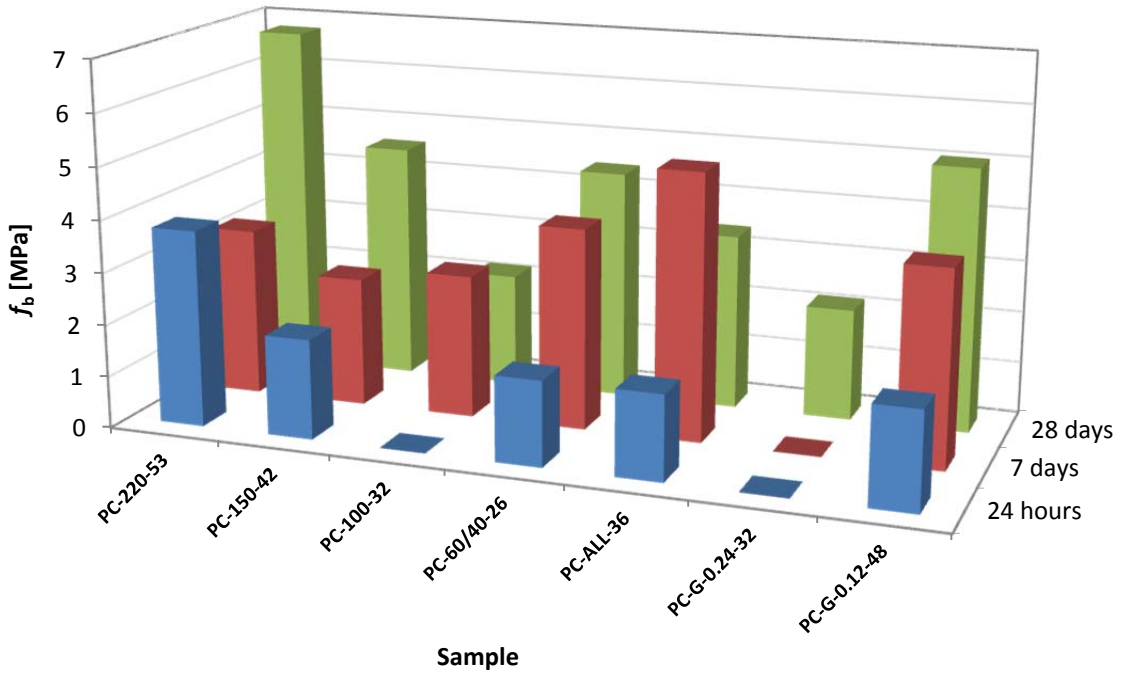

Fig. 34: *Development of flexural strengths of mortars based on Portland cement CEM I 52.5 N reinforced with 1 g of Kuralon fibers*

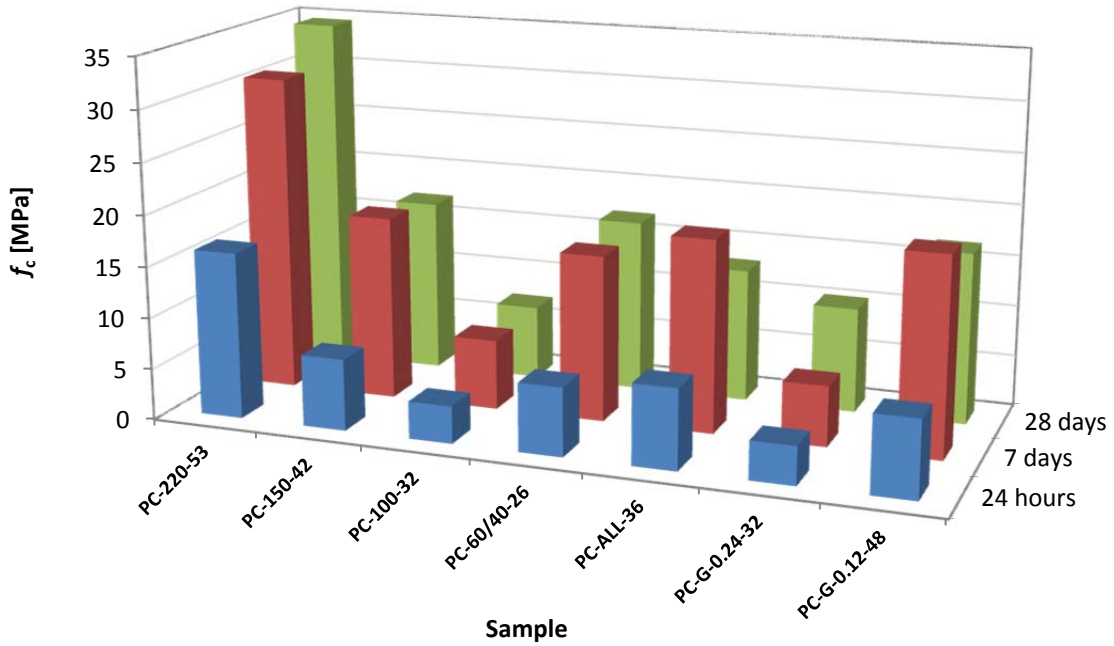

Fig. 35: *Development of compressive strengths of mortars based on Portland cement CEM I 52.5 N reinforced with 1 g of Kuralon fibers*

The water which would be used as rheological is then missing and that is cause of workability loss. That is the reason of the selected composition. So flexural strengths are generally not too high here but it would not be a problem because in the case of flat filtration units, which those of prepared for this thesis are, are mostly put on a support (e.g. perforated metal board) which is to ensure the barrier not to break. So the main purpose is to find such mixture which has sufficient integrity in the water not only stationary but also in rapid (turbulent) water flow.

Compressive strengths do not exceed 30 MPa, but for aims of filtration barriers preparation, it is satisfactory.

Next set of PC samples with the same composition as those discussed above was modified by addition of PP fibers Kuralon as the reinforcement. The fibers were added to enhance mechanical properties especially flexural strengths. The other advancement which was considered to be achieved by this fibers modification was the potential improving of sieving effect of the filtration barriers, but this theory was not verified anyway. Some of the mixes were omitted and only the particular fractions of SiC and the 1:1 blend of all the fractions were dealt with.

Table 20: *Strengths of mortars based on Portland cement CEM I 52.5 N reinforced with 2 g of Kuralon fibers*

Sample	PC-220-53	PC-150-42	PC-100-32	PC-60/40-26	PC-ALL-36
f_b (24 h) [MPa]	4.13	2.16	1.75	1.76	1.96
f_c (24 h) [MPa]	17.00	10.18	5.56	7.23	12.35
f_b (7 days) [MPa]	4.19	3.90	2.93	2.42	3.17
f_c (7 days) [MPa]	17.00	15.78	10.16	15.72	15.93
f_b (28 days) [MPa]	6.34	4.52	3.13	2.82	3.22
f_c (28 days) [MPa]	29.88	17.42	10.72	10.86	14.05

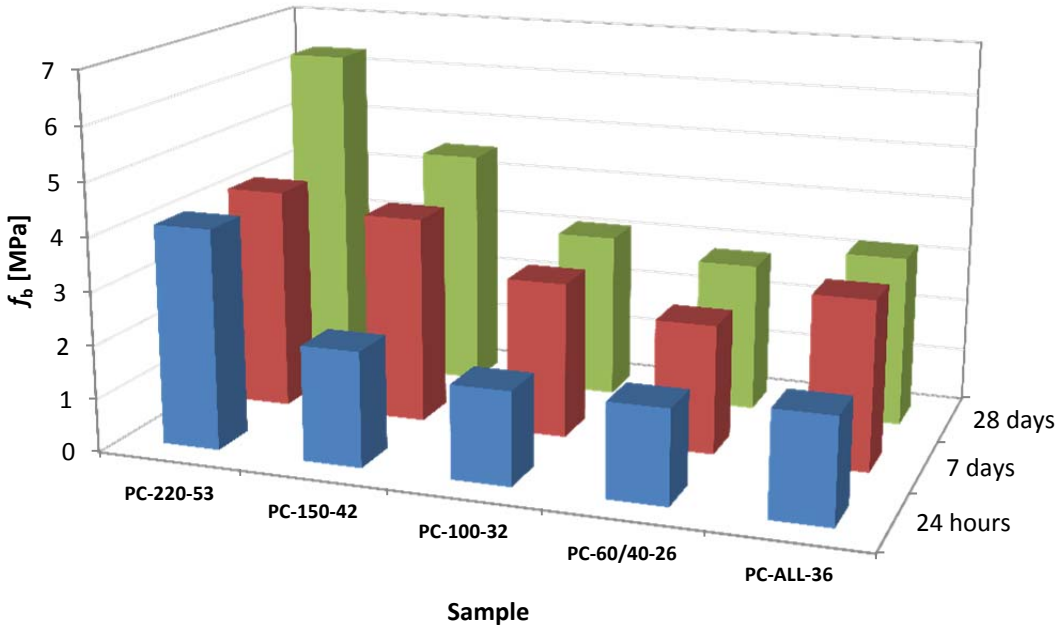

Fig. 36: *Development of flexural strengths of mortars based on Portland cement CEM I 52.5 N reinforced with 2 g of Kuralon fibers*

At first, the amount of 1 g of the Kuralon fibers was added (the fibers were added to water, then the cement was admixed and finally the aggregates were added and then homogenized). The amount of the fibers is very low by weight but the volume, which the amount occupies, is quite large, therefore the weight of the fibers added was not higher than 2 g for 40 cm^3, 100 g of cement and corresponding amount of aggregates. The main reason of adding no more fibers was worsened workability of the mortars and more difficult ramming. Thus the mechanical strengths of these mixes are not too recognizable because of the worse compaction. But if the strengths of mortars without Kuralon fibers are compared with those with it, the certain enhancement of the strength is observable. So the additional improvement by means of fiber reinforcement can advance the properties of these composites and thus to be more usable for certain applications.

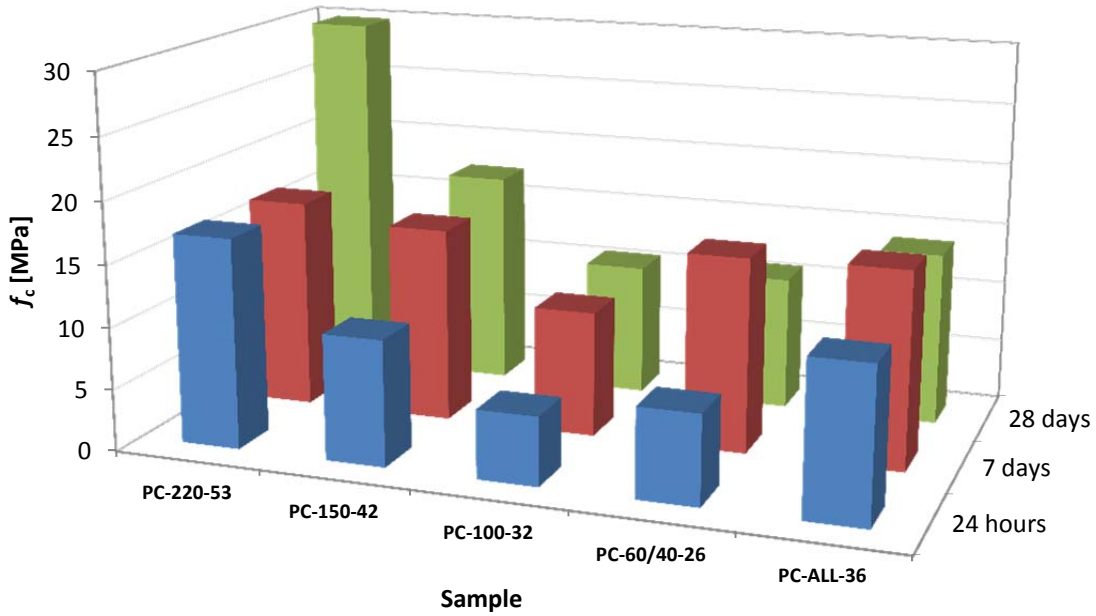

Fig. 37: *Development of compressive strengths of mortars based on Portland cement CEM I 52.5 N reinforced with 2 g of Kuralon fibers*

Finally, the last material, which was used as aggregates, was milled porcelain with fraction of particle size under 0.8 mm. This material was tested with use of PC and AC, too and the mortars were mixed with gradually increasing binder percentage from 30 to 70 %. The strengths development of PC mortars is obvious from Fig. 38 and 39, for resulting strengths see Table 21. There is a large difference between strengths with 40 and 50 % of binder. The mortar with the 40 % content of binder was almost dry and incompactable with the help of vibration table and it is possible to say that barriers pressed of this mortar would be suitable for filtration. However, the strengths are relatively small as in the case of those with the SiC with binder content of 40 % and lower. With the increase of binder percentage up to 50 %, the abrupt growth of strengths is seen and with the more increasing content of binder up to 70 % the strengths slowly descend. The distinction of strengths between specimens PC-Por-40 and PC-Por-50 is double more for flexural strengths and almost quintuple for compressive strengths.

Table 21: *Strengths of mortars based on Portland cement CEM I 52.5 R and milled porcelain*

Sample	PC-Por-30	PC-Por-40	PC-Por-50	PC-Por-60	PC-Por-70
f_b (24 h) [MPa]	1.63	4.08	10.56	7.64	6.47
f_c (24 h) [MPa]	4.32	18.27	63.72	58.38	48.98
f_b (7 days) [MPa]	1.96	5.23	12.17	11.01	7.21
f_c (7 days) [MPa]	7.51	21.63	99.49	91.98	85.74
f_b (28 days) [MPa]	2.90	6.02	12.85	12.68	11.96
f_c (28 days) [MPa]	7.71	22.14	107.06	98.14	93.76

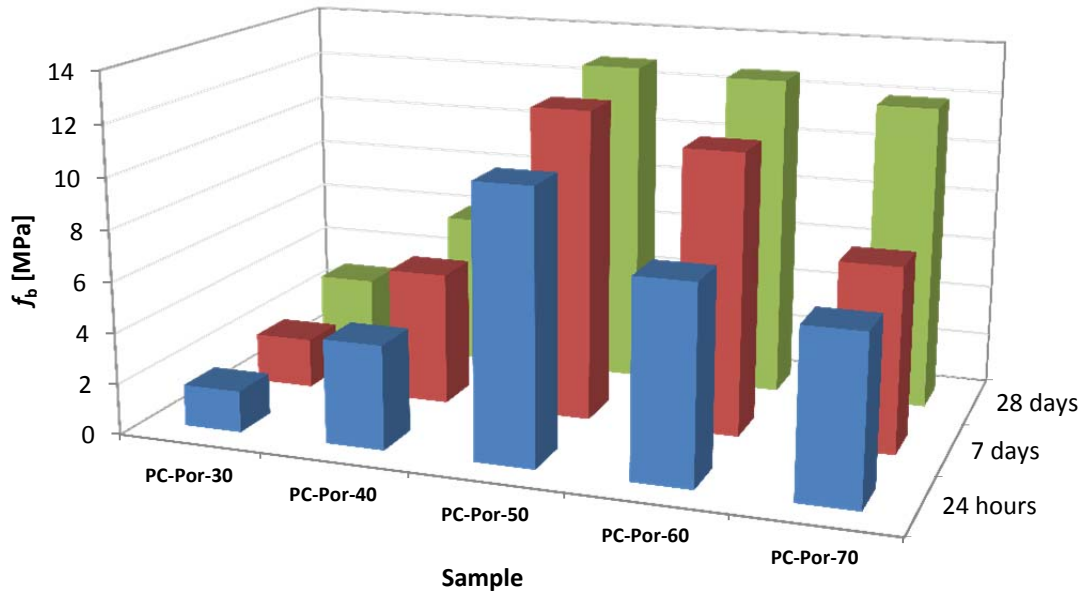

Fig. 38: *Development of flexural strengths of mortars based on Portland cement CEM I 52.5 R and milled porcelain*

So the mortar with 50 % of binder can be, in the case of milled porcelain, ideal proportion between binder and aggregates with water-cement ratio 0.40. This must be, however, considered with the regard to the grain size composition. The milled porcelain was sieved and the fraction with particle size below 0.80 mm was used without additional dividing into subfractions. So in the range under 0.80 mm is probably such distribution of particle sizes that it approximate to the optimal granulometric curve and therefore the high values of strengths.

Table 22: *Strengths of mortars based on aluminate cement Secar 71 and milled porcelain*

Sample	AC-Por-30	AC-Por-40	AC-Por-50	AC-Por-60	AC-Por-70
f_b (24 h) [MPa]	1.81	3.74	9.01	8.37	6.43
f_c (24 h) [MPa]	6.87	18.27	70.09	41.35	31.91
f_b (7 days) [MPa]	2.57	3.92	12.95	12.11	10.46
f_c (7 days) [MPa]	11.97	29.12	91.00	57.96	30.07
f_b (28 days) [MPa]	3.00	6.69	15.94	15.79	12.82
f_c (28 days) [MPa]	9.67	39.06	116.34	78.04	55.92

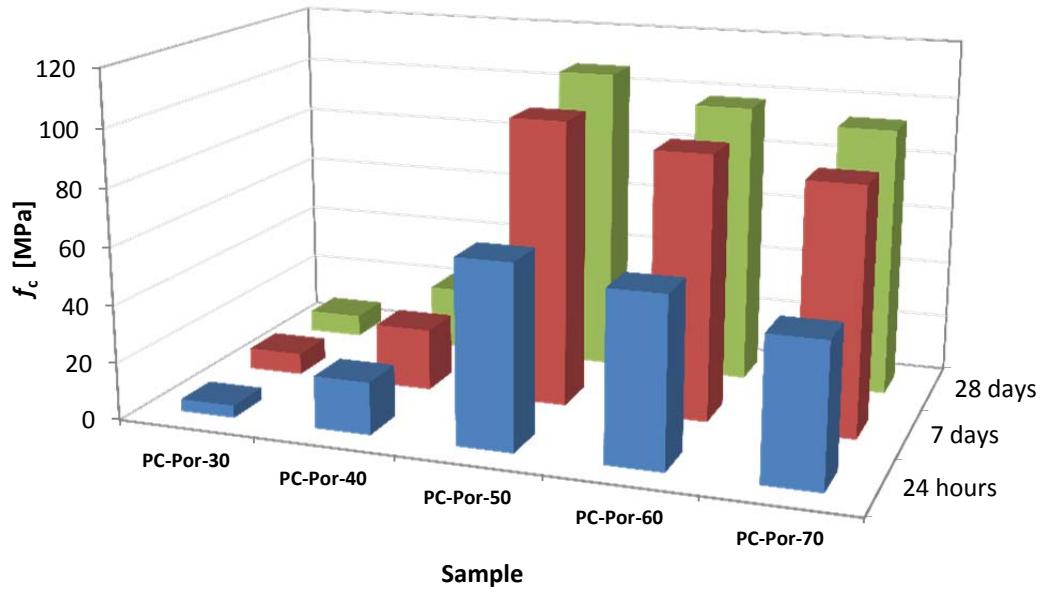

Fig. 39: *Development of compressive strengths of mortars based on Portland cement CEM I 52.5 R and milled porcelain*

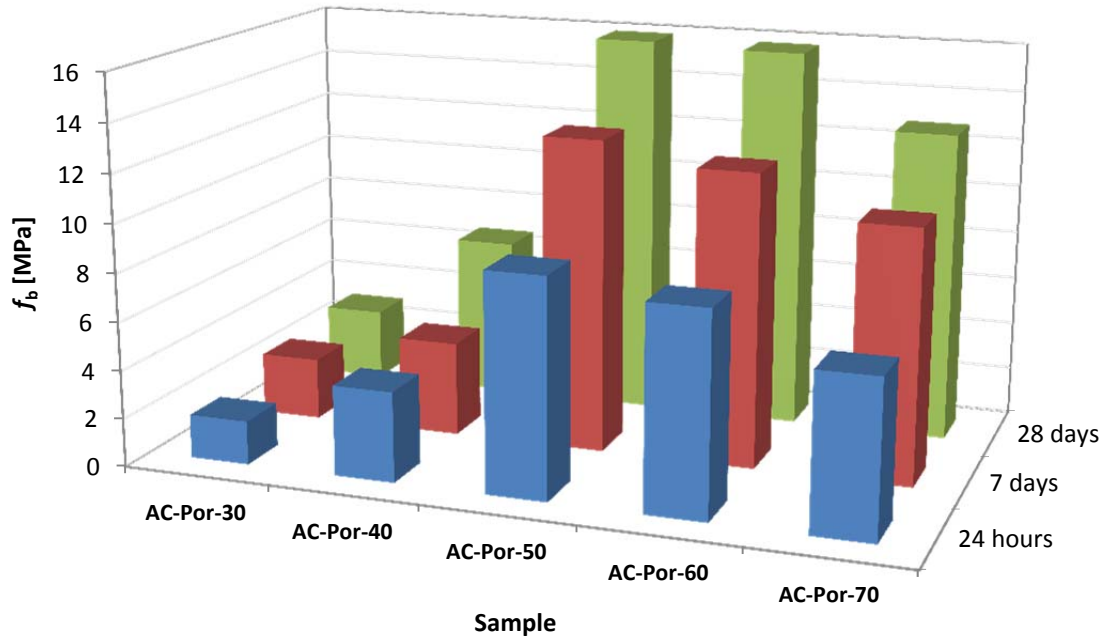

Fig. 40: *Development of flexural strengths of mortars based on aluminate cement Secar 71 and milled porcelain*

A similar trend in the strengths development is perceptible in the case of AC. The final strengths are slightly even larger in the case of 50 % binder content but the drop of the strength with content of binder over 50 % is more rapid than in the case of PC. It is important to point out that in the case of porcelain the PC CEM I 52.5 R (instead of 52.5 N used in the previous cases). The main difference between these two PC is in the initial setting rate. The PC CEM I 52.5 R has accelerated initial setting and hardening which means that the same mixture prepared on the basis of 52.5 N and 52.5 R will not have the same strength – 52.5 R

sets and hardens more quickly in the early period. AC is characterized by moderate setting followed by rapid hardening and it is probably a random that the compressive strengths of PC-Por-40 and AC-Por-40 after 24 hours are equal to each other (18.27 MPa).

For the purposes of the barriers are suitable the mortars with binder content of 40 % then the mixture are too wet and it leads to the almost quite elimination of pores. The pores are there constantly even in the case of pure cement paste but they are very small, in range of nanometers, and that is the reason of high hydraulic resistance of the barriers with increased binder content and thus impossibility of a liquid to flow through.

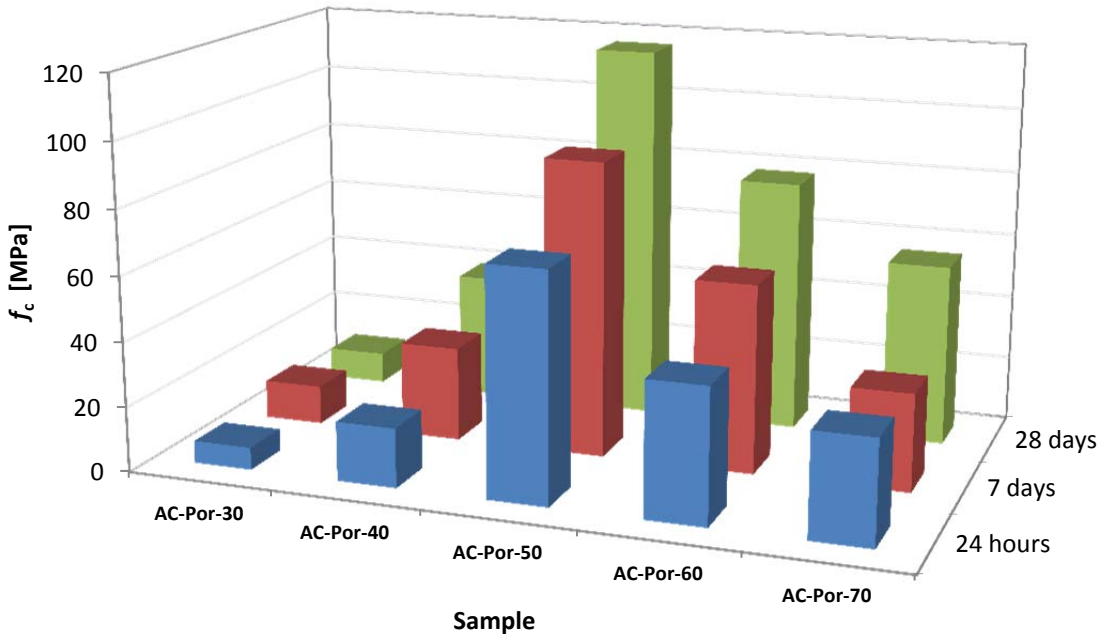

Fig. 41: *Development of compressive strengths of mortars based on aluminate cement Secar 71 and milled porcelain*

6.2 Distributions of particle sizes of input materials

In this chapter, the size of particles of the initial material is dealt with. The main effort of the work is to influence pore size distribution by particle size distribution therefore this measurement is important. Data from laser diffraction granulometry were worked into clearer charts in form of integral distribution functions which express portion of particles whose size is same or lower than selected value (so called cumulative distribution of particle size) and differential distribution functions which express portion of particles with certain size (so called density distribution of occurrence of given particle).

At Fig. 41 – 43 are shown integral distribution curves of particle sizes of used binders, SiC as aggregates and the other aggregates (porcelain, glass etc.), respectively. Fig. 44 – 46 display differential distribution curves of the same materials. In Table 23 there are summarized quantiles of the distributions ($x_{0.5}$ – median, $x_{0.9}$ and $x_{0.99}$).

Table 23: *Quantiles of normal distribution of the particle sizes*

Material	$x_{0.5}$ [µm]	$x_{0.9}$ [µm]	$x_{0.99}$ [µm]
CEM I 52,5 N	8.71	33.03	60.52
MK Mefisto L05	2.06	6.56	10.86
MK Mefisto K05	3.38	8.06	12.06
Sekar 71	4.27	13.34	19.12
F 40	540.41	738.04	1076.35
F 60	284.16	412.47	503.85
F 100	163.49	260.92	353.23
F 150	122.12	184.19	245.72
F 220	78.03	122.27	174.05
Porcelain	223.22	562.68	723.65
G 0.24-0.40	337.54	528.32	683.02
G 0.12-0.24	192.29	341.45	468.56
FGQ	30.00	91.93	180.05

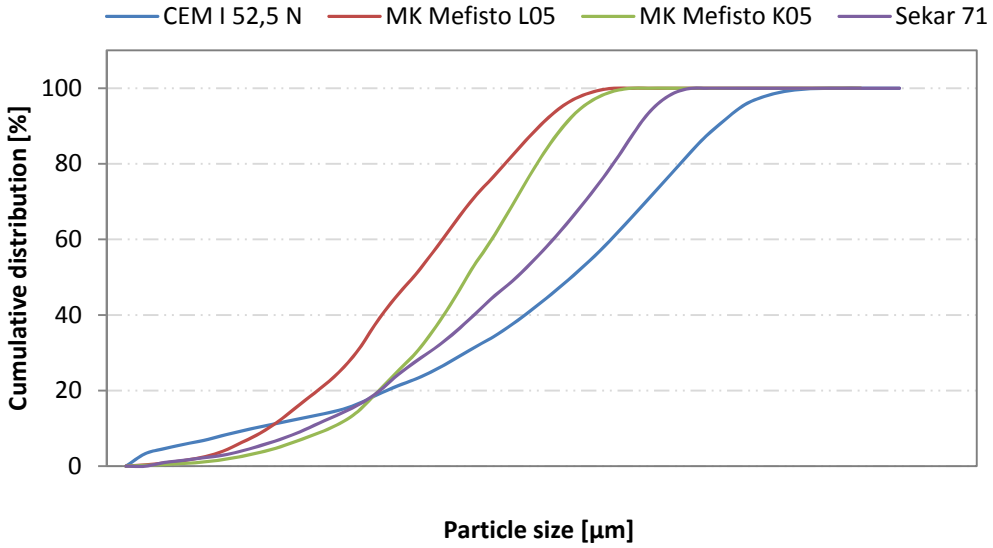

Fig. 42: *Cumulative distribution functions of used binders*

The distribution curves are arranged in groups into graphs and that is the reason of non-scaled *x*-axes because the particle sizes are wide-spread and therefore the plots could not be displayed together side by side. These plots were arranged into these forms to compare the shape of curves of individual materials. The best defined distributions can be seen at Fig. 43 and 46 which belong to SiC. This is an example of commercially available material of high quality with accurately defined distributions of particle sizes.

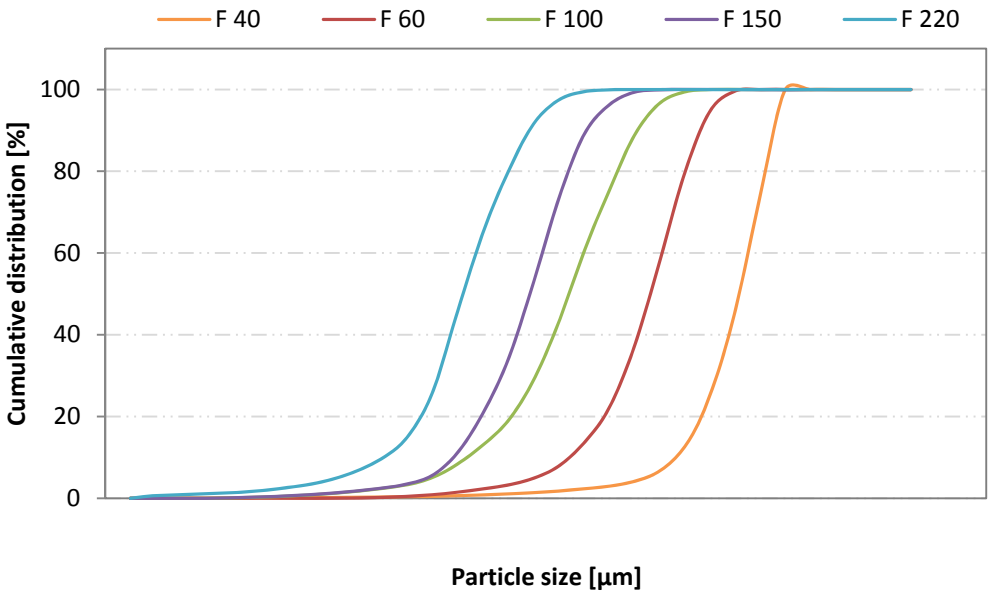

Fig. 43: *Cumulative distribution functions of individual fraction of silicon carbide*

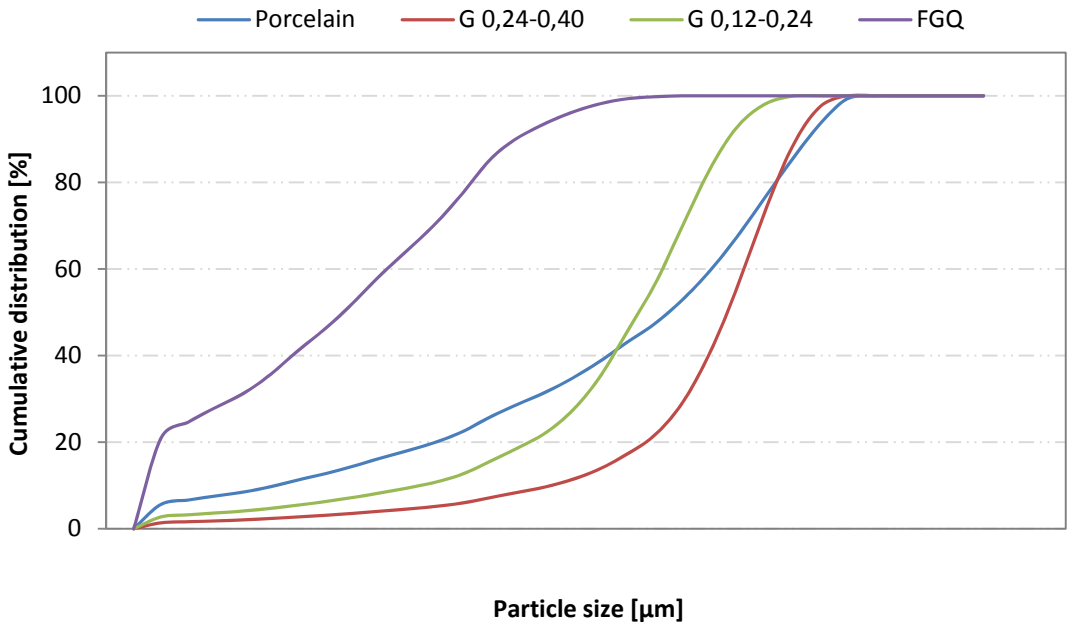

Fig. 44: *Cumulative distribution functions of secondary materials (milled porcelain and glass) and finely grounded quartz*

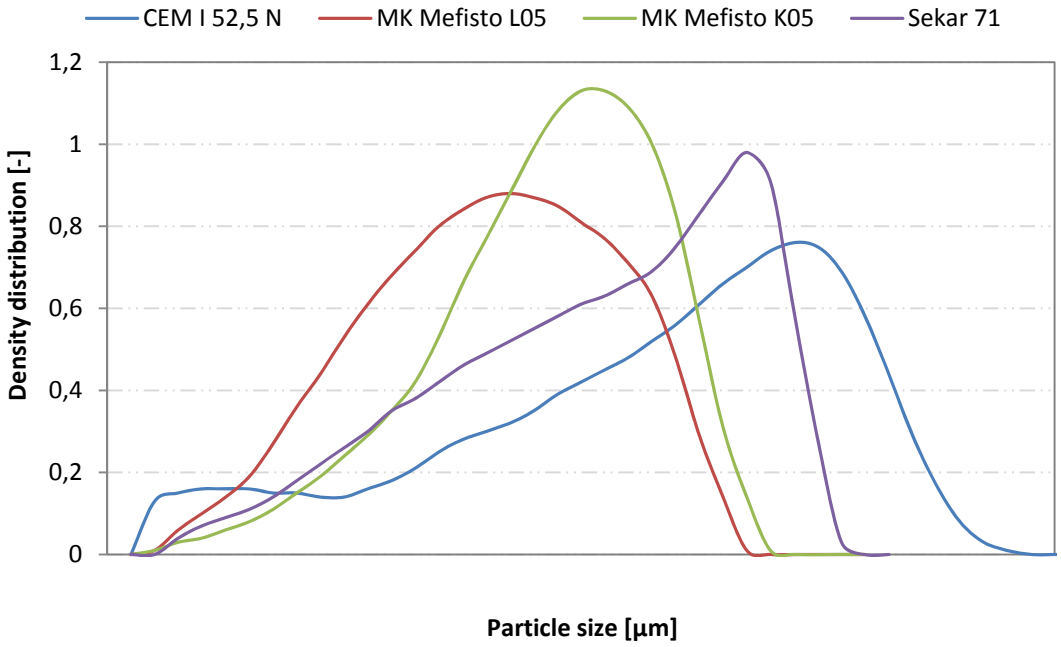

Fig. 45: *Differential distribution functions of used binders*

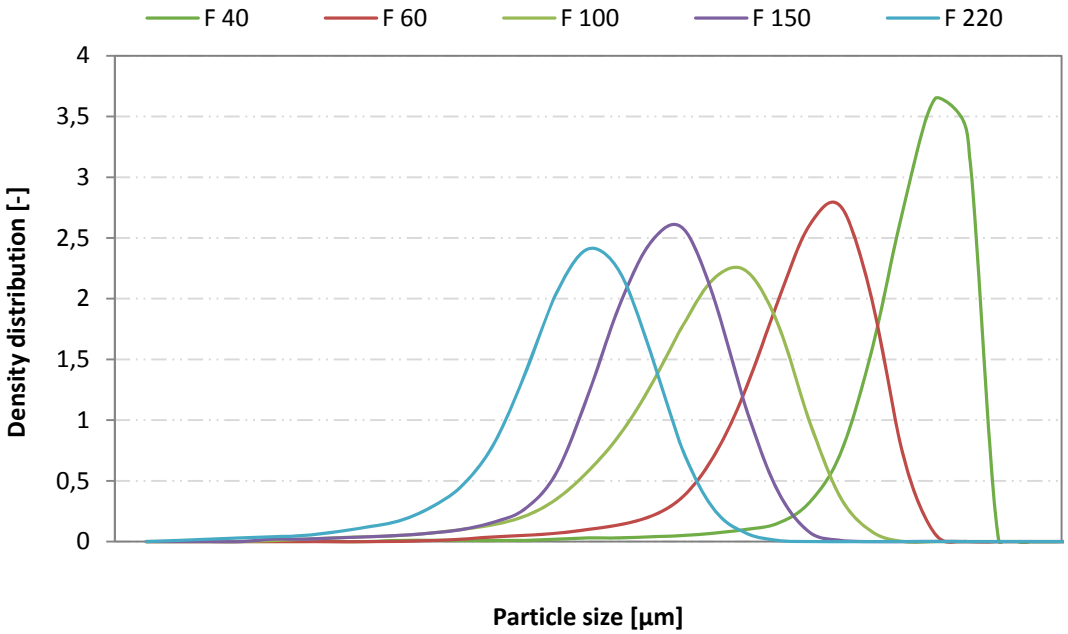

Fig. 46: *Differential distribution functions of individual fractions of silicon carbide*

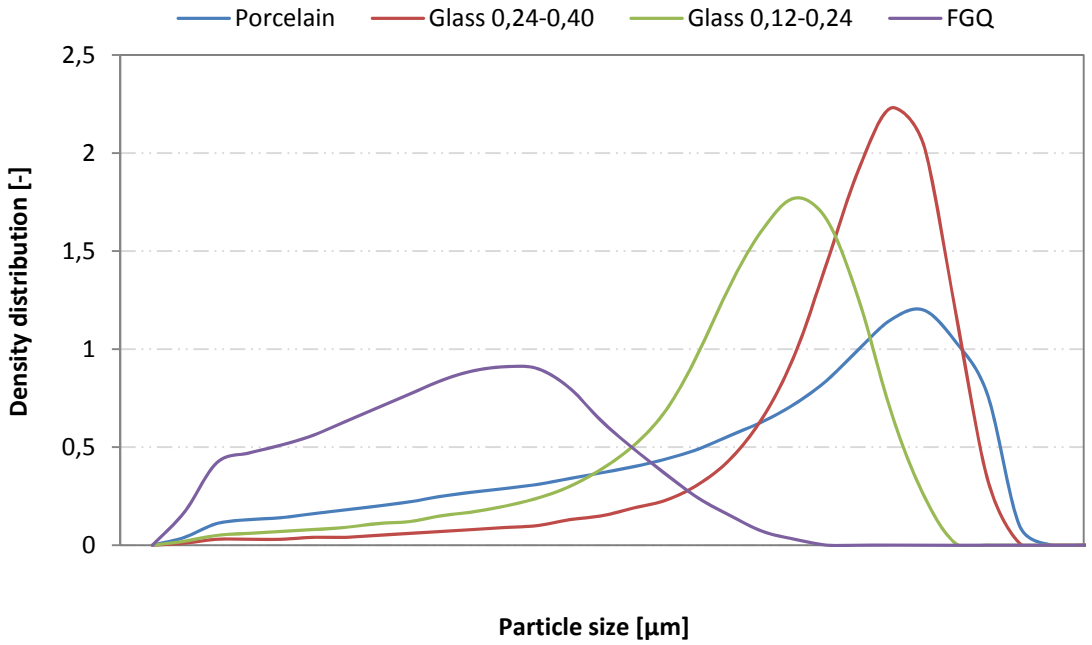

Fig. 47: *Differential distribution functions of secondary materials (milled porcelain and glass) and finely grounded quartz*

6.3 Evaluation of results from porosimetry

The porosimetry measurement was carried out to get general information about pore structure of prepared samples. This measurement was done in collaboration with Faculty of civil engineering; two samples were characterized (AC-220-53 and AC-150-42) to get some basic idea about pore structure of materials prepared in the manner as done for this thesis.

Table 24 shows some basic parameters of the pore structure of the characterized materials and some of the characteristics can be thus compared with those determined by pycnometry.

Table 24: *The structural parameters obtained by mercury intrusion porosimetry*

Sample	AC-220-53	AC-150-42
Total intrusion volume [$cm^3 \cdot g^{-1}$]	0.0710	0.0698
Total pore area [$m^2 \cdot g^{-1}$]	5.2616	4.8867
Median pore diameter (volume) [µm]	0.6181	5.8433
Median pore diameter (area) [µm]	0.0099	0.0103
Average pore diameter (4V/A) [µm]	0.0540	0.0571
Bulk density [$g \cdot cm^{-3}$]	2.1846	2.2449
Apparent (skeletal) density [$g \cdot cm^{-3}$]	2.5858	2.6618

At Fig. 48, the chart of the cumulative pore volume distribution can be seen. In the case of sample AC-220-53, we can see gradual increase of the cumulative volume which means that pore size diminishes evenly; there is no step change in the cumulative volume. Something else is observable in the case of the other sample (AC-150-42). In the range of 10 µm pore diameter, we see the cumulative volume increase from 0.01 to almost 0.04 $cm^3 \cdot g^{-1}$. So in this area, there is higher amount of pores with about10 µm in diameter. Generally, in ranges with a steep cumulative pore volume curve, more pore volume is "concentrated" than in flatter ones. [60] Next course of the curve is similar to AC-220-53 but it has less steep bias and the curves end at $d_p < 0.01$ µm.

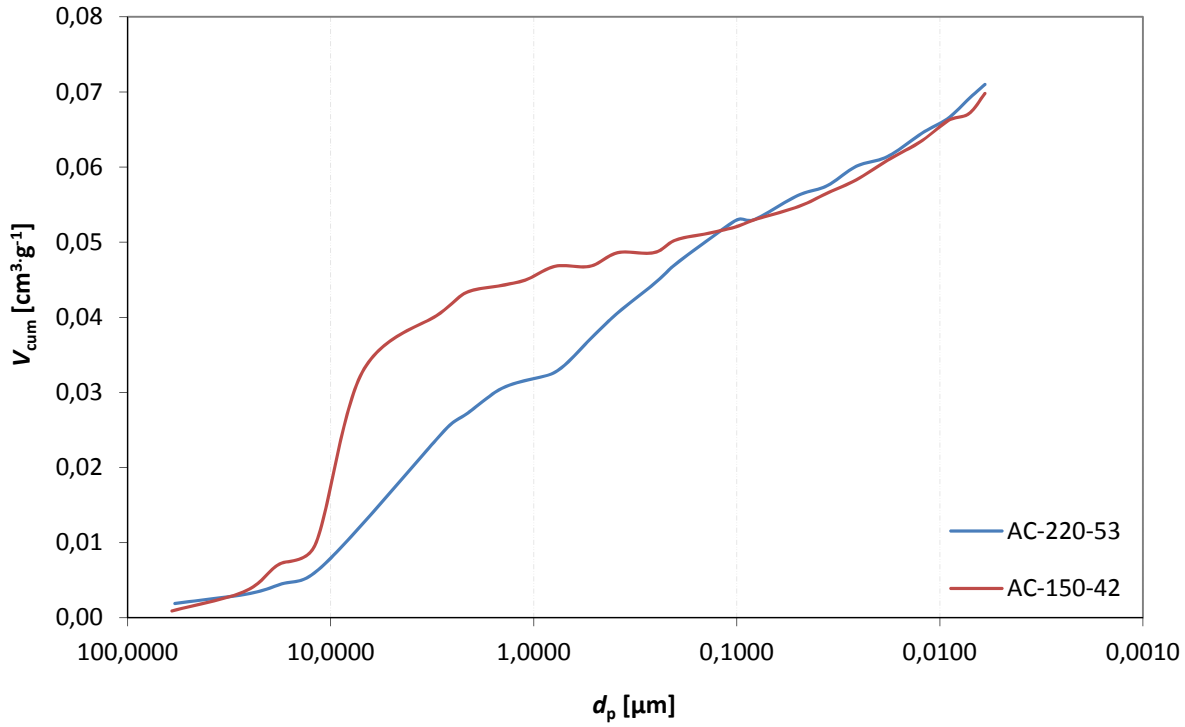

Fig. 48: *Cumulative pore volume distribution*

The curves of cumulative surface area (Fig. 49) are of typical appearance. The cumulative surface area increases towards lower pore diameters. For AC-220-53 the total pore area equals to 5.1626 $cm^2 \cdot g^{-1}$ and average pore diameter is 0.0540 µm whereas for the other sample the values, in the aforesaid order, are 4.8867 $cm^2 \cdot g^{-1}$ and 0.0571 µm. So with the pore decrement the total pore area aggrandizement is observable although it is very low in this case.

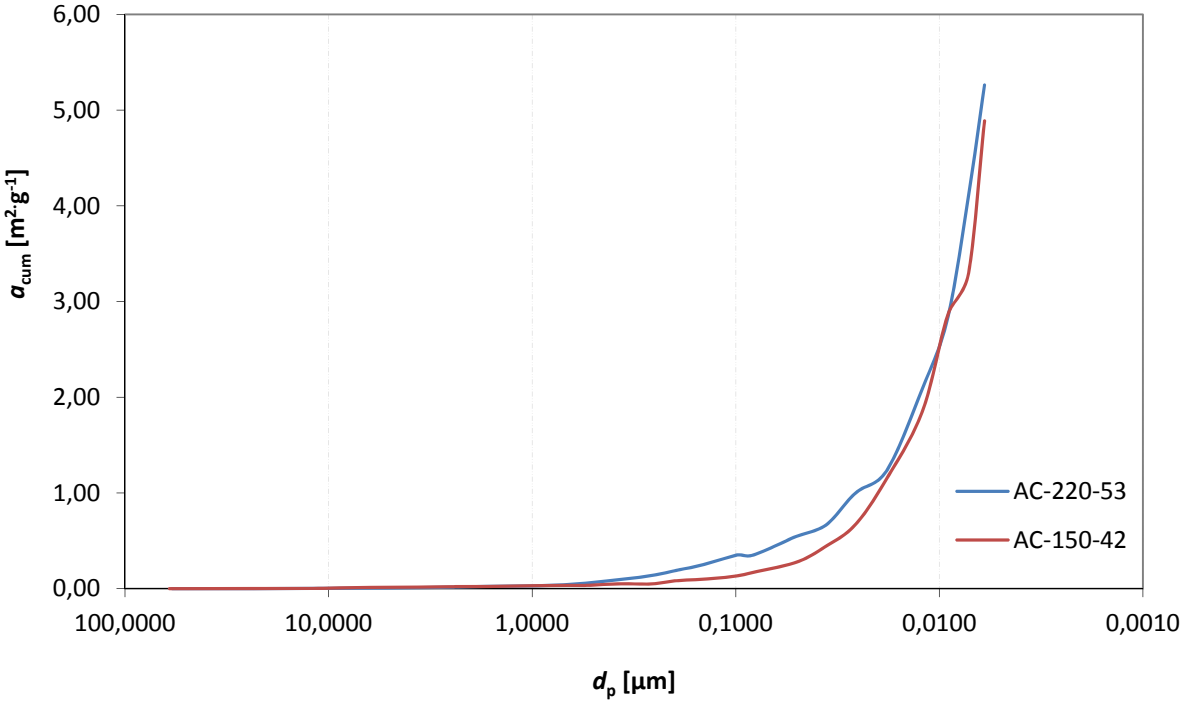

Fig. 49: *Cumulative surface area distribution*

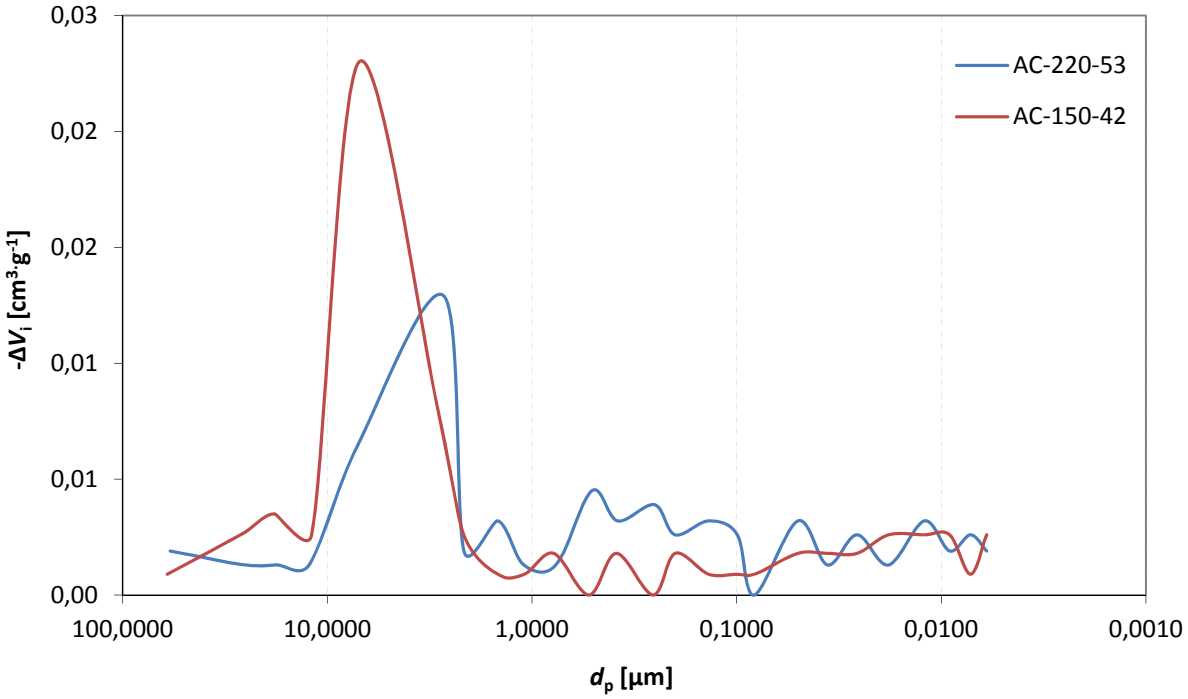

Fig. 50: *Incremental pore volume distribution*

The next plot (Fig. 50) is incremental pore volume distribution which confirms the previous two. The highest volume increments are in the range of 10 µm pore diameter and at the same area is lowest cumulative surface area. All of that is confirmed by chart of differential pore volume distribution (Fig. 51).

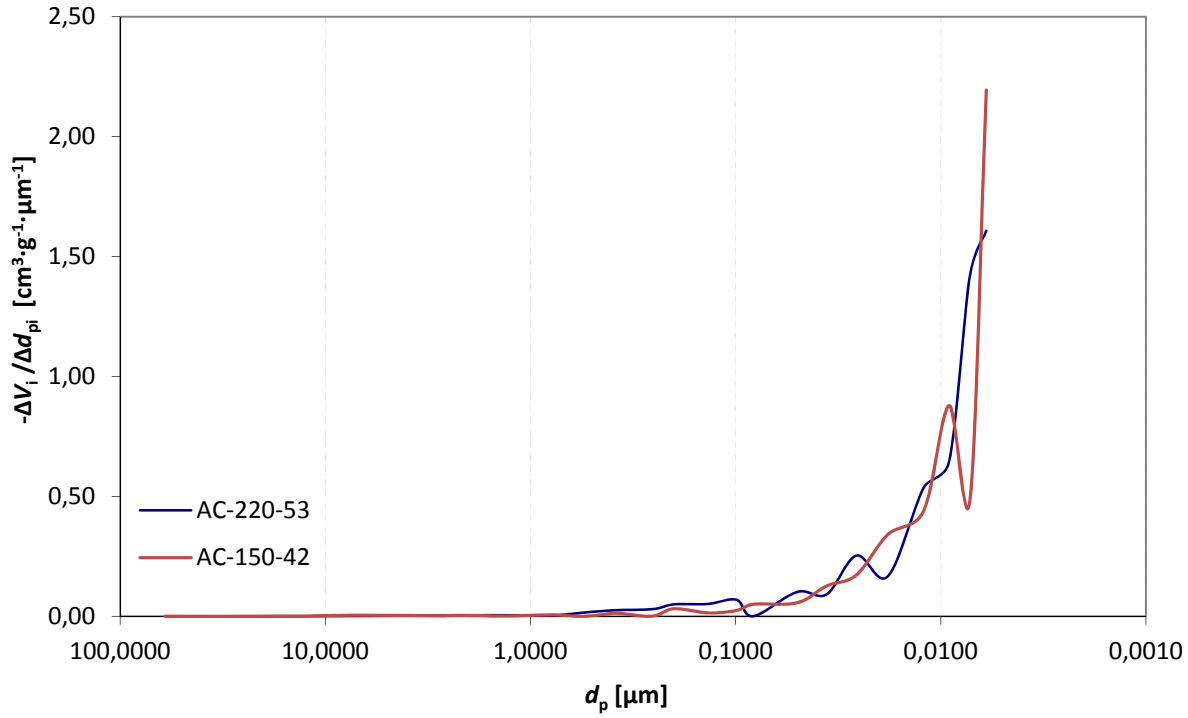

Fig. 51: *Differential pore volume distribution*

6.4 Microscopic structure observation

In this section, pictures from light and scanning electron microscopy are shown. For observation were taken samples with porcelain with binder content 40 % and 60 % to compare the structures and to display the particles of milled porcelain which are supposed to be porous. Some specimens made of SiC were observed too for comparison with those made of porcelain.

6.4.1 Optical microscopy

The structure of specimen L05-40-5 is shown at Fig. 52 and we can observe randomly arranged SiC grains and their irregular shape together with interstices between them. From this picture is obvious that regular pore structure with defined pore size distribution and pore shape may not be expected. The mixtures will always have different parameters which are caused by not quite accurate and definable properties of input materials and moreover, the stochastic process, which with no doubt blending is, amplifies all of that.

Fig. 53 shows structure of specimen with porcelain and 60 % of PC. The single grains of porcelain are recognizable and pervaded by continuum of cement paste. The porosity is obvious but not sufficient for filtration applications. Such barrier would probably have high resistance to flow of fluids.

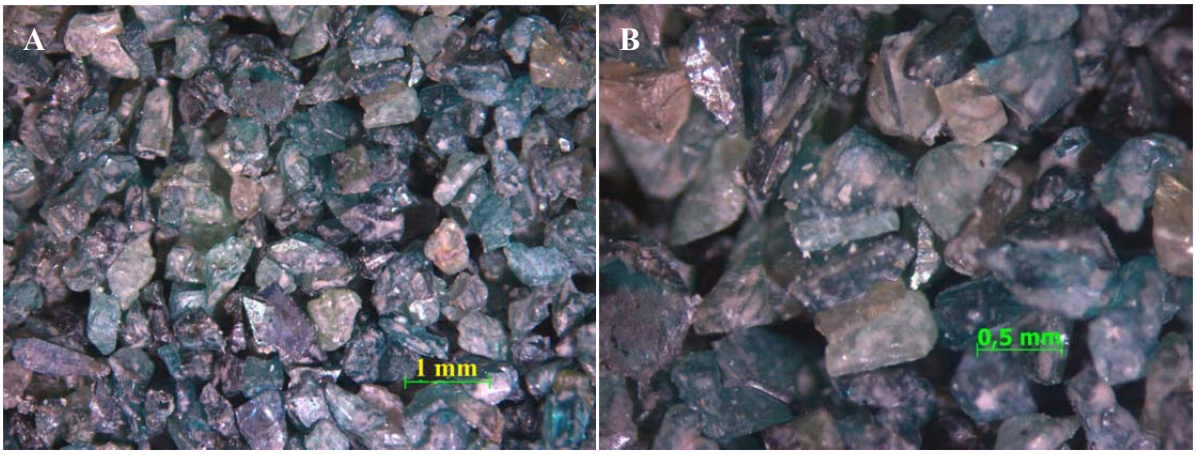

Fig. 52: *Surface of specimen L05-40-5 (A) and the same at double magnification (B), light microscope Zeiss Stemi 2000-C*

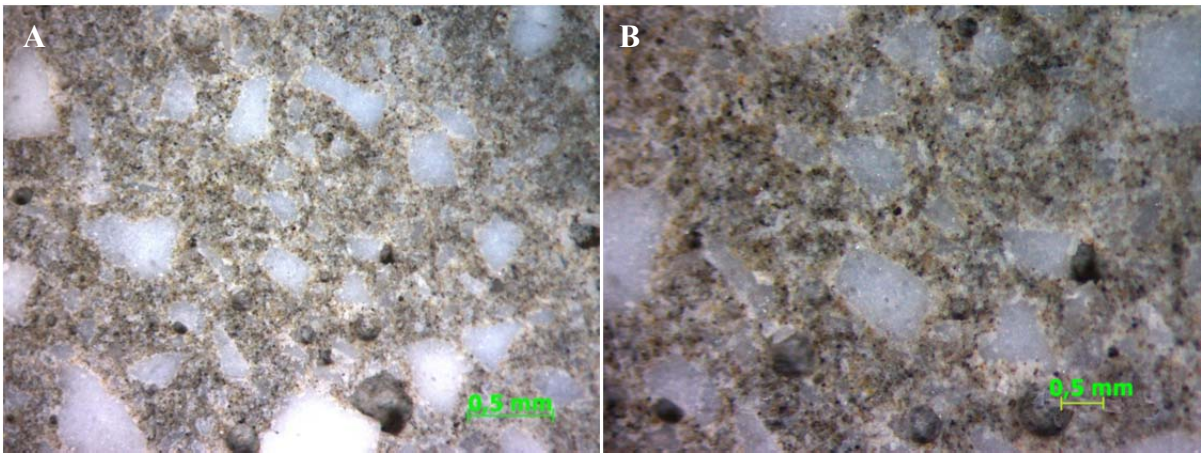

Fig. 53: *Cut of specimen PC-Por-60 (A) and the same at double magnification (B), light microscope Zeiss Stemi 2000-C*

Fig. 54 shows more porous structure even though worse visible and distinguishable because of the same color of the compounds (white cement, white porcelain). Nevertheless, this composition can be suitable for filtration, as there gaps that should be sufficient for fluid flux.

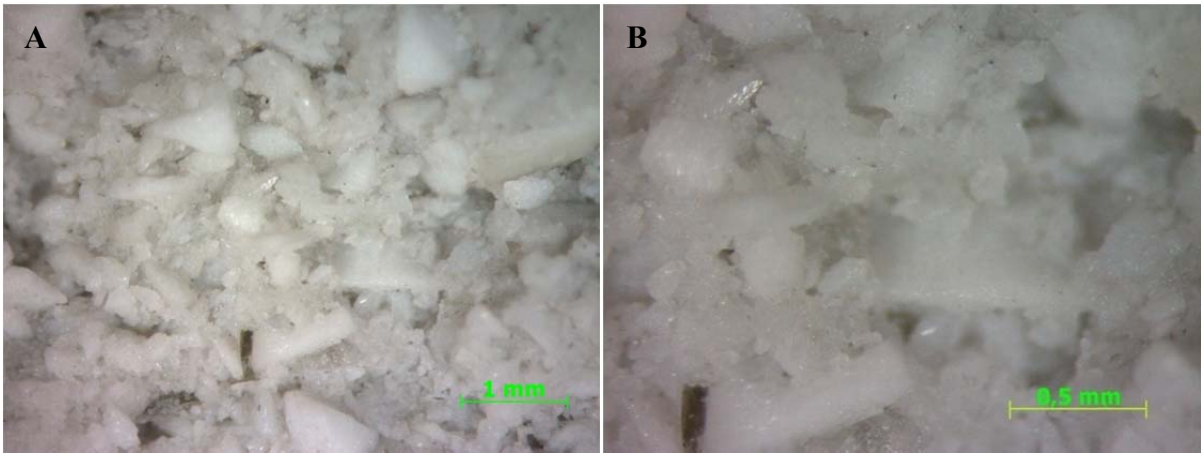

Fig. 54: *Cross-section of specimen AC-Por-40 (A) and the same at double magnification (B), light microscope Zeiss Stemi 2000-C*

6.4.2 Scanning electron microscopy

The Fig. 55 represents cut of sample with 60 % of binder and 40 % of porcelain. Similarly to the Fig. 53 from the light microscope, we can see particles of porcelain (2) and the continuous matter between them which is binder (1). As expected, the porcelain particles have intrinsic (intra-particle) pores which is observable at Fig. 55 and in larger detail at Fig. 56 (the circled areas in the picture) and Fig. 57. The particles are porous though but the pores are certainly not penetrable so for the filtration purposes it does not matter if the particles are porous or not. The relevant for the passage of fluids are inter-particle pores.

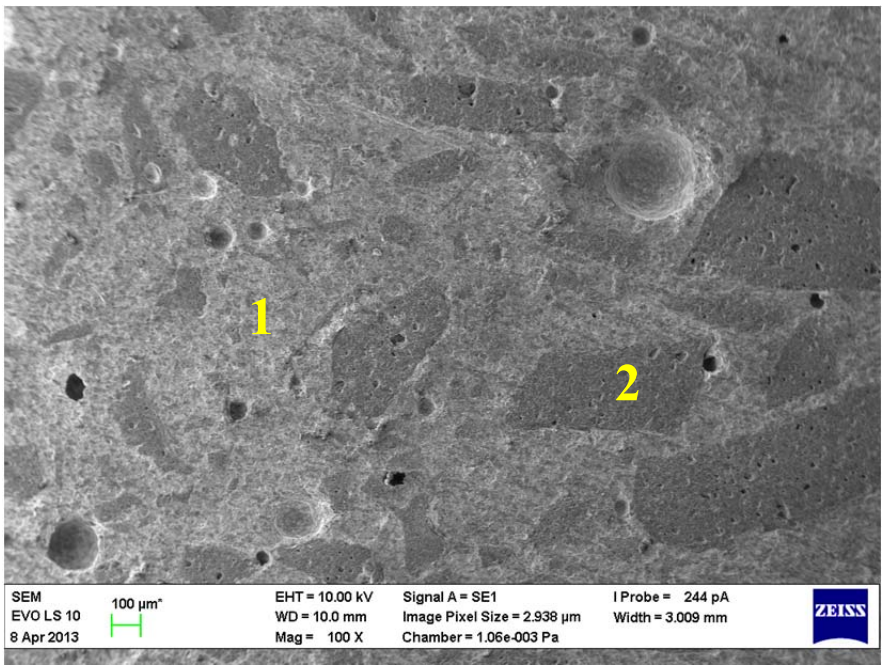

Fig. 55: *The structure of sample PC-Por-60,1 – binder, 2 – porcelain particle, scanning electron microscope Zeiss EVO LS. Magnification: X 100*

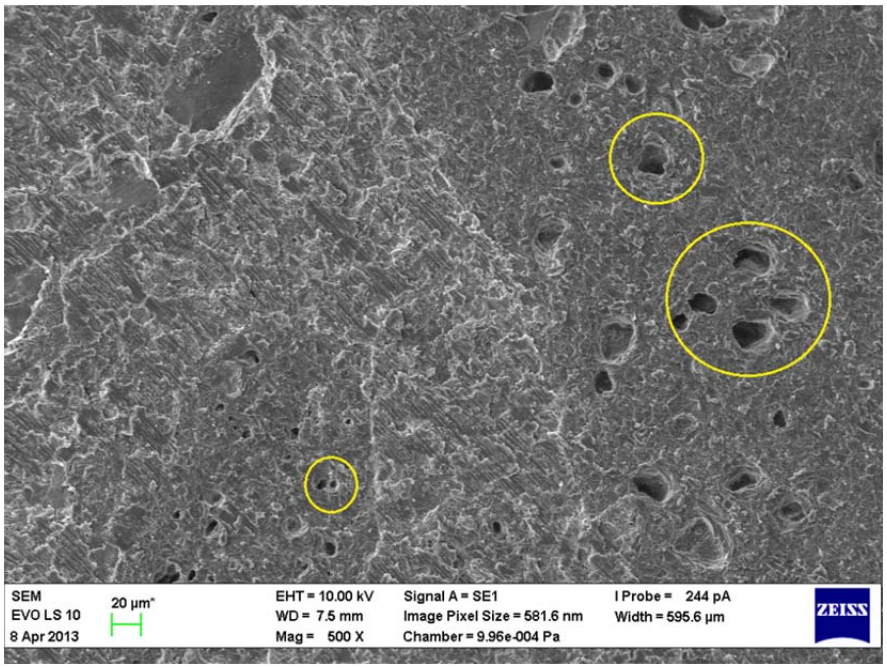

Fig. 56: *The structure of sample AC-Por-60, in the picture marked porcelain intra-particle pores, scanning electron microscope Zeiss EVO LS. Magnification:X 500*

Fig. 58 represents the sample with SiC where a particle of SiC is observable (2) and coated with cement (1). For better display of structure where the interstices between particles would be observable, the more detailed contemplation should be done. This is a fracture surface of the sample without additional adjustment.

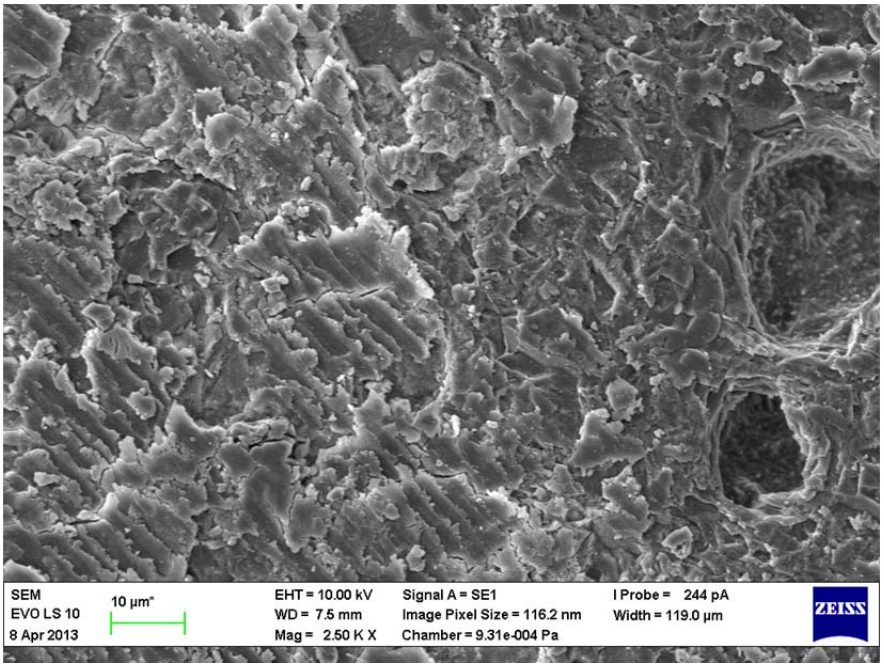

Fig. 57: *The structure of sample AC-Por-40, scanning electron microscope Zeiss EVO LS. Magnification: X 2500*

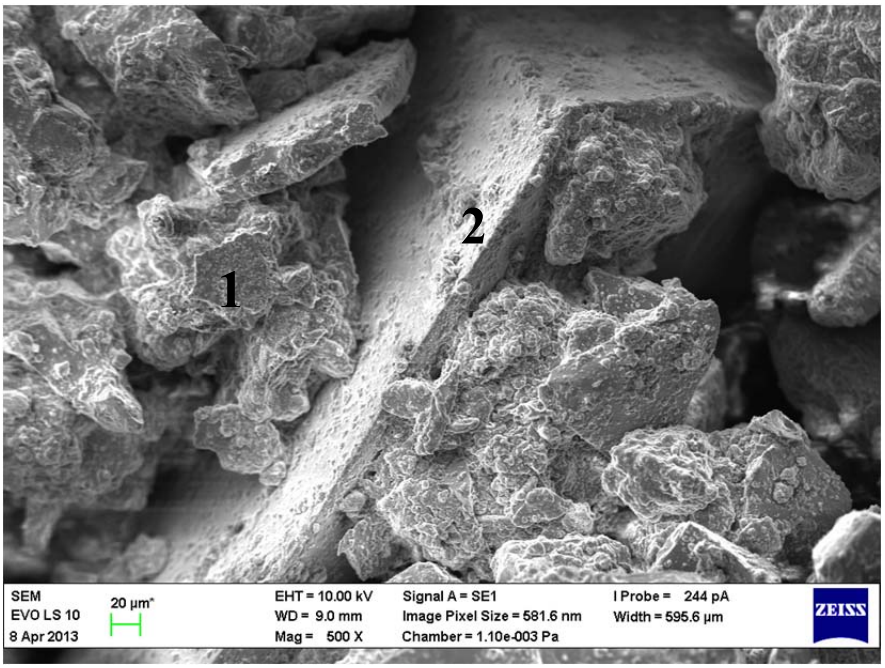

Fig. 58: *The structure of sample AC-150-42, 1 – binder, 2 –a particle of silicon carbide, scanning electron microscope Zeiss EVO LS. Magnification: X 500*

6.5 XRD analysis of initial materials

This analysis was carried out to get overview structure characterization of the input materials.XRD spectra were provided for every material used; in this chapter two representatives of each kind of materials (two of binder and two of aggregates) are demonstrated.

The resultant XRD spectrum of Portland cement CEM I 52.5 N represents Fig. 58. It is obvious the presence of basic clinker minerals such as tricalcium silicate C_3S, dikalcium silicate C_2S, tetracalcium aluminoferrite C_4AF and tricalcium aluminate C_3A. The other components which act as setting retarder (gypsum $CaSO_4$ resp. $CaSO_4 \cdot 2H_2O$) and certain amount of clear quartz can be seen, as well.

The next XRD spectrum (see Fig. 59) describes aluminate cement Secar 71 from which is obvious very well defined composition consisting purely of 81 % of calcium aluminate CA and remaining 19 % is calcium dialuminate CA_2.

The spectrum shown at Fig. 60 is pertinent to green silicon carbide whose manufacturer guarantee 99.5 % purity. The spectrum shows very well defined structure, which consist of SiC hexagonal modification called moissanite, rhomboedral modification and small residual amount of graphite (probably unreacted graphite from manufacturing). From the Fig. 60 is obvious almost zero background which is mark of perfect crystalline structure.

XRD spectrum of milled porcelain which was used as aggregate represents Fig. 61. The basic components occurring at fired ceramic such as mullite, corundum and quartz can be seen. Small amount of sekaninaite which is silicate mineral (iron rich analogue of cordierite) can be found in this ceramic.

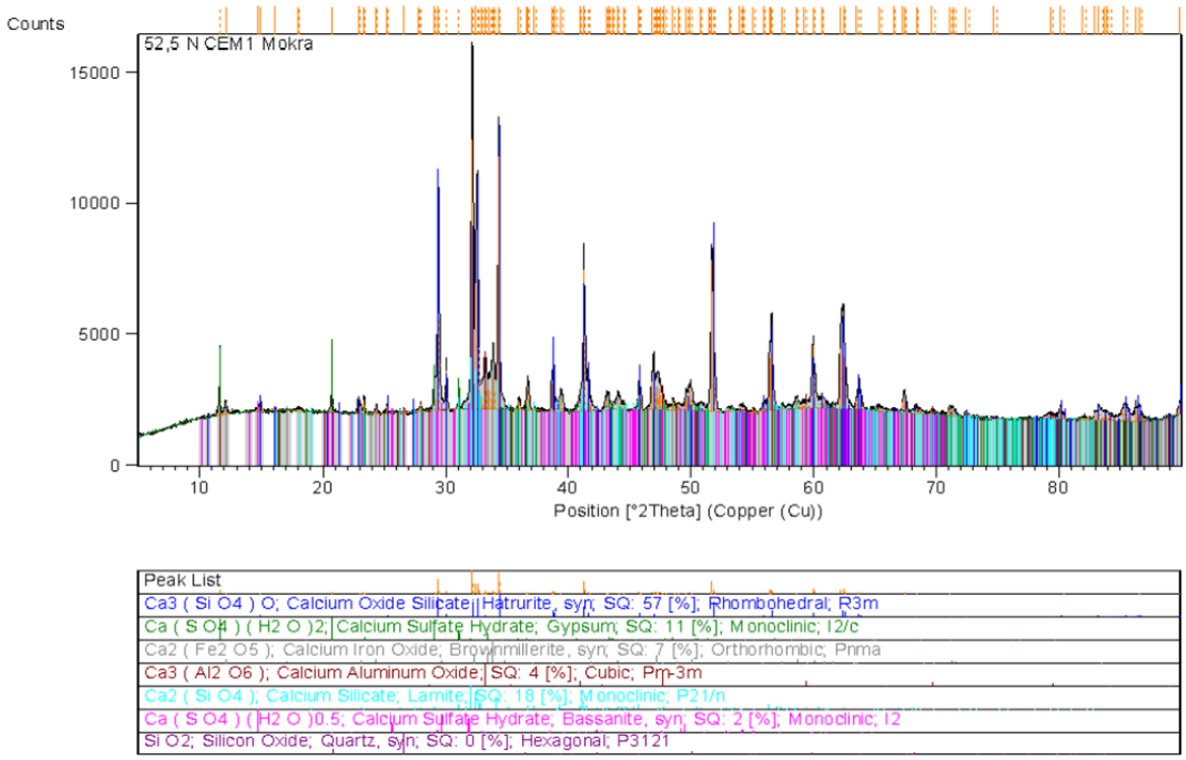

Fig. 59: *XRD spectrum of PC CEM I 52.5 N*

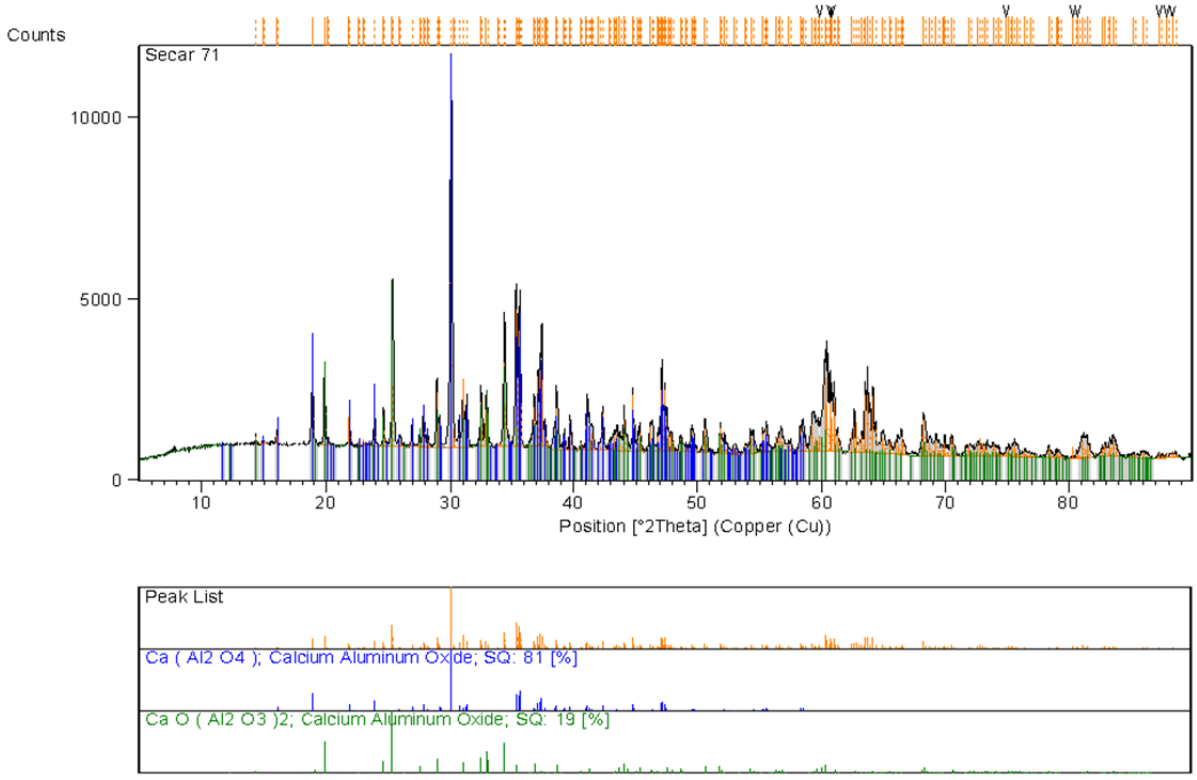

Fig. 60: *XRD spectrum of AC Secar 71*

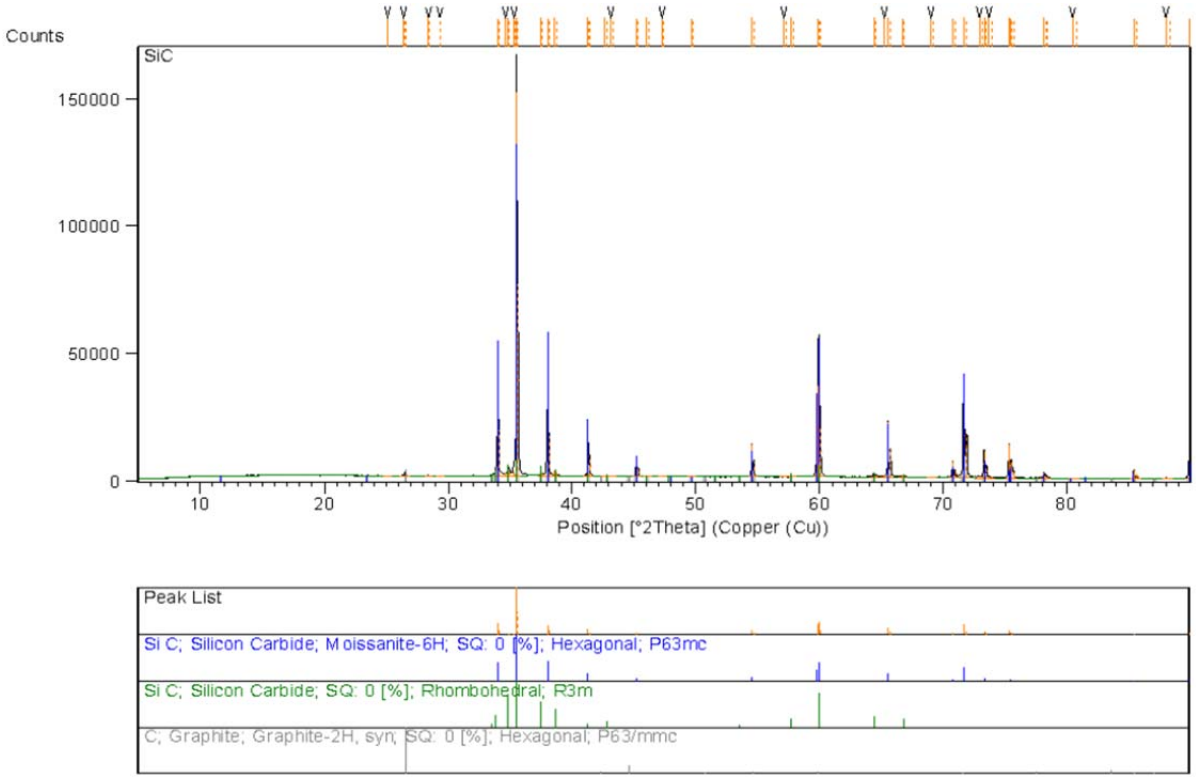

Fig. 61: *XRD spectrum of SiC*

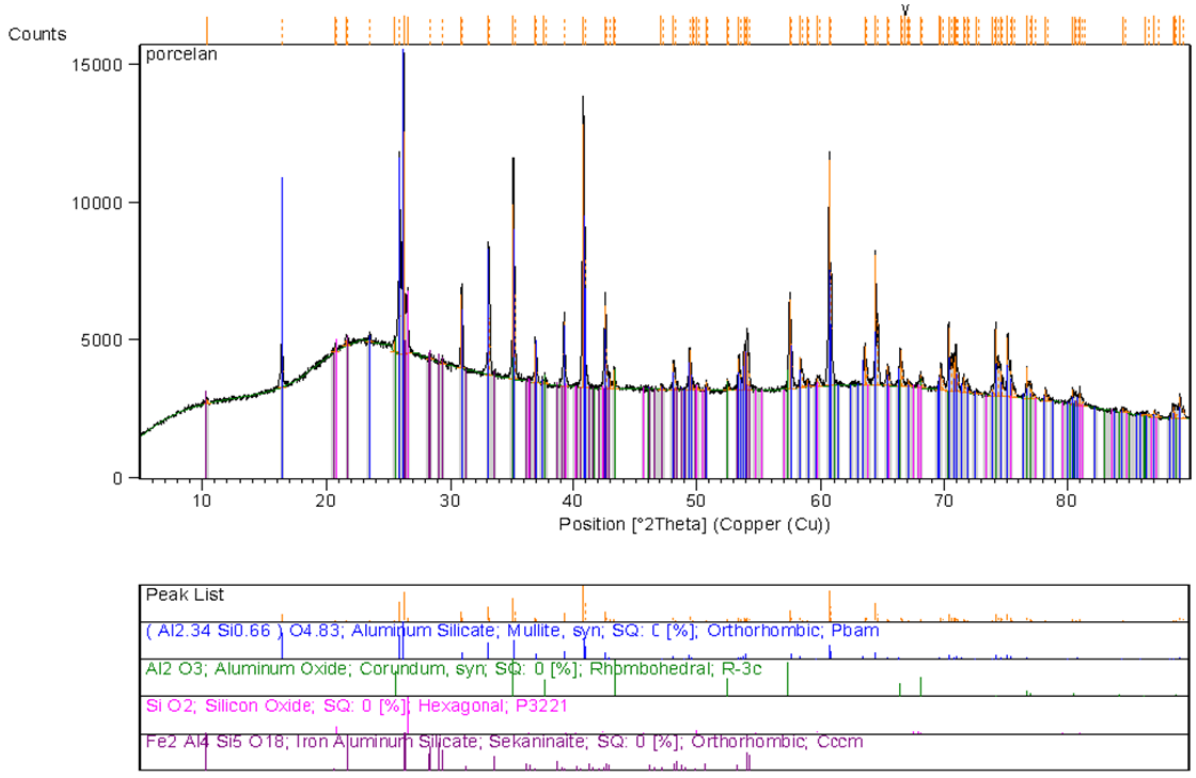

Fig. 62: *XRD spectrum of milled porcelain*

6.6 Capillarity testing

Capillarity experiments were performed as described in section 5.4.6 and output of this measurement were dependences of height of raised liquid on time and dependence of weight increment on time. The mean radii of capillaries in the material were calculated according to Eq. 37.

Table 25: *Values obtained from capillarity measurement for set of MK K05 based specimens*

	***h* [mm]**					
***t* (min)**	**K05-220/150-25**	**K05-220/150/100-28**	**K05-220-28**	**K05-150-25**	**K05-100-22**	**K05-220/ČSN1-22**
0	0	0	0	0	0	0
3	42	15	25	52	30	65
6	90	50	45	70	62	75
9	95	50	51	74	63	85
12	100	53	55	75	70	90
15	100	70	60	90	80	100
18	100	78	60	100	80	100
21	100	78	60	100	84	100
24	100	80	60	100	85	100
27	100	80	60	100	85	100
30	100	80	60	100	85	100

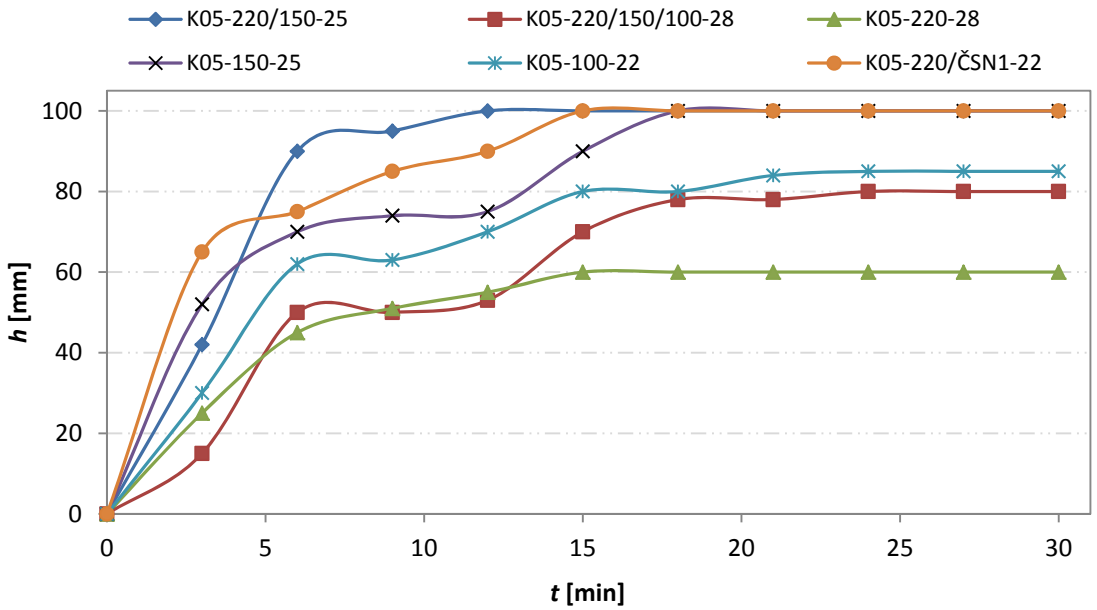

Fig. 63: *Capillarity curves of MK K05 based specimens*

The next values obtained from this measurement are diffusion coefficients of water in the material (Eq. 38). These characteristics can be important for description of porous structure of

the materials as mean radius of capillary gives information about pore size and diffusion coefficient provides characterization of mass transfer in the material.

Table 26: *Values obtained from capillarity measurement for set of PC-SiC based specimens*

	***h* [mm]**					
***t* (min)**	**PC-220-53**	**PC-150-42**	**PC-100-32**	**PC-60/40-26**	**PC-ALL-36**	**PC-G0.24-32**
0	0	0	0	0	0	0
3	20	30	80	90	45	100
6	40	50	100	95	55	100
9	50	60	100	100	70	100
12	50	65	100	100	80	100
15	60	70	100	100	80	100
18	60	70	100	100	90	100
21	60	70	100	100	90	100
24	63	70	100	100	90	100
27	65	76	100	100	90	100
30	65	78	100	100	93	100

All the curves as shown at Fig. 63 – 66 are characteristic by parabolic course which is in accordance with the theory introduced in chapter 5.4.6. Some specimens are characteristic by jump increase of height of the water raised in the material. For example, in the case of the sample PC-G0.24-32 where milled glass was used as aggregates, water reached height of 100 mm within 3 minutes. That probably means high porosity and permeability for water and high diffusion ability of water in the material of the specimen characterized by the highest diffusion coefficient of all the samples (D_g = 0.556 cm^2·s^{-1}).

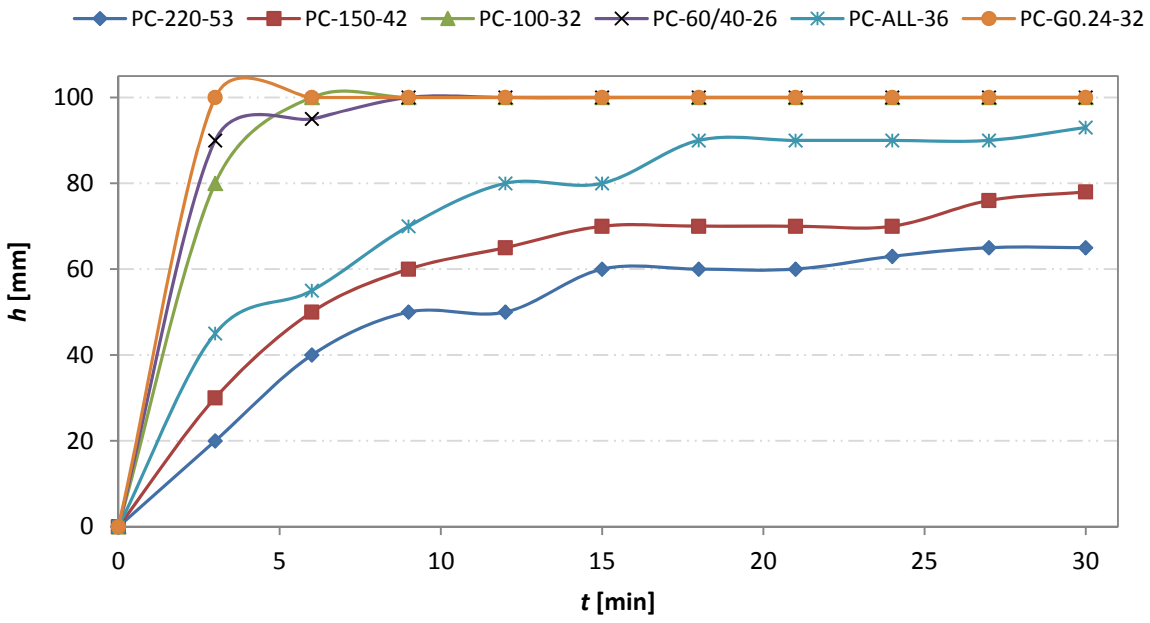

Fig. 64: *Capillarity curves of PC-SiC based specimens (one sample of glass)*

The filtration barrier made of this material would probably be of low hydraulic resistance because water has big ability to pass through the material. Together with the appropriate mechanical strengths (for this sample f_b = 3.38 MPa, f_c = 23.90 MPa, see Table 18) would be a suitable for filtration applications.

Other characteristics are observable in the case of the sample PC-Por-50. It is obvious that larger amount of binder cause porosity reduction (a therefore mechanical strengths increase) and that is why the water in the sample material arose only by 2 mm within 30 minutes and hence diffusion coefficient equals only to 0.001 $cm^2 \cdot s^{-1}$.

Table 27: *Values obtained from capillarity measurement for set of various specimens*

	***h* [mm]**			
***t* (min)**	**PC-Por-40**	**PC-Por-50**	**L05-150-26**	**K05-150/ČSN1-20**
0	0	0	0	0
3	60	8	50	65
6	66	8	63	75
9	70	8	70	85
12	70	8	80	90
15	70	9	85	100
18	75	9	93	100
21	80	9	100	100
24	80	10	100	100
27	85	10	100	100
30	85	10	100	100

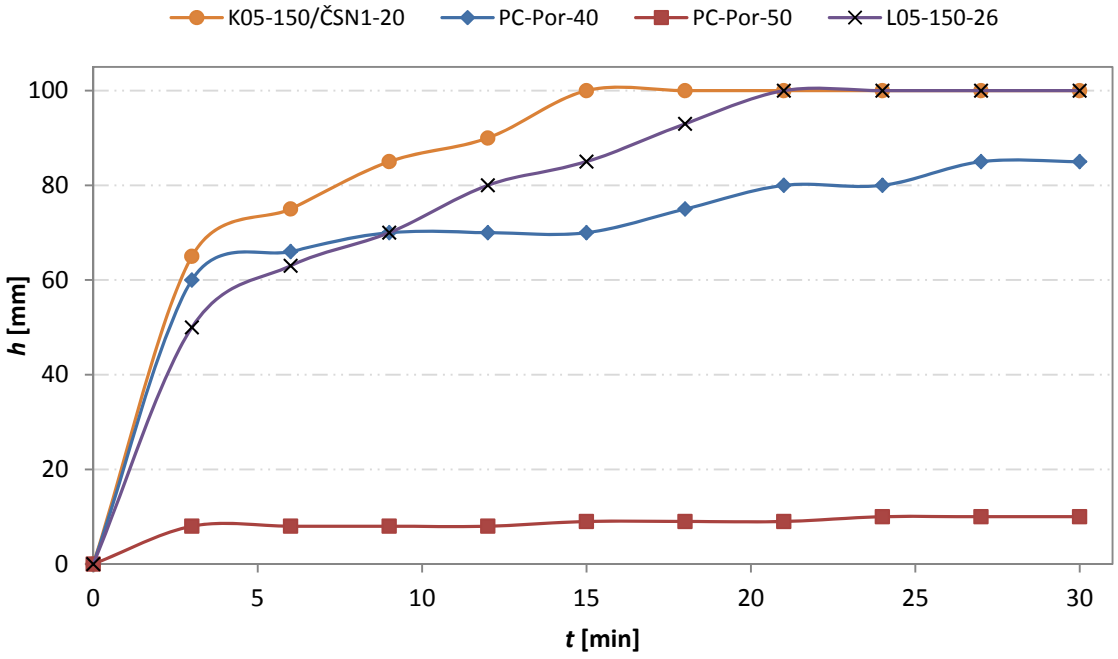

Fig. 65: *Capillarity curves of various specimens*

As the height of the raised water in the column is very low, the mean pore radius on the contrary is characterized by high value which is conformable with Eq. 37 but the reality is

quite different, apparently. It is likely truth that the relation (Eq. 37) is accepted only if the pores are penetrable and can be characterized by one capillary which has mean radius. If the pores are not connected, the fluid cannot pass through the material. In the case of the sample PC-Por-50, it is probably not accomplished.

Table 28: *Values obtained from capillarity measurement for set of PC and MK based specimens (specific capillarity)*

	***m* [g]**			
***t* (min)**	**PC-Por-40**	**PC-Por-50**	**L05-150-26**	**K05-150/ČSN1-20**
0	72.0	80.5	77.1	75.4
3	76.1	80.7	82.2	80.6
6	76.6	80.7	82.7	81.2
9	77.0	80.7	83.6	82.0
12	77.1	80.7	84.2	82.4
15	77.2	80.7	84.8	82.7
18	77.2	80.7	85.4	83.0
21	77.3	80.7	85.6	83.1
24	77.3	80.7	85.8	83.4
27	77.3	80.7	85.8	83.4
30	77.3	80.7	85.9	83.4

Table 29: *Calculated values of diffusion coefficients of water in the materials and mean radii of capillaries in the material*

Sample	D_g **[cm^2·s^{-1}]**	r_c **[mm]**
K05-220/150-25	0.139	0.149
K05-220/150/100-28	0.044	0.186
K05-220-28	0.040	0.248
K05-150-25	0.093	0.149
K05-100-22	0.050	0.175
K05-220/ČSN1-22	0.111	0.149
PC-220-53	0.023	0.229
PC-150-42	0.034	0.191
PC-100-32	0.278	0.149
PC-60/40-26	0.185	0.149
PC-ALL-36	0.048	0.160
PC-G0.24-32	0.556	0.149
PC-Por-40	0.040	0.175
PC-Por-50	0.001	1.490
L05-150-26	0.079	0.149
K05-150/ČSN1-20	0.111	0.149

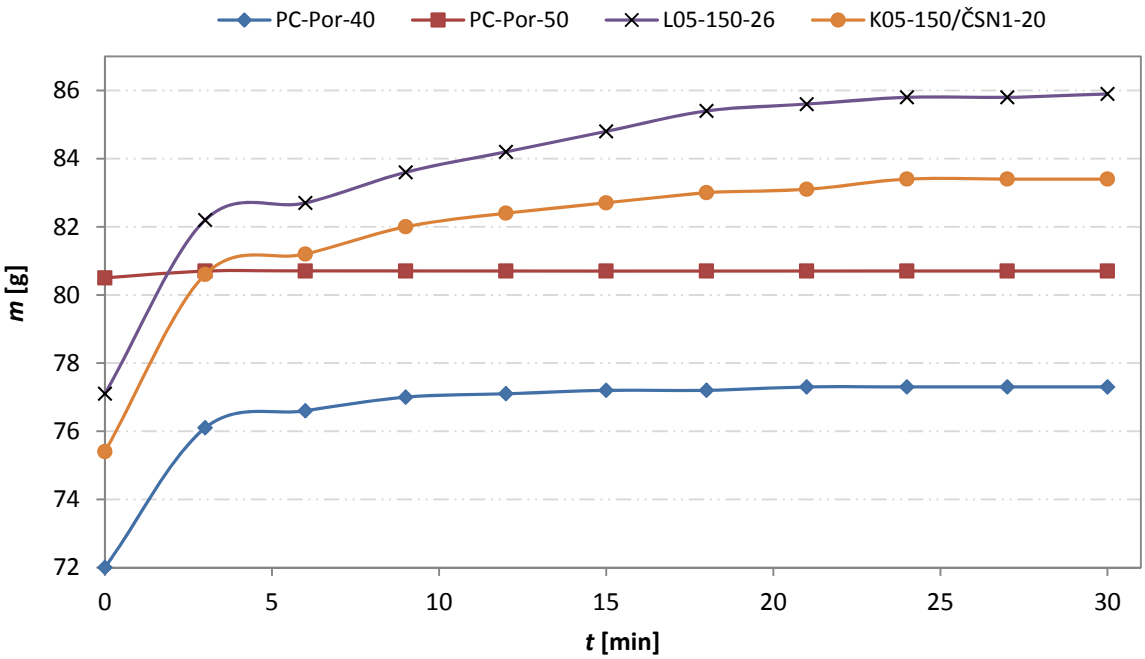

Fig. 66: *Specific capillarity curves of PC and MK based specimens*

6.7 Permeation measurement

This experiment was applied to investigate permeability (penetrability, channel capacity) of the prepared barriers. It was done with disk with 90 mm in diameter with the equipment as shown at Fig. 25. The barrier was inserted into the chamber, sealed, closed up with lid and to the inlet was attached air supplier. For demonstration data from measurement see Tab. 30. The measurement was performed for each prepared barrier three times.

Table 30: *Example of output data from permeation test for two barriers*

AC-150-42 (1)								
t_1 [s]	**Δp [kPa]**	**$\ln(\Delta p/\Delta p_0)$**	**t_2 [s]**	**Δp [kPa]**	**$\ln(\Delta p/\Delta p_0)$**	**t_3 [s]**	**Δp [kPa]**	**$\ln(\Delta p/\Delta p_0)$**
0	115	0	0	115	0	0	115	0
0.4	90	-0.2451	0.4	90	-0.2451	0.5	90	-0.1398
1.1	70	-0.4964	1.1	70	-0.4964	1.1	70	-0.3629
2.4	50	-0.8329	2.4	50	-0.8329	2.3	50	-0.6506
4.5	30	-1.3437	4.3	30	-1.3437	4.4	30	-1.0561
8.6	10	-2.4423	8.3	10	-2.4423	8.4	10	-1.7492
11.3	0	-	11.2	0	-	11.4	0	-
PC-ALL-36								
0.0	115	0	0.0	115	0	0.0	115	0
0.6	90	-0.2451	0.4	90	-0.2451	0.7	90	-0.2451
1.1	70	-0.4964	1.0	70	-0.4964	1.2	70	-0.4964
1.9	50	-0.8329	1.9	50	-0.8329	2.1	50	-0.8329
3.0	30	-1.3437	2.8	30	-1.3437	3.2	30	-1.3437
5.0	10	-2.4423	4.6	10	-2.4423	5.2	10	-2.4423
6.9	0	-	6.5	0	-	6.8	0	-

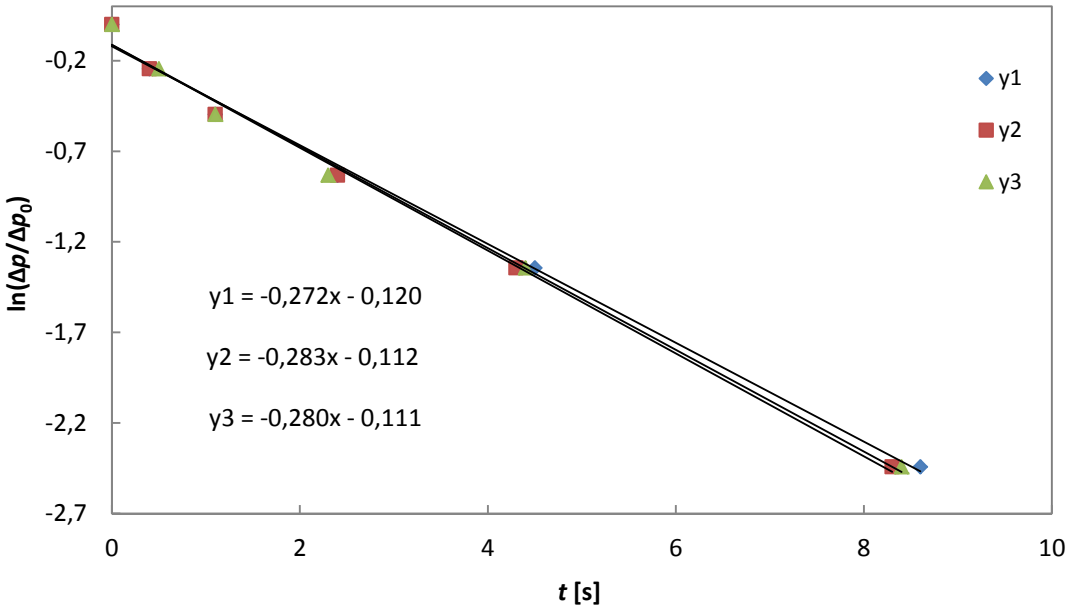

Fig. 67: *Permeation measurement plot – sample AC-150-42 (1)*

At Fig. 67 – 69 examples of output data plots from permeation measurement are shown. The times of permeation (penetrating the air through the barrier) vary mostly from five to eight seconds. Only one barrier (Fig. 69) is different, the time of permeation is almost 16 s. It is the barrier with 60 % of binder so the flow of air through this barrier is more difficult and penetrates for longer time. So the resulting value of effective permeability is lower. Generally, the longer the air flux time the lower effective permeability results are observable.

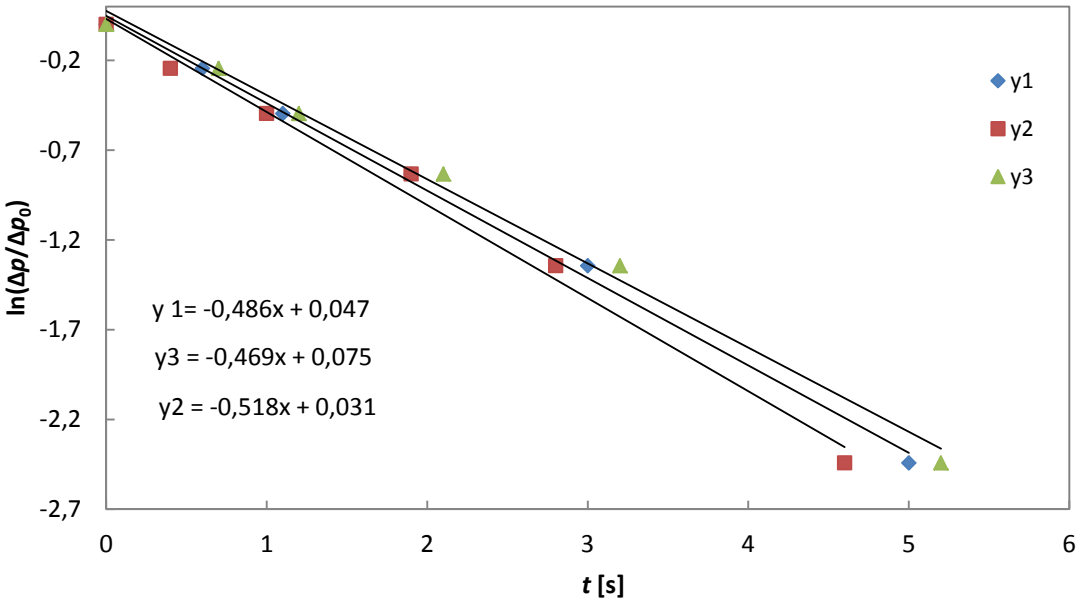

Fig. 68: *Permeation measurement plot – sample PC-ALL-36*

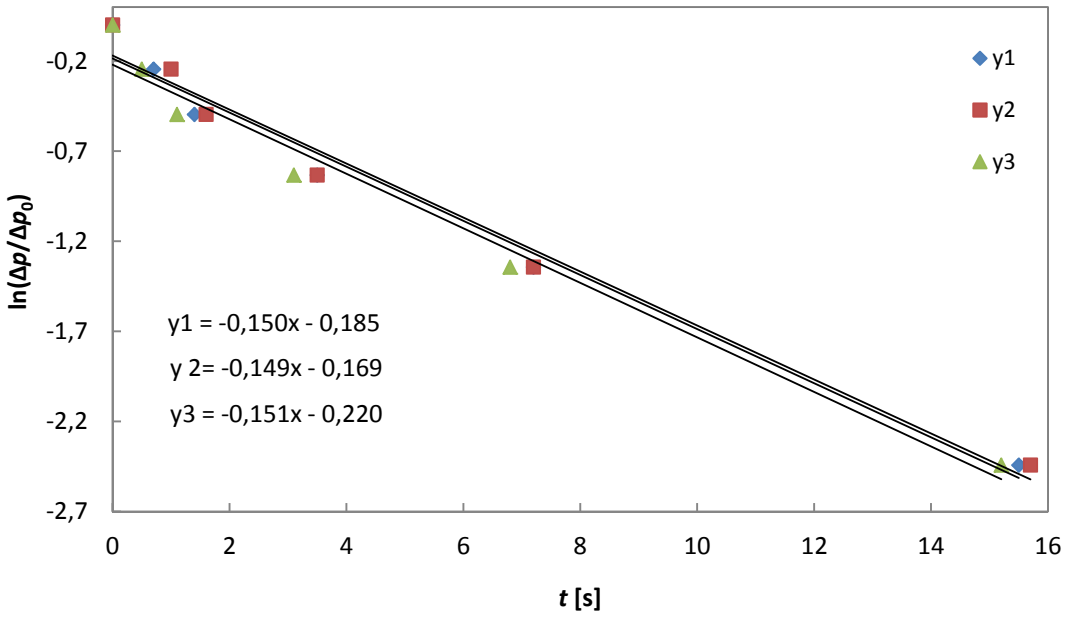

Fig. 69: *Permeation measurement plot – sample AC-Por-60*

The resulting effective permeabilities of particular barriers are show in Table 31. Some of the barriers were measured more times for results comparison and to find out how the results are different. The similar results of permeabilities as in the case of barriers AC-100-32 (1), AC-100-32 (2) and AC-100-32 (3) which equals to $3.062 \cdot 10^{-7}$, $3.072 \cdot 10^{-7}$ and $3.059 \cdot 10^{-7}$ $mol \cdot m^{-1} \cdot s^{-1} \cdot Pa^{-1}$, respectively, are the proof of good reproducibility of the barrier preparation by pressing the mortars in mold. Something different is seen in the case of AC-150-42 where the single values are more different. It can be caused by many influences such as unequal compacting pressure; possible is a sealing flaw at chamber and of course stochastic character of blending procedure of granular materials.

The difference between permeabilities can be caused by the age of barrier and way of storage (compare specimens AC-100-32 which was prepared five months ago and the other made of the same composition but more lately – AC-100-32 (1), AC-100-32 (2), AC-100-32 (3)). Elder barriers have probably lower permeability which can be caused by more advanced hydration period where the structure of cement hydration products are more developed and fills the spaces among grains of aggregates. The same can be observed if the barriers are stored in water which is needed in the case of hydraulic binders or if it is stored on a dry place where the hydration process is slowed down.

Table 31: *Angular coefficients from the permeation measurement plot and resulting values of effective permeability*

Sample	β_1 [s^{-1}]	β_2 [s^{-1}]	β_3 [s^{-1}]	h_b [mm]	K_{eff} [10^{-7} mol·m^{-1}·s^{-1}·Pa^{-1}]
AC-100-32	0.399	0.436	0.390	5.85	2.188
PC-ALL-36	0.486	0.518	0.469	5.90	2.653
AC-60/40-26 (1)	0.366	0.417	0.378	5.80	2.056
AC-60/40-26 (2)	0.486	0.518	0.469	6.86	3.085
AC-150-42 (1)	0.272	0.283	0.280	5.08	1.295
AC-150-42 (2)	0.539	0.502	0.517	5.30	2.521
AC-150-42 (3)	0.557	0.627	0.590	5.85	3.168
AC-Por-40	0.527	0.559	0.568	5.16	2.605
AC-Por-60	0.150	0.149	0.151	5.79	0.795
PC-G-0.24-32	0.589	0.599	0.594	4.98	2.709
AC-G-0.24-32	0.620	0.626	0.613	5.25	2.979
AC-100-32 (1)	0.610	0.589	0.625	5.50	3.062
AC-100-32 (2)	0.643	0.568	0.622	5.49	3.072
AC-100-32 (3)	0.590	0.629	0.603	5.50	3.059

6.8 Determination of porosity by pycnometry

In Table 32 we can see results of pycnometric measurement. An anomaly in the form of final results of apparent and total porosities can be seen. In some cases the total porosity is lower than the apparent one which is impossible as the total porosity includes open and closed pores whereas the apparent porosity contains only percentage of open pores. This is probably caused by boiling the samples as they are less tenacious and during the boiling the samples crumbled which caused weight loss and hence inaccurate calculation.

Table 32: *Values obtained by pycnometric measurement*

Sample	m_1 [g]	m_2 [g]	m_3 [g]	m_4 [g]	ρ_b [kg·m^{-3}]	A_C [%]
PC-Por-40	1.9805	59.1187	58.2601	2.1808	1761.4	10.11
AC-220-53	2.7312	59.4656	57.8943	2.9498	2349.4	8.00
AC-150-42	2.9384	57.3769	55.7175	3.2332	2292.3	10.03
AC-100-32	2.5602	59.5851	58.2601	3.0062	2068.1	17.42
AC-60/40-26	2.4735	59.4328	57.8943	2.7881	2639.6	12.72
AC-ALL-36	3.0291	57.5178	55.7175	3.2958	2459.6	8.80
AC-G-0.12-48	1.5250	58.9492	58.2601	1.7005	1820.3	11.51
	m_1 [g]	m_2 [g]	m_3 [g]	ρ_{sw} [kg·m^{-3}]	ε_a [%]	ε_t [%]
PC-Por-40	1.9805	59.2579	58.1477	2268.3	17.81	22.35
AC-220-53	2.7312	59.5954	57.8985	2632.1	18.80	10.74
AC-150-42	2.9384	57.8396	55.8814	2988.1	23.00	23.29
AC-100-32	2.5602	59.8674	58.1477	3036.2	36.03	31.89
AC-60/40-26	2.4735	59.5434	57.8985	2975.5	33.57	11.29
AC-ALL-36	3.0291	57.9265	55.8814	3068.4	21.66	19.84
AC-G-0.12-48	1.5250	59.0504	58.1477	2442.7	20.95	25.48

6.9 Filtration testing

As a demonstration, data from filtrations measurement are shown here. Filtrations were contrived at device as shown at Fig. 25. Firstly, the flux of pure water through the barrier was measured. A certain volume of water was poured into chamber with the barrier and closed up, the pressure was applied and the amount of water passed through was measured in given time intervals. The same was done with suspension of lime hydrate and limestone. The acquired data were then plotted in the form of linear dependences (Eq. 45).

Table 33: *Values from filtration test at p = 30 kPa (pure water)*

Water			
t [s]	V_f [cm^3]	V_f/A [10^{-3} m]	$t(A/V_f)$ [10^4 m^{-1}·s]
30	37	8.37	0.36
60	37	8.37	0.72
90	34	7.69	1.17
120	31	7.01	1.71
150	35	7.92	1.89
180	31	7.01	2.57
210	31	7.01	2.99
240	29	6.56	3.66
270	30	6.79	3.98

Table 34: *Parameters of suspension of lime hydrate and filtration cake*

m_{H2O} [g]	300.0
m_{sp} [g]	50.0
m_{ss} [g]	350.0
h_c [mm]	11.9
m_c [g]	74.8
m_f [g]	250.0

Table 35: *Values from filtration test at p = 30 kPa (suspension of lime hydrate)*[2]

t [s]	V_f [cm^3]	V_f/A [10^{-3} m]	$t(A/V_f)$ [10^4 m^{-1}·s]
60	36	8.14	0.73
120*	25	5.66	2.12
180*	23	5.20	3.46
240*	21	4.75	5.05
300*	19	4.30	6.98
360	25	5.66	6.37
420	28	6.33	6.63
480	25	5.66	8.49
540	31	7.01	7.70

[2] By the asterisk are marked values taken to be plotted

Calculations of filtration parameters (suspension):

1. Calculation of residual amount of water in cake and calculation of porosity

- Cake humidity:

$$m_{ss} - m_f = \frac{m_c}{1 - x_c'} \cdot x_c' \Rightarrow x_c' = \frac{m_{ss} - m_f}{m_{ss} - m_f + m_c}$$

$$x_c' = \frac{350 - 250}{350 - 250 + 74.8}$$

$$x_c' = 0.5721$$

- Weight of water in cake:

$$m_{H_2O}' = m_{sp} \cdot \frac{x_c'}{1 - x_c'} = 50 \cdot \frac{0{,}5721}{1 - 0{,}5721} = 66.86 \text{ g}$$

- Cake porosity[3]:

$$\varepsilon = \frac{V_p}{V} = \frac{V - V_{sp}}{V} = \frac{A \cdot h_c - \frac{m_{sp}}{\rho_s}}{A \cdot h_c} = 1 - \frac{m_{sp}}{A \cdot h_c \cdot \rho_s} = 1 - \frac{50 \cdot 10^{-3}}{4.42 \cdot 10^{-3} \cdot 11.9 \cdot 10^{-3} \cdot 2240} = 0{,}4244$$

2. Calculation of filtration constants

- The system of two equations with two unknowns:

$t = 180$ s

$$\left(\frac{V_f}{A}\right)^2 + 2 \cdot \left(\frac{V_f}{A}\right) \cdot V_{fb} = 2 \cdot C \cdot \tau$$

$$\left(\frac{23 \cdot 10^{-6}}{4.42 \cdot 10^{-3}}\right)^2 + 2 \cdot \left(\frac{23 \cdot 10^{-6}}{4.42 \cdot 10^{-3}}\right) \cdot V_{fb} = 2 \cdot C \cdot 180 \Rightarrow C = \frac{\left(5.204 \cdot 10^{-3}\right)^2 + 2 \cdot \left(5.204 \cdot 10^{-3}\right) \cdot V_{fb}}{2 \cdot 180}$$

$t = 240$ s

$$\left(\frac{21 \cdot 10^{-6}}{4.42 \cdot 10^{-3}}\right)^2 + 2 \cdot \left(\frac{21 \cdot 10^{-6}}{4.42 \cdot 10^{-3}}\right) \cdot V_{fb} = 2 \cdot C \cdot 240$$

$$\left(4.751 \cdot 10^{-3}\right)^2 + 2 \cdot \left(4.751 \cdot 10^{-3}\right) \cdot V_{fb} = 2 \cdot \frac{\left(5.204 \cdot 10^{-3}\right)^2 + 2 \cdot \left(5.204 \cdot 10^{-3}\right) \cdot V_{fb}}{2 \cdot 180} \cdot 240$$

$$V_{fb} = -3.095 \cdot 10^{-3} \text{ m}^3$$

$$C = -1{,}640 \cdot 10^{-7} \text{ m}^6 \cdot \text{s}^{-1}$$

- Graphical analysis:

$$\left(\frac{V_f}{A}\right)^2 + 2 \cdot \left(\frac{V_f}{A}\right) \cdot V_{fb} = 2 \cdot C \cdot \tau \Big| \cdot \frac{A}{2 \cdot C \cdot V_f}$$

[3] The value of lime hydrate density (ρ_t) is according to [61]

$$\frac{1}{2\cdot C}\cdot\frac{V_f}{A}+\frac{V_{fb}}{C}=\tau\cdot\frac{A}{V_f}$$

$$y=ax+b\rightarrow y=-4\cdot10^{7}+22183$$

$$a=-4\cdot10^{7};\ b=22183$$

$$C=\frac{1}{2\cdot a}=\frac{1}{2\cdot(-4\cdot10^{7})}$$

$$C=-1.250\cdot10^{-8}\,m^{6}\cdot s^{-1}$$

$$V_{fb}=b\cdot C=22183\cdot(-1.25\cdot10^{-8})$$

$$V_{fb}=-2.773\cdot10^{-4}\ \mathrm{m}^3$$

Table 36: *Results of calculation and comparison of values of filtration constants obtained by numerical and graphical solution for both suspension and water filtration (p = 40 kPa)*

	Constants	**Suspension**	**Water**
Equations solution	C [m^6·s^{-1}]	$-1.640\cdot10^{-7}$	$-6.730\cdot10^{-8}$
	V_{fb} [m^3]	$-6.448\cdot10^{-3}$	$-5.233\cdot10^{-3}$
Graphical solution	C [m^6·s^{-1}]	$-1.250\cdot10^{-8}$	$-2.500\cdot10^{-8}$
	V_{fb} [m^3]	$-2.773\cdot10^{-4}$	$-3.606\cdot10^{-4}$
m'_{H_2O} [g]		66.86	-
ε [%]		42.44	-

Table 37: *Comparison of water flow in free column and column with the barrier (p = 40 kPa)*

Barrier	t **[s]**	$\dot{V}$ **[10^{-6} m^3·s^{-1}]**	u **[10^{-3} m·s^{-1}]**	ε **[%]**	u_ε **[10^{-2} m·s^{-1}]**
PC-ALL-36	48.6	5.14	1.16	21.66	3.20
AC-150-42	41.0	6.10	1.38	23.00	3.01
AC-100-32	23.3	10.7	2.43	36.03	1.92
AC-60/40-26	53.9	4.64	1.05	33.57	2.06
AC-Por-40	33.4	7.48	1.69	17.81	3.89
AC-220-53[4]	155.7	0.32	0.07	18.80	3.69
V_1 **[cm^3]**	V_2 **[cm^3]**	t **[s]**	$\dot{V}$ **[10^{-5} m^3·s^{-1}]**	u **[10^{-3} m·s^{-1}]**	A **[10^{-3} m^2]**
250	50	8.16	3.06	6.93	4.42

When we look at the Table 36 where the resulting constants of filtration are summarized, the large difference is observable between the values gained by numerical and graphical calculation. The numerical calculation comes directly out of concrete values of time and filtrate volume. The graphical calculation is carried out with the help of regression analysis which is quite different as the regression equation is of shape which is dependent on measured values so that they follow one another. So the graphical solution is more accurate.

For the calculation of velocity in the channels of the barrier were used values of porosity determined by pycnometric measurement. As expected and supported by theory of flow through a porous barrier, the flow velocity in the barrier (in the channels) is higher than that in free column, but overall flow rate is lower.

[4] The water volume V_2 was used for the barrier AC-220-53

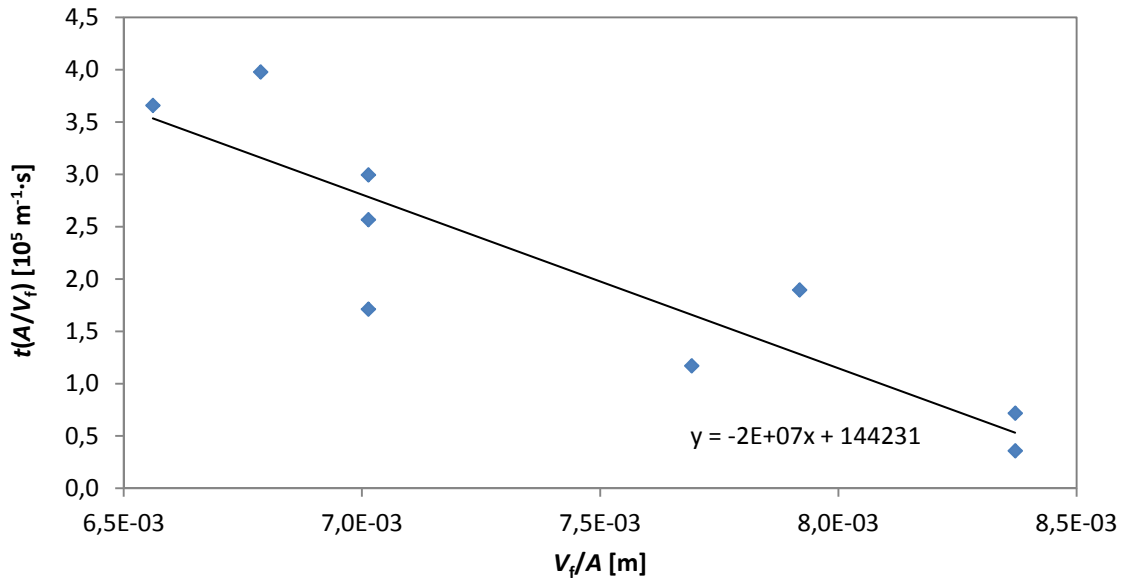

Fig. 70: *Graphical representation of filtration equation for water flux*

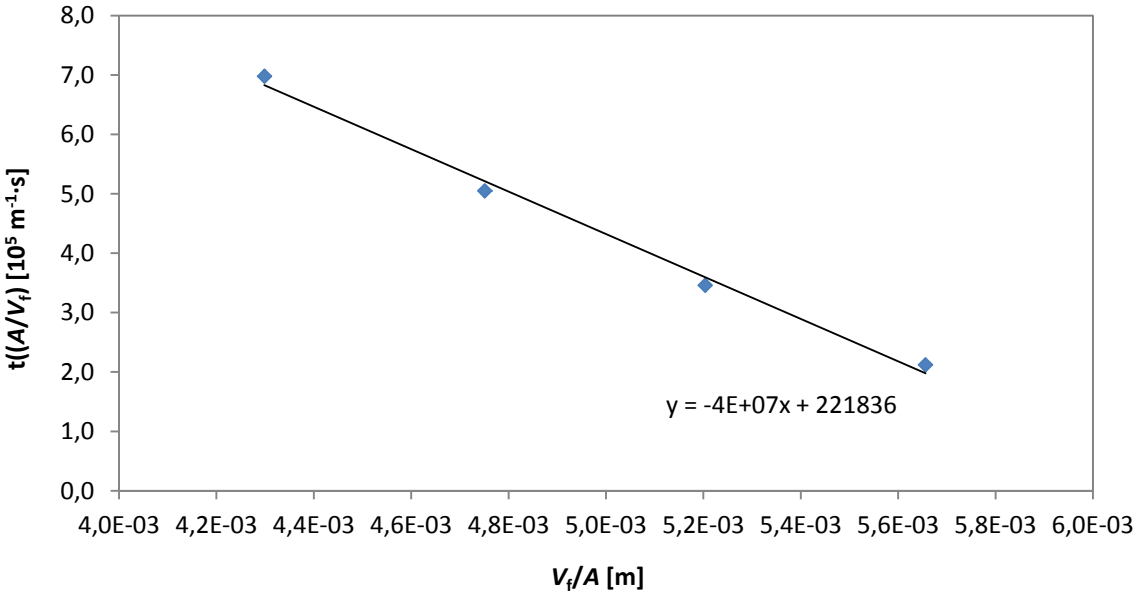

Fig. 71: *Graphical representation of filtration equation – filtration of lime hydrate suspension*

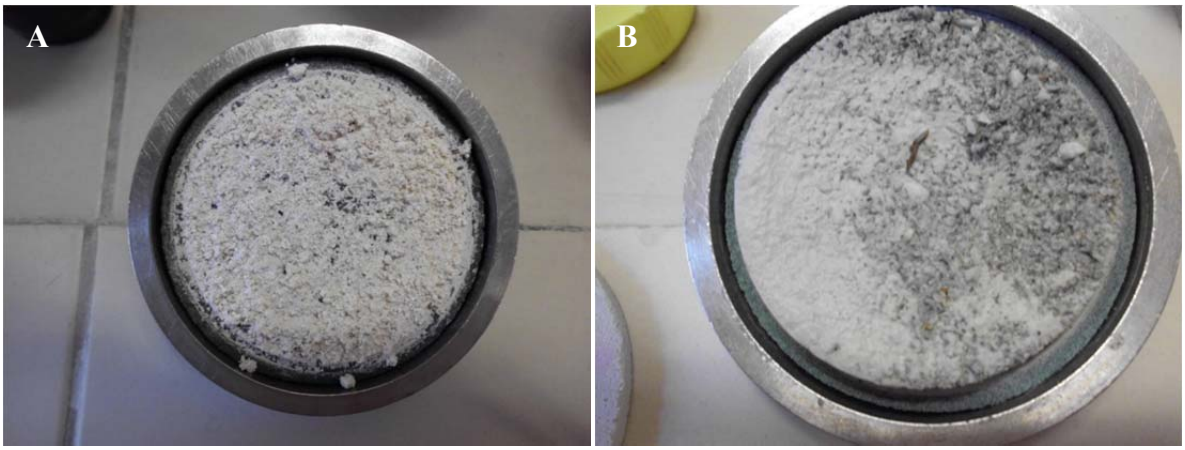

Fig. 72: *Filtration cake of lime hydrate (A) and limestone (B)*

7 CONCLUSION

The main endeavor of this work was to find a way to reduce cost of filtration process by replacing filtration units whose cost is high due to the manufacturing process which involves not only the forming of the matter which the units should have been made of (precursor material) into desired shape but the additional heat treatment by firing that the final cost of the units and hence the cost of overall filtration process makes more expensive. The way how to abate the units is mainly to avoid the additional heat treatment which involves temperatures higher than 1000 °C, because firing is expensive process which is concerned in cost from 30 % up to 50 %.So this work was based upon the attempt to make the units without additional heat treatment, by so called cementation which makes compacted bodies by bonding the grains of a granular material together using a binder which provides bridges between the grains and let the spaces between them continuous for the flow of a fluid. All of that is very simple idea but the main problem is in the porosity which caused deterioration of mechanical properties as Eq. 6 and 7 describe and Fig. 4 shows. Porosity is deleterious to mechanical properties; 10 % vol. porosity decreases the flexural strength by 50 % from the measured value for the non-porous material (see chapter 4.3.4). The first attempt to prepare such body for filtration usage was done and the results are very interesting. It does work. The main problem remains in the mechanical properties but there are many ways how to enhance them.

To summarized the result of mechanical properties testing, at first must be said that to find out the appropriate and fitting mixtures for preparation of units for various application on the field of filtration (not only the liquid suspensions but suspension broadly, thus the gaseous suspension, as well), many more blends and many more mechanical testing must be done. Necessary is to introduce additives and admixtures such as superplasticizers to reduce W/C ratio in order to enhance the strengths, maybe some foaming agents, admixtures such as blast-furnace slag, fly ash and binders on the geopolymer and alkali-activated materials basis, generally. It is truth that the binders based on geopolymer were not dealt with in too large manner here and for this purposes it is irremissible to do larger research on this field. The truth is that the disagreement between the porosity and the values of mechanical properties is of rudimental nature and trying to change it would be an attempt of falsifying basic relations and rules as written in section 4.3.4 which is pre-sentenced to fail. There are only certain ways how to enhance them as forth as possible. So this is the problem of mechanical properties but the way how to solve them is about next eventual research to enhance mechanical properties and preserve porosity, simultaneously. This thesis offers the basic sketch in form of some examples of potential mixtures for the filtration units' manufacture as described in sections 5.2 and 6.1.

The next section dealt with porosimetry which was done in case of two specimens only but this was enough to get basic idea about the porous structure of barriers prepared in the manner as done in this thesis so the blending the mortars with subsequent pressing in mold. The basic relations between pore volume, specific surface area and pore diameters were confirmed in all ways. So the lower the pore diameter, higher specific surface area and higher the cumulative pore volumes, lower the surface area. The samples (AC-220-53 and AC-150-42) are comparable by average pore diameter as shown in Table 24 (0.540 and 0.571 μm, respectively) so there is a need to try to blend many more mortars with gradual increasing of ratio of aggregates and binder and to measure porosities and to find the relationships between these properties. It is truth that it was not expect to get to so low pore diameters as mentioned

above. These pores are still considered to be mesopores (according to IUPAC) as they are larger than 50 nm in diameter. With the lower pore diameter, the penetrability of the barriers is more complicated and the barriers are of high resistance to flow of fluids. Another system is in the case of membrane processes. The membrane is a thin layer or foil (thickness in range of decimal of millimeters down to micrometers) of which is permeable for certain matter and they are being placed on a macroporous supportive body. That is the difference between membranes and our barriers. From the definition, our barriers are macroporous elements which have high thickness (range of millimeters) and if we want to go down with the pore sizes we will encounter an obstacle in the form of the resistance to fluid as mentioned above.

So the low pore size together with higher thickness of the barrier leads to so high flow of fluid resistance that the fluid is almost not able to pass through even if the pressure is elevated. In principle, it is possible to filtrate through barriers of pure cement paste but the resistance would be so high that fluid would not pass through. So it is necessary to find out such composition between the granulometry of aggregates and binder (of course together with W/C ratio) to preserve porosity insomuch that the prepared barrier will be penetrable for fluids. It is truth that the cement grains are getting lower as they are subjected to hydration process but almost never the reaction is complete. It is commonly known that the hydration process, which take place in e.g. concrete and other materials based on hydraulic binders, proceeds throughout the whole time of the using it e.g. in some concrete construction.

The pictures from microscopy show not particularly significant results which would be revolutionary. It is though better to have some idea about microstructure and that was the main purpose why the microscopy was carried out. Some various structures are observable from those with milled porcelain which is characteristic by intrinsic porosity of particles and comparison of structure with different binder content. As was mentioned, the intra-particle pores are not penetrable (at least majority of them) so they are not of essential importance as the main pores for fluid flow are the inter-particle pores i.e. voids and channel among particles of aggregates.

The capillarity experiments provide information about the ability of a fluid to pass through the porous material or a material, generally. The level of capillary forces in the case of our porous materials in the form of columns is relatively high as some of the specimens were completely permeated by water in a very short period of time (e.g. sample PC-G-0.24-32 reached the final height of 100 mm within three minutes and there are next similar to this). This may be a good indicator of material permeability and mainly very simple, because enough is if the material is observed in the touch of liquid. If the liquid rises into the material it is a sign of good permeability and potential applicability for filtration. On this very simple principle is based the calculation of diffusion coefficients of water in the porous materials which comes out of the parabolic dependence of raised liquid height squared on time. On very simple principle is based the capillary radius calculation, as well.

As concerns of the permeation measurement, this gave us a simple dependence of the logarithm of quotient of immediate and initial overpressure of air on time from which the effective permeability was calculated. The results vary according to composition as expected. The lowest effective permeability has sample AC-Por-60 which contains higher amount of binder which close the pores between the aggregates particles and hence the penetrability for fluid is more difficult.

The results of pycnometric measurement are in compliance with the results of permeation test. For example, sample AC-100-32 (2) has the highest permeability 3.072 $mol \cdot m^{-1} \cdot s^{-1} \cdot Pa^{-1}$

(not counting AC-150-42 (3) and AC-60/40-26 (2) which has K_{eff} = 3.168 and 3.085 $mol \cdot m^{-1} \cdot s^{-1} \cdot Pa^{-1}$, respectively) and it corresponds with the value of apparent porosity determined by pycnometric method (ε_a = 36.03 %). The certain deviations from the expected results are justifiable because high porosity does not need to signify high permeability. The porosity can be at high level but it does not mean that the pores are pervious for liquid thereby the permeability can decrease.

The performed filtration experiments are of demonstrative character with some basic calculations of filtration parameters including the filtration equation constants. As testing suspensions, the suspensions of lime hydrate were used. Lime hydrate is very fine material for build purposes whose milling fineness is very high (1200 $m^2 \cdot g^{-1}$ [62]). The capturing efficiency of the barriers shows Fig. 72 (picture of barrier with filtration cake). So the major fraction is captured but some smallest particles are not caught up and the filtrate is clouded so the used barrier does not capture everything. For the evaluation of amount of solid which is not captured would be needed more sophisticated equipment with turbidimeter and other units such as manometers, rotameters and others which are necessary to characterize the fluid flow in porous barriers. This is only an example and a demonstration of the utility of the barriers presented in this work.

One more time about materials based on geopolymers. The usage of geopolymers on field of filtration applications is relatively faintly researched. The geopolymers are materials which have maybe greater potential than we can ever imagine. It is not only the building application (geopolymer based concrete) and solidification of toxic waste but many more such as filtration and catalysis without exception. If we look at the structure of geopolymer (Fig. 12) and its porous nature (Fig. 15 B) the ideas about applicability of this material raises into higher levels. To use this material as functional e.g. on the field of membrane technology would bring not only the cost reduce but next utilization of secondary materials as in the case of geopolymer concretes. High surface area of those materials can lead to utilization in catalysis or adsorption processes. But it is a vision of maybe not too far future. Geopolymer material itself has its own porosity as described in chapter 4.7.2.5 and as the Fig. 14 B shows which only waits for its higher expansion. The main problem remains in the evolving of alkaline solutions if the geopolymer based material is in contact with water and other negative aspects. There would be no problem with mechanical properties as these materials are "amorphous ceramics via solution" as Šoukal, et al. [42] introduced, which means that the materials have the same properties as fired ceramics but prepared through reaction in solution at ambient temperature. And this is the rudimental mark of the replacement of fired ceramic membranes which has great potential for future.

The barriers prepared in terms of this work are of certain utility, too. The next engagement needs to be performed for the practical implementation. The barriers with PC would be used e.g. as cheap (disposable) membranes for water suspensions and waste sludge in wastewater treatment or for filtration of gaseous suspension. The barriers with AC extends the usage to the suspensions which can be of high temperature (AC resistant to high temperature, used as refractory material) or e.g. filtration of hot oils or filtration of gases entering the heat exchanger etc. AC is one order of magnitude more expensive than PC but compared to the firing and sintering, usage of AC based barriers is still cheaper and reduces the cost of not only the barriers but the overall filtration process in greater manner. The concrete cost comparison was not done but everybody can imagine that to get something to temperature of about 1000 °C runs out of the financial sources in great manner.

8 REFERENCES

[1] SPIRATOS, N., et al. *Superplasticizers for concrete: Fundamentals, technology, and practice*. 1st ed. Ottawa, Ontario: Supplementary Cementing Materials for Sustainable Development, Inc. ©2003, 2003. 322 p. ISBN 0-9731-507-1-8.

[2] JANČÁŘ, J. *Mechanics and failure of plastics*. 1st ed. Brno: FCH VUT, 2005. 140 p. ISBN 80-214-2971-2.

[3] MOHAZZABI, P., HILL, W. C. A simple method for accurate determination of porosity using ideal gas law. *Journal of Porous Materials* [online]. 2012. DOI: 10.1007/s10934-012-9613-y. Available from http://link.springer.com/article/10.1007/s10934-012-9613-y/fulltext.html. ISSN 1573-4854.

[4] WANG, J., GAN, M., SHI, J. Detection and characterization of penetrating pores in porous materials. *Materials characterization* [online]. 2007, vol. 58, no. 1 [cited 2013-03-18], p. 8–12. Available from http://www.sciencedirect.com/science/article/pii/S1044580306000817. ISSN 1044-5803.

[5] BAI, J., et al. Fabrication of porous Al2O3-based ceramics using combustion synthetized powders. *Ceramics - Silikáty* [online]. 2012, vol. 56, no. 1 [cited 2013-03-18], p. 20–24. Available from http://www.ceramics-silikaty.cz/2012/pdf/2012_01_20.pdf. ISSN 1804-5847.

[6] RIGBY, S. P., FLETCHER, R. S., RILEY, S. N. Characterization of porous solids using integrated nitrogen sorption and mercury porosimetry. *Chem .Eng. Sci.* [online]. 2004, vol. 59, no. 1 [cited 2013-03-18], p. 41–51. Available from http://www.sciencedirect.com/science/article/pii/S0009250903004792. ISSN 0009-2509.

[7] ŽIVCOVÁ-VLČKOVÁ, Z., et al. Microstructural comparison of porous oxide ceramics from the system Al2O3–ZrO2 prepared with starch as a pore-forming agent. *Journal of the European Ceramic Society* [online]. 2012, vol. 32, no. 10 [cited 2013-03-18], p. 2163–2172. Available from http://www.sciencedirect.com/science/article/pii/S0955221912000635. ISSN 0955-2219.

[8] SHE, F. H., TUNG, K. L., KONG, L. X. Calculation of effective pore diameters in porous filtration membranes with image analysis. *Robotics and Computer-Integrated Manufacturing* [online].2008, vol. 24, no. 3 [cited 2013-02-12], p. 427–434.Available from http://www.sciencedirect.com/science/article/pii/S0736584507000555. ISSN 0736-5845

[9] GUOCHENG, L., et al. Preparation and characterization of red mud sintered porous materials for water defluoridation. *Applied Clay Science* [online]. 2012 [cited 2013-03-18]. Available from http://www.sciencedirect.com/science/article/pii/S0169131712002621. ISSN 0169-1317.

[10] NANDI, B. K., UPPALURI, R., PURKAIT, M. K. Preparation and characterization of low cost ceramic membranes for micro-filtration applications. *Applied Clay Science* [online]. 2008, vol. 42, no. 1-2 [cited 2013-03-26], p. 102–110. Available from http://www.sciencedirect.com/science/article/pii/S0169131707002037. ISSN 0169-1317.

[11] KUDOVÁ, J., et al. Keramické porézní elementy pro filtraci plynů a příbuzné aplikace. *Chemické Listy* [online]. 2004, vol. 98, no. 1 [cited 2013-03-26], p. 29–32.

Available from http://www.chemicke-listy.cz/docs/full/2004_01_05.pdf . ISSN 1213-7103.

[12] DONG, Y., et al. Cost-effective tubular cordierite micro-filtration membranes processed by co-sintering. *J. Alloys Compd.* [online]. 2009, vol. 477, no. 1-2 [cited 2013-03-26], p. L35–L40. Available from http://www.sciencedirect.com/science/article/pii/S0925838808020124. ISSN 0925-8388.

[13] HANYKÝŘ, V., KUTZENDÖRFER, J. *Technologie keramiky*. 1st ed. Hradec Králové: Vega s.r.o., 2000. 310 p. ISBN 80-900860-6-3.

[14] HLAVÁČ, J. *Základy technologie silikátů*. 1st ed. Praha: SNTL - Nakladatelství technické literatury, 1981. 520 p.

[15] PTÁČEK, P., et al. *Praktikum z preparativních a testovacích metod II*. 1st ed. Brno: VUT v Brně, Fakulta chemická, 2012. 225 p. ISBN 978-80-214-4435-5.

[16] ROUQUEROL, J., et al. Recommendation for the characterization of porous solids. *Pure Appl. Chem.* [online]. 1994, vol. 66, no. 8 [cited 2013-02-25], p. 1739–1758. Available from http://www.iupac.org/publications/pac/1994/pdf/6608x1739.pdf. ISSN 1365-3075.

[17] NIELD, D. A., BEJAN, A. *Convection in Porous Media*. 3rd ed. NY: Springer Science + Business Media, Inc., 2006. 654 p. ISBN 978-0387-29096-6.

[18] LU, G. Q., ZHAO, X. S. *Nanoporous Materials: Science and Engineering*. 2004. 912 p. ISBN 978-1-86094-210-5.

[19] KANEKO, K. Determination of pore size and pore size distribution: 1. Adsorbents and catalysts. *J. Membr. Sci.* [online].1994, vol. 96, no. 1-2 [cited 2013-02-15], p. 59. Available from http://www.sciencedirect.com/science/article/pii/037673889400126X. ISSN: 0376-7388

[20] ZDRAVKOV, B. D., et al. Kategorizace pórů v porézních matricích. *Chemické listy* [online]. 2008, vol. 102, no. 6 [cited 2013-02-25], p. 434–438. Available from http://www.chemicke-listy.cz/docs/full/2008_06_434-438.pdf. ISSN 1213-7103.

[21] ZDRAVKOV, B. D., et al. Pore classification in the characterization of porous materials: A perspective. *Central European Journal of Chemistry* [online]. 2007, vol. 5, no. 2 [cited 2013-02-25], p. 385–395. Available from http://link.springer.com/article/10.2478%2Fs11532-007-0017-9?LI=true .ISSN 1644-3624.

[22] ASKELAND, D. R. *The Science and Engineering of Materials*. 2nd ed. London, UK: Chapman & Hall, 1988. 880 p. ISBN 0-412-34260-X

[23] CALLISTER, W. D. *Materials Science and Engineering: An Introduction*. 6thed. New York, NY: John Wiley & Sons, Inc., 2003. 820 p. ISBN 0-471-22471-5

[24] GALCERAN, M. Sol-gel modified Pechini method for obtaining nanocrystalline KRE(WO4) 2 (RE = Gd and Yb). *Journal of Sol-Gel Science and Technology* [online]. 2007, vol. 42 [cited 2013-03-20], p. 79–88. Available from http://www.dt-crys.net/recent_results/published/Galceran_JofSolGel_0407.pdf. ISSN 1573-4846.

[25] PALATÝ, Z., et al. *Membránové procesy*. 1st ed. Praha: vydavatelství VŠCHT, 2012. 296 p. ISBN 978-80-7080-808-5.

[26] PTÁČEK, P. Sol-gel proces, 2012. *E-learning VUT Brno*. [online] https://www.vutbr.cz/elearning/mod/resource/view.php?id=202971 (accessed March 27, 2013), Lecture on Advanced ceramic technologies.

[27] PTÁČEK, P. Společné srážení z roztoku, ostatní metody přes roztok, 2012. *E-learning VUT Brno*. [online]https://www.vutbr.cz/elearning/mod/resource/view.php?id=202972 (accessed March 27, 2013), Lecture on Advanced ceramic technologies.

[28] PTÁČEK, P. Reakce v plynné fázi, 2012. *E-learning VUT Brno*. [online] https://www.vutbr.cz/elearning/mod/resource/view.php?id=202973 (accessed March 27, 2013), Lecture on Advanced ceramic technologies.

[29] AALTOSALMI, U. *Fluid flow in porous media with the Lattice-Boltzmann method*: Ph.D. Dissertation. Department of physics: University of Jyvaskyla, 2005. 158 p.

[30] BUDD, D. A. The Relative Roles of Compaction and Early Cementation in the Destruction of Permeability in Carbonate Grainstones: A Case Study from the Paleogene of West-Central Florida, U.S.A.. *Journal of Sedimentary Research* [online]. 2002, vol. 72, no. 1 [cited 2013-03-20], p. 166–128. Available from http://jsedres.sepmonline.org/content/72/1/116.short. ISSN 1527-1404.

[31] ŠEMBERA, J. Mechanika kontinua II. část - Mechanika tekutin, TU Liberec, 2004.

[32] BADGER, W. L., BANCHERO, J. T. *Introduction to Chemical Engineering*. 1st ed. Toronto: McGraw-Hill Book Company, Inc., 1955. 753 p. ISBN 0-07-002995-4.

[33] RAKESH, P., et al. Overview of industrial filtration technology and its applications. *Indian Journal of Science and Technology* [online]. 2010, vol. 3, no. 10 [cited 2013-03-27], p. 1121–1127. Available from http://ajsih.in/index.php/indjst/article/view/29843/25803. ISSN 0974-6846.

[34] ŠNITA, D., et al. *Chemické inženýrství I*. 1st ed. Praha: vydavatelství VŠCHT, 2005. 318 p. ISBN 80-7080-589-7.

[35] RICHTER, J., STEHLÍK, P., SVĚRÁK, T. *Chemické inženýrství I*. 1st ed. Brno: VUT, Fakulta chemická, 2004. 228 p. ISBN 80-214-2568-7.

[36] ČERŇANSKÝ, A., PECIAR, M. *Separačné procesy I: Hydromechanické procesy*. 1st ed. Bratislava: Vydavateľstvo STU, 2008. 277 p. ISBN 978-80-227-2800-3.

[37] Understanding Geotextiles, 2013. Swicofil Passion for Success. http://www.swicofil.com/othermarket_geotextiles.html (accessed April 15, 2013).

[38] [AÏTCIN, P. *Vysokohodnotný beton*. 1st ed. Praha: ČKAIT, 2009. P. 74. ISBN 80-86769-39-9.

[39] COLLEPARDI, M. *Moderní beton*. 2nd ed. ČKAIT, s.r.o., 2009. P. 11–25. ISBN 978-80-87093-75-7.

[40] PYTLÍK, P. *Technologie betonu*. 2nd ed. Brno: VUTIUM, 2000. P. 9–56. ISBN 80-214-1647-5.

[41] BÍLEK, V. A bez cementu by to nešlo? In *11. Betonářské dny 2004*. ČBS Servis s.r.o. 2004. pp. 97–101. ISBN 80-903501-3-5

[42] ŠOUKAL, F., et al. Geopolymers – amorphous ceramics via solution. In *Some thermodynamic, structurals and behavioral aspects of materials accentuating non-crystalline states*. Pilsen 2009. Plzeň, CZ: OPS Nymburk, 2009. pp. 556-584. ISBN: 978-80-87269-06-0.

[43] ZHANG, Y. S., SUN, W., LI, Z. J. Hydration process of potassium polysialate (K-PSDS) geopolymer cement. *Advances in Cement Research*, 2005, vol. 17, no. 1, p. 23–28.

[44] DUXSON, P., et al. The role of inorganic polymer technology in the development of 'green concrete'. *Cem. Concr. Res.* [online]. 2007, vol. 37, no. 12 [cited 2013-03-23],

p. 1590–1597. Available from http://www.sciencedirect.com/science/article/pii/S0008884607002001. ISSN 0008-8846.

[45] ŠKVÁRA, F. Alkali activated material - geopolymer. In *Alkali Activated Materials – Research, Production and Utilization: 2007 - INTERNATIONAL CONFERENCE. 2007*, p. 661–676. ISBN 978-80-86742-18-2.

[46] [DAVIDOVITS, J. *Geopolymer Chemistry and Applications*. 2nd ed. Saint-Quentin France: Institut Géopolymère, 2008. 589 p. ISBN 2-9514820-1-9.

[47] DOMBROWSKI, K., BUCHWALD, A., WEIL, M. The influence of calcium content on the structure and thermal performance of fly ash based geopolymers. *J. Mater. Sci.* [online]. 2007, vol. 42, no. 9 [cited 2013-03-20], p. 3033–3043. DOI: 10.1007/s10853-006-0532-7. Available from http://link.springer.com/article/10.1007%2Fs10853-006-0532-7?LI=true#page-1.

[48] [48] ŠKVÁRA, F., JÍLEK, T., KOPECKÝ, L. Geopolymer materials based on fly ash. *Ceramics - Silikáty*, 2005, vol. 49, p. 198. Available from http://www.geopolymery.eu/aitom/upload/documents/ceramics_2005-03-195.pdfISSN 1804-5847.

[49] Secar 71 Product Data Sheet, 2006. Kerneos Aluminate Technologies. http://www.kerneosinc.com/pdfs/new/Secar71.pdf (accessed April 15, 2013).

[50] CEM I 52,5 N, 2013. Českomoravský cement. http://www.heidelbergcement.com/NR/rdonlyres/12140417-3206-4AE1-AD83-905CC208C681/0/TechnickylistPortlandskycementCEMI525NMokra20130322.pdf (accessed April 15, 2013).

[51] CEM I 52,5 R, 2013. Českomoravský cement. http://www.heidelbergcement.com/NR/rdonlyres/1927525C-5119-4C49-91AD-A802FC44931F/0/TechnickylistPortlandskycementCEMI525RMokra20130322.pdf (accessed April 15, 2013).

[52] Common Types of Manufactured Abrasives, 2009. *UnifiedAbrasives Manufacturers' Association*. http://www.uama.org/Abrasives101/101Types.html (accessed April 20, 2013).

[53] HELOS. Sympatec. http://www.sympatec.com/EN/LaserDiffraction/HELOS.html (accessed April 15, 2013).

[54] EXNAR, P. Characterization of porous glasses by means of porosimetry. *Ceramics - Silikáty* [online]. 1994, vol. 38, no. 1 [cited 2013-04-15], p. 16–22. Available from http://www.kch.tul.cz/publications/cc06.pdf. ISSN 1804-5847.

[55] Porosimetry. Micromeritics. http://www.micromeritics.com/Repository/Files/Porosimetry_brochure.pdf(accessed April 15, 2013).

[56] LEDNICKÝ, F. *Mikroskopie a morfologie polymerů: Mikroskopie polymerů a preparační technologie.* 1. Praha: Fastr typo-tisk, 2009. 71 s. ISBN 978-80-7372-486-3.

[57] SWAPP, S. Scanning Electron Microscopy, 2012. *Geochemical Instrumentation and Analysis.*http://serc.carleton.edu/research_education/geochemsheets/techniques/SEM.html(accessed April 19, 2013).

[58] DUTROV, B. L.; CLARK, C. M. X-ray Powder Diffraction (XRD), 2012. *Geochemical Instrumentation and Analysis*. http://serc.carleton.edu/research_education/geochemsheets/techniques/XRD.html (accessed April 21, 2013).

[59] FRIDRICH, P.; VEDRA, P.; KACÁLEK, P. Možnosti sanace vlhkého zdiva typu THERM, 2011. *Konference JUNIORSTAV 2011 FAST VUT Brno*.

http://www.fce.vutbr.cz/veda/JUNIORSTAV2011/pdf/1.2/Fridrich_Pavel_CL.pdf(accessed April 21, 2013).

[60] MEYER, K., KLOBES, P. Comparison between different presentations of pore size distribution in porous materials. *Fresenius' J. Anal. Chem.* [online]. 1999, vol. 363, no. 2 [cited 2013-04-27], p. 174–178. DOI: 10.1007/s002160051166. Available from http://link.springer.com/article/10.1007%2Fs002160051166. ISSN 1432-1130.

[61] Vápenný hydrát - bezpečnostní list, 2004. *Carmeuse natural chemicals*. http://www.carmeuse.cz/files/files/pdf_vyrobky/bl/bl_v__penn___hydr__t.pdf(accessed April 28, 2013).

[62] Profi vápenný hydrát - Jurat Kalk, 2010. *Profi stavební hmoty*. http://www.profiambau.cz/photo/sekce/file/1Profi_Jurat-Kalk.pdf (accessed April 29, 2013).

9 LIST OF ABBREVIATIONS AND SYMBOLS

a	column length	[mm]
a_{cum}	cumulative surface area	$[m^2 \cdot g^{-1}]$
A	filtration area	$[m^2]$
A_C	absorptive capacity	[%]
A_p	wall area	$[m^2]$
A_s	specific surface area	$[m^2 \cdot g^{-1}]$
AAC	alkali activated cement	
AAFA	alkali activated fly ash	
AAS	alkali activated slag	
AC	aluminate cement	
ACS	accelerated concrete setting	
b	testing column width	[mm]
BET	Brunauner-Emmett-Teller	
C	constant of filtration equation	$[m^6 \cdot s^{-1}]$
C_3A	tricalcium aluminate	
C_4AF	tetracalcium aluminoferrite	
CAH	calcium aluminate hydrate	
C_2S	dicalcium silicate	
C_3S	tricalcium silicate	
CSH	calcium silicate hydrate	
ČSN1	standard sand fine	
d	crystal inter-planar spacing	[nm]
d_{crit}	critical pore diameter	[nm]
d_e	equivalent diameter	[m]
d_p	pore diameter	[nm]
D	column diameter	[m]
D_g	diffusion coefficient of water in a material	$[cm^2 \cdot s^{-1}]$
E	modulus of elasticity	[GPa]
E_0	modulus of elasticity of non-porous material	[GPa]
EDTA	ethylenediaminetetraacetic acid	
f_b	flexural strength	[MPa]
f_c	compressive strength	[MPa]
F	force acting perpendicularly to the surface	[kN]
FA	fly ash	
FGQ	finely ground quartz	
g	gravity acceleration	$[m \cdot s^{-2}]$
G	glass	
h	height	[mm]
h_b	filtration barrier thickness	[mm]
h_c	cake thickness	[mm]
IUPAC	International union of pure and applied chemistry	
K	specific permeability	$[m^2]$
K_{eff}	effective permeability	$[mol \cdot m^{-1} \cdot s^{-1} \cdot Pa^{-1}]$
K	specific permeability tensor	$[m^2]$
l	distance between supports at bending test	[mm]

m_c	weight of filtration cake	[g]
m_d	weight of dry sample	[g]
m_f	weight of filtrate	[g]
m_{H2O}	weight of water in filtration cake	[g]
m_s	weight of sample suspended in water	[g]
m_{sf}	weight of solid corresponding to filtrate volume	[g]
m_{sl}	weight of solid elusive for barrier	[g]
m_{sp}	weight of solid phase	[g]
m_{ss}	weight of suspension	[g]
m_w	weight of wet sample	[g]
MK	metakaolin	
n	order of reflection at Bragg's equation	
NCS	normal concrete setting	
OM	optical (light) microscopy	
p	pressure	[Pa]
Δp	pressure drop	[Pa]
Δp_b	pressure drop in filtration barrier	[Pa]
Δp_c	pressure drop in filtration cake	[Pa]
Δp_0	initial overpressure at permeation test	[Pa]
PC	Portland cement	
Por	porcelain	
PP	polypropylene	
q	experimental constant at Eq. 7	[-]
r_h	hydraulic radius	[μm]
r_p	pore radius	[μm]
r_c	capillary radius	[mm]
R	molar gas constant	$[J \cdot mol^{-1} \cdot K^{-1}]$
Re	Reynolds number	[-]
s	index of cake compressibility	[-]
SEM	scanning electron microscopy	
SiC	silicon carbide	
t	time	[s]
T	thermodynamic temperature	[K]
TEOT	tetraethylorthotitanate	
TMOS	tetramethoxysilane	
u	flow rate	$[m \cdot s^{-1}]$
u_ε	flow rate in channels of barrier	$[m \cdot s^{-1}]$
$\mathbf{u}$	flow rate vector	$[m \cdot s^{-1}]$
V	total volume	$[m^3]$
$\dot{V}$	volume flow	$[m^3 \cdot s^{-1}]$
V_a	volume of compressor air jet	$[m^3]$
V_{cum}	cumulative volume	$[cm^3 \cdot g^{-1}]$
V_f	volume of filtrate	$[m^3]$
V_{fb}	volume of filtrate forming filtration cake	$[m^3]$
V_p	pore volume	$[cm^3]$
V_{sp}	volume of solid phase	$[cm^3]$

ΔV_i	incremental pore volume	[$cm^3 \cdot g^{-1}$]
W/C	water cement ratio	
WG Na	sodium water glass	
$x_{0.5}$	median of particle sizes	[μm]
$x_{0.9}$	0.9 quantile of particle sizes	[μm]
$x_{0.99}$	0.99 quantile of particle sizes	[μm]
$x_c^{'}$	humidity of filtration cake	[%]
x_s	weight concentration of suspension	[%]
XRD	X-ray diffraction	
α	specific cake resistance	[$kg^{-1} \cdot m$]
β	angular coefficient in Eq. 39	[s^{-1}]
γ	surface tension	[$N \cdot m^{-1}$]
ε	porosity	[%]
ε_a	apparent porosity	[%]
ε_t	true porosity	[%]
η	dynamic viscosity	[Pa·s]
θ	incident angle	[°]
λ	wavelength	[nm]
λ_s	friction coefficient for flow in porous barrier	[-]
φ	contact angle	[°]
ρ_b	bulk density	[$kg \cdot m^{-3}$]
ρ_{H2O}	density of water	[$kg \cdot m^{-3}$]
ρ_l	liquid density	[$kg \cdot m^{-3}$]
ρ_s	solid phase density	[$kg \cdot m^{-3}$]
ρ_{sp}	solid phase density	[$kg \cdot m^{-3}$]
ρ_{sw}	specific weight	[$kg \cdot m^{-3}$]
ρ_t	true density	[$kg \cdot m^{-3}$]
σ_{fs}	flexural strength	[MPa]
σ_0	flexural strength of non-porous material	[MPa]
∇	Hamilton's operator	

10 LIST OF SUPPLEMENTS

Supplement 1: *Distribution of particle sizes – PC CEM I 52.5 N*
Supplement 2: *Distribution of particle sizes – PC CEM I 52.5 N*
Supplement 3: *Distribution of particle sizes – Metakaolin Mefisto L05*
Supplement 4: *Distribution of particle sizes – Metakaolin Mefisto K05*
Supplement 5: *Distribution of particle sizes – SiC F40*
Supplement 6: *Distribution of particle sizes – SiC F60*
Supplement 7: *Distribution of particle sizes – SiC F100*
Supplement 8: *Distribution of particle sizes – SiC F150*
Supplement 9: *Distribution of particle sizes – SiC F220*
Supplement 10: *Distribution of particle sizes – milled porcelain*
Supplement 11: *Distribution of particle sizes – milled glass 0.12 – 0.24 mm*
Supplement 12: *Distribution of particle sizes – milled glass 0.24 – 0.40 mm*
Supplement 13: *Distribution of particle sizes – FGQ*
Supplement 14: *XRD spectrum – Metakaolin Mefisto L05*
Supplement 15: *XRD spectrum – Metakaolin Mefisto K05*
Supplement 16: *XRD spectrum – standard sand fine (ČSN 1)*
Supplement 17: *Structure of PC-Por-40. Magnification: X100 (SEM)*
Supplement 18: *Structure of PC-Por-40. Magnification: X500 (SEM)*
Supplement 19: *Structure of PC-Por-40. Magnification: X1000 (SEM)*
Supplement 20: *Structure of PC-Por-40. Magnification: X2500 (SEM)*
Supplement 21: *Structure of PC-Por-60. Magnification: X500 (SEM)*
Supplement 22: *Structure of PC-Por-60. Magnification: X1000 (SEM)*
Supplement 23: *Structure of PC-Por-60. Magnification: X2500 (SEM)*
Supplement 24: *Structure of AC-Por-40. Magnification: X100 (SEM)*
Supplement 25: *Structure of AC-Por-40. Magnification: X500 (SEM)*
Supplement 26: *Structure of AC-Por-40. Magnification: X1000 (SEM)*
Supplement 27: *Structure of AC-Por-40. Magnification: X2500 (SEM)*
Supplement 28: *Structure of AC-Por-60. Magnification: X100 (SEM)*
Supplement 29: *Structure of AC-Por-60. Magnification: X1000 (SEM)*
Supplement 30: *Structure of AC-150-42. Magnification: X100 (SEM)*
Supplement 31: *Structure of AC-150-42. Magnification: X1000 (SEM)*
Supplement 32: *Structure of AC-150-42. Magnification: X2500 (SEM)*
Supplement 33: *Permeation measurement plot – AC-100-32*
Supplement 34: *Permeation measurement plot – AC-60/40-26 (1)*
Supplement 35: *Permeation measurement plot – AC-60/40-26 (2)*
Supplement 36: *Permeation measurement plot – AC-150-42 (2)*
Supplement 37: *Permeation measurement plot – AC-150-42 (3)*
Supplement 38: *Permeation measurement plot – AC-Por-40*
Supplement 39: *Permeation measurement plot – PC-G-0.24-32*
Supplement 40: *Permeation measurement plot – AC-G-0.24-32*
Supplement 41: *Permeation measurement plot – AC-100-32 (1)*
Supplement 42: *Permeation measurement plot – AC-100-32 (2)*
Supplement 43: *Permeation measurement plot – AC-100-32 (3)*

11 SUPPLEMENT

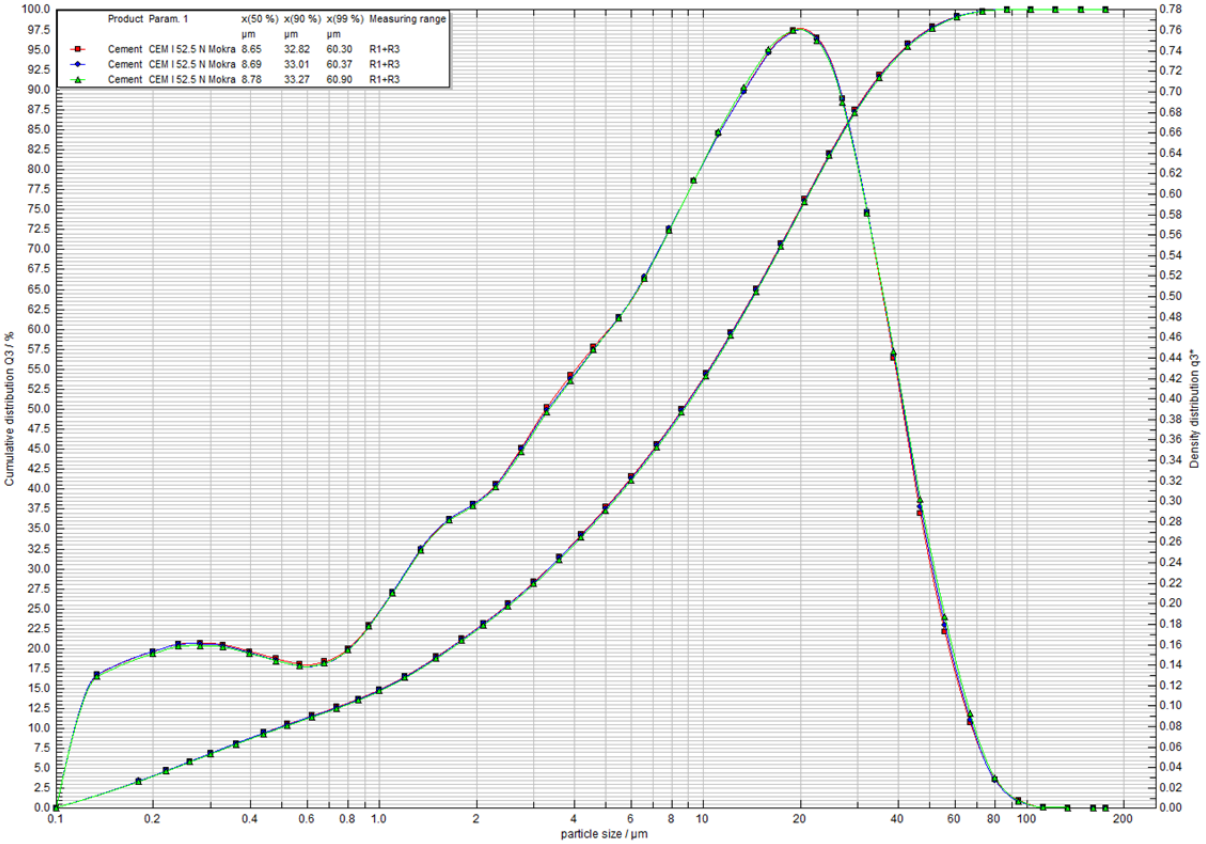

Supplement 1: *Distribution of particle sizes – PC CEM I 52.5 N*

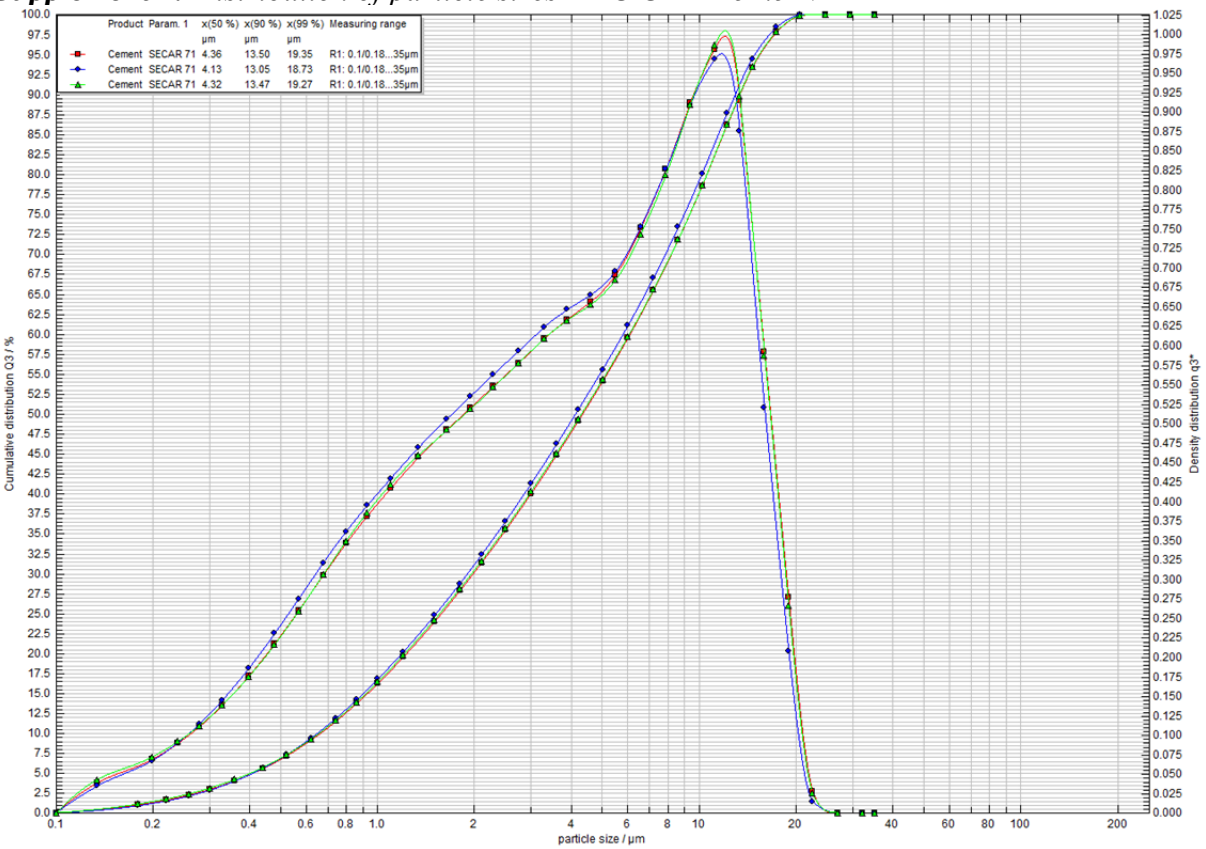

Supplement 2: *Distribution of particle sizes – PC CEM I 52.5 N*

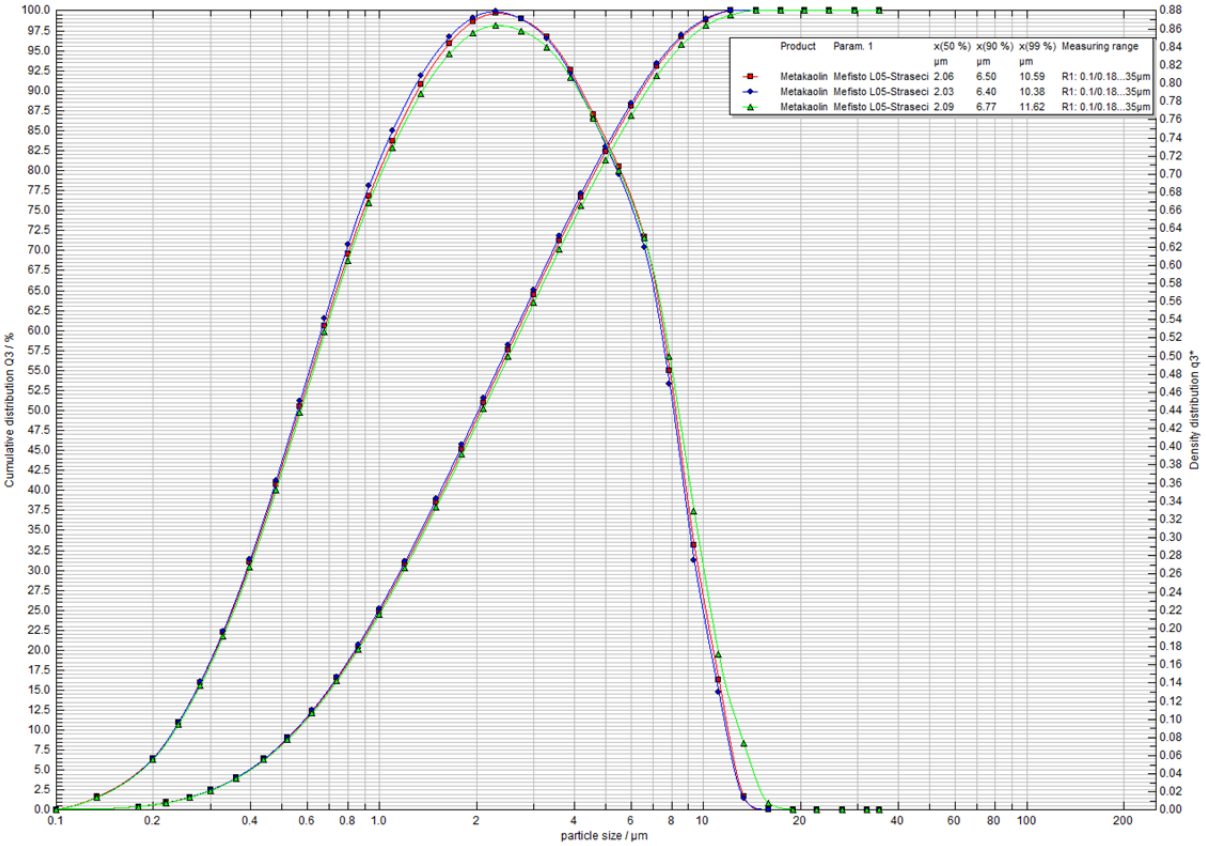

Supplement 3: *Distribution of particle sizes – Metakaolin Mefisto L05*

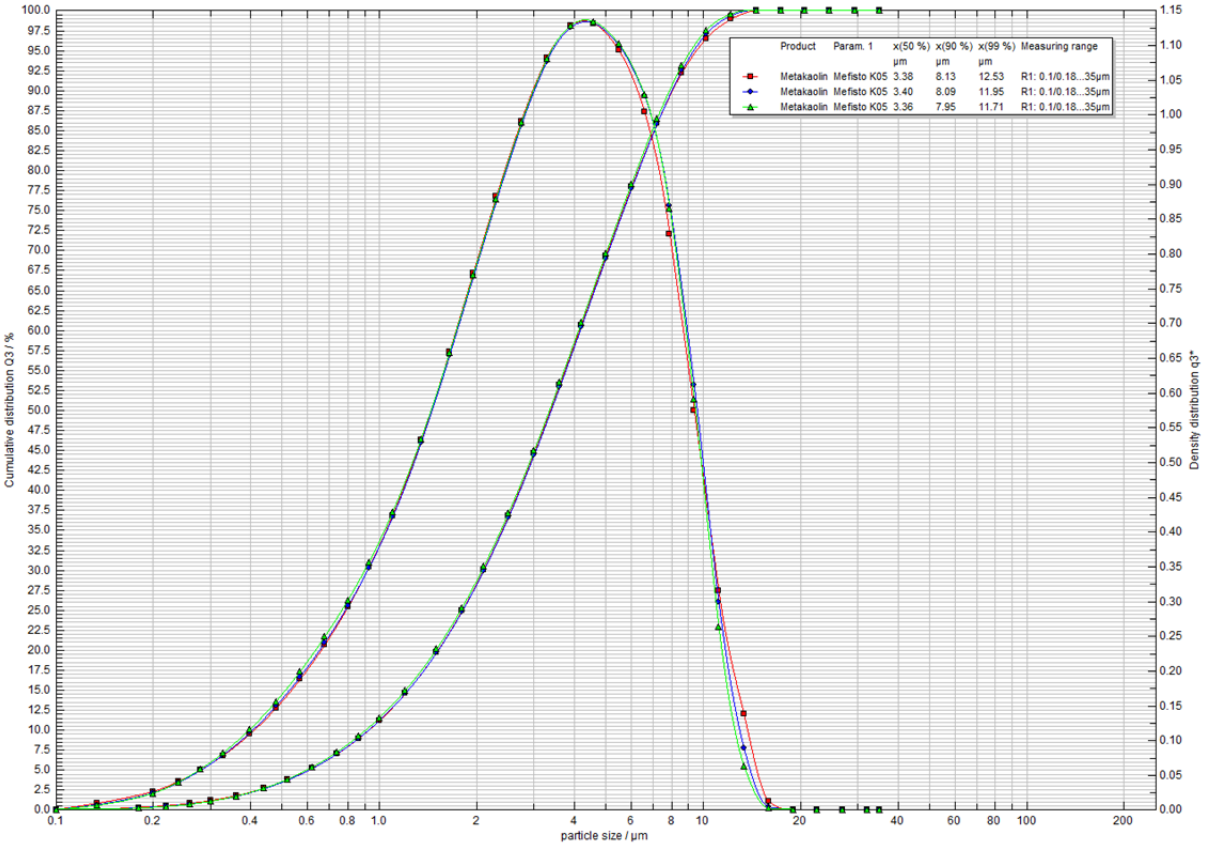

Supplement 4: *Distribution of particle sizes – Metakaolin Mefisto K05*

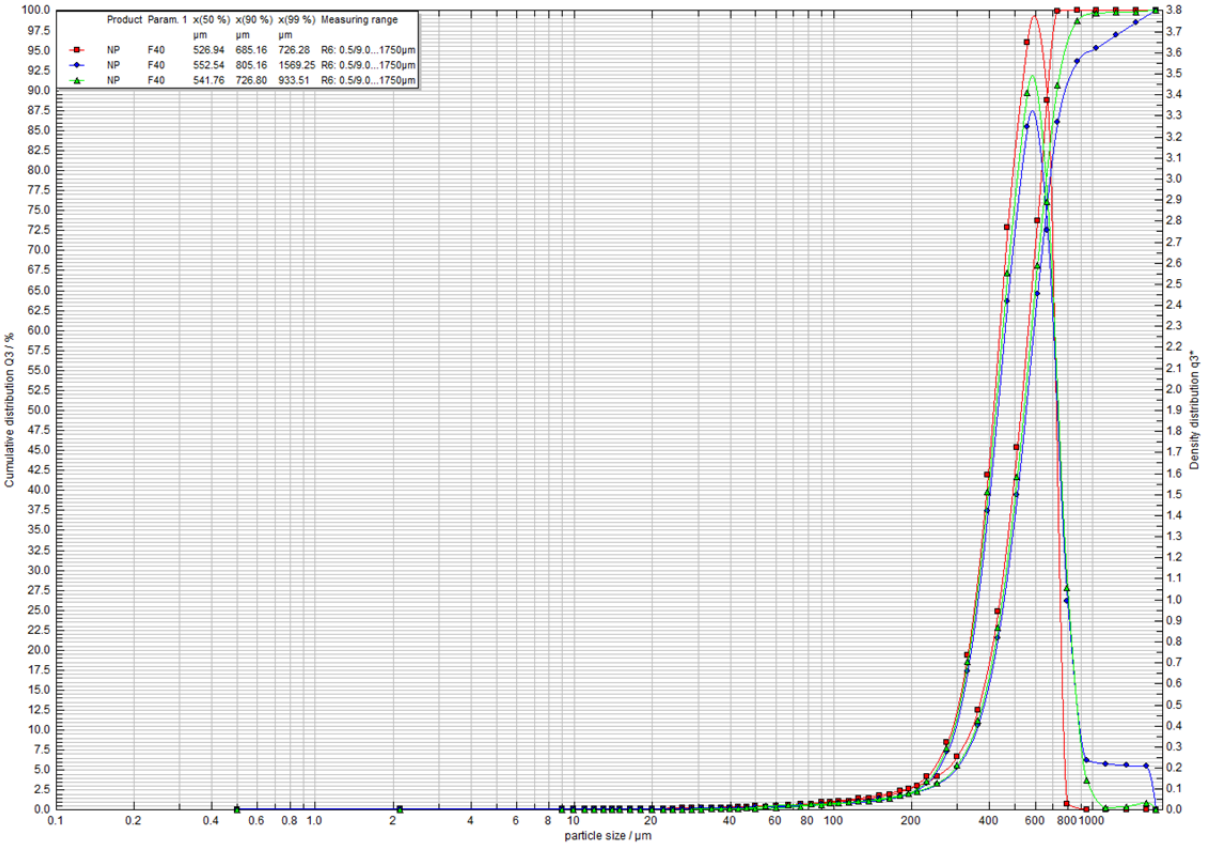

Supplement 5: *Distribution of particle sizes – SiC F40*

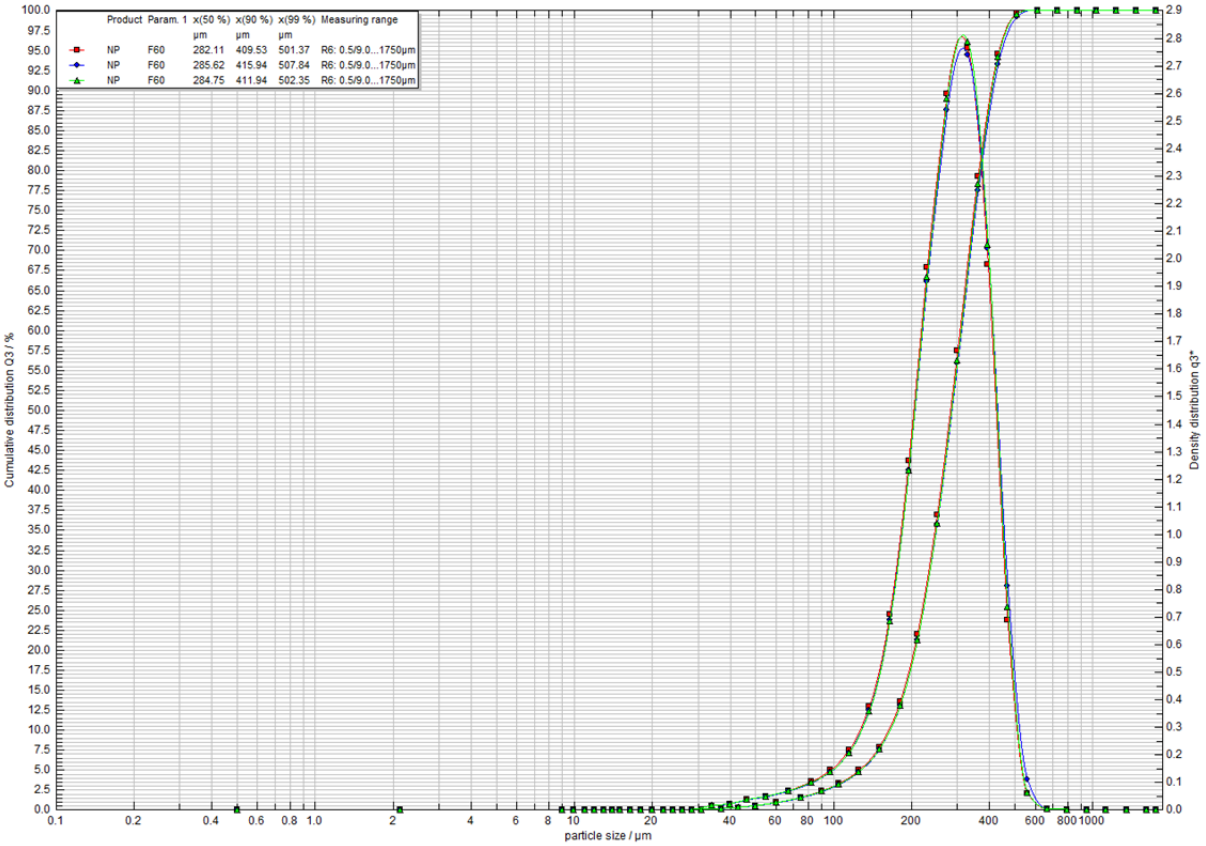

Supplement 6: *Distribution of particle sizes – SiC F60*

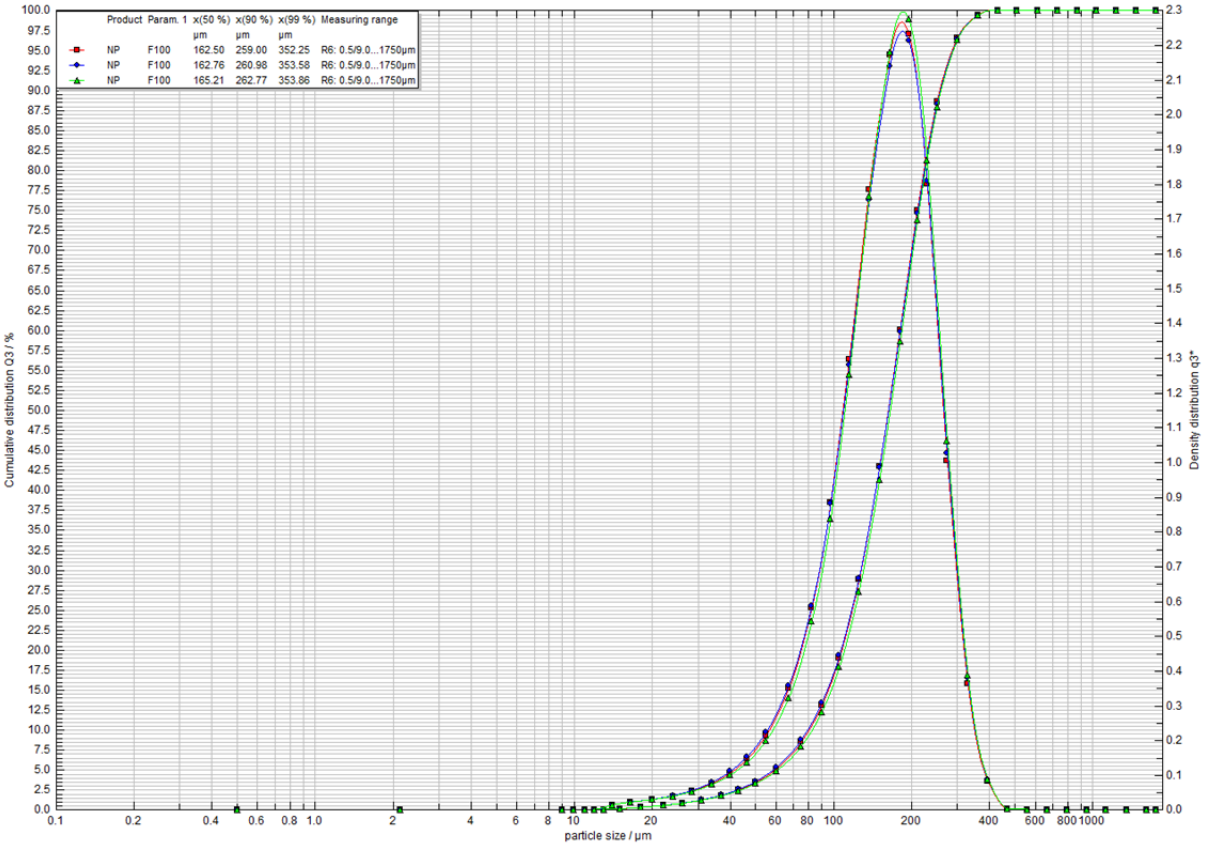

Supplement 7: *Distribution of particle sizes – SiC F100*

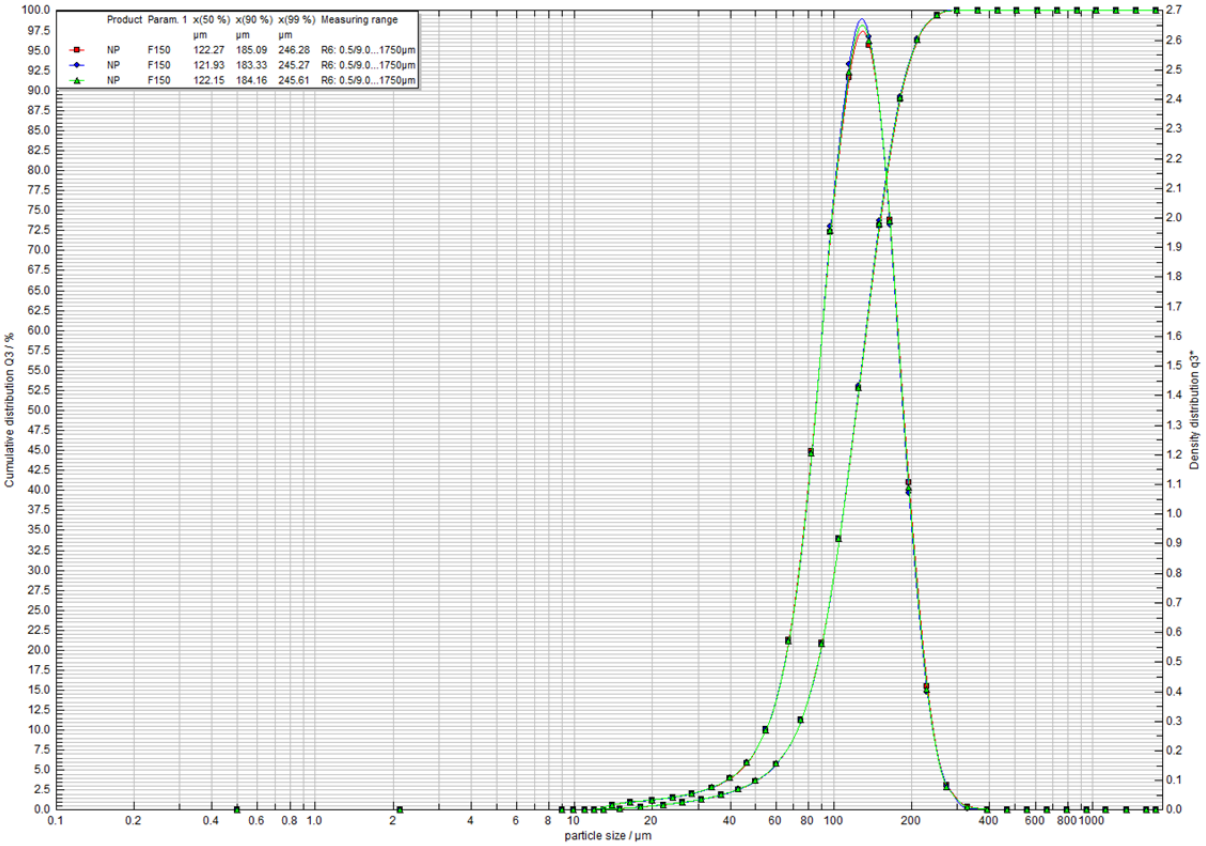

Supplement 8: *Distribution of particle sizes – SiC F150*

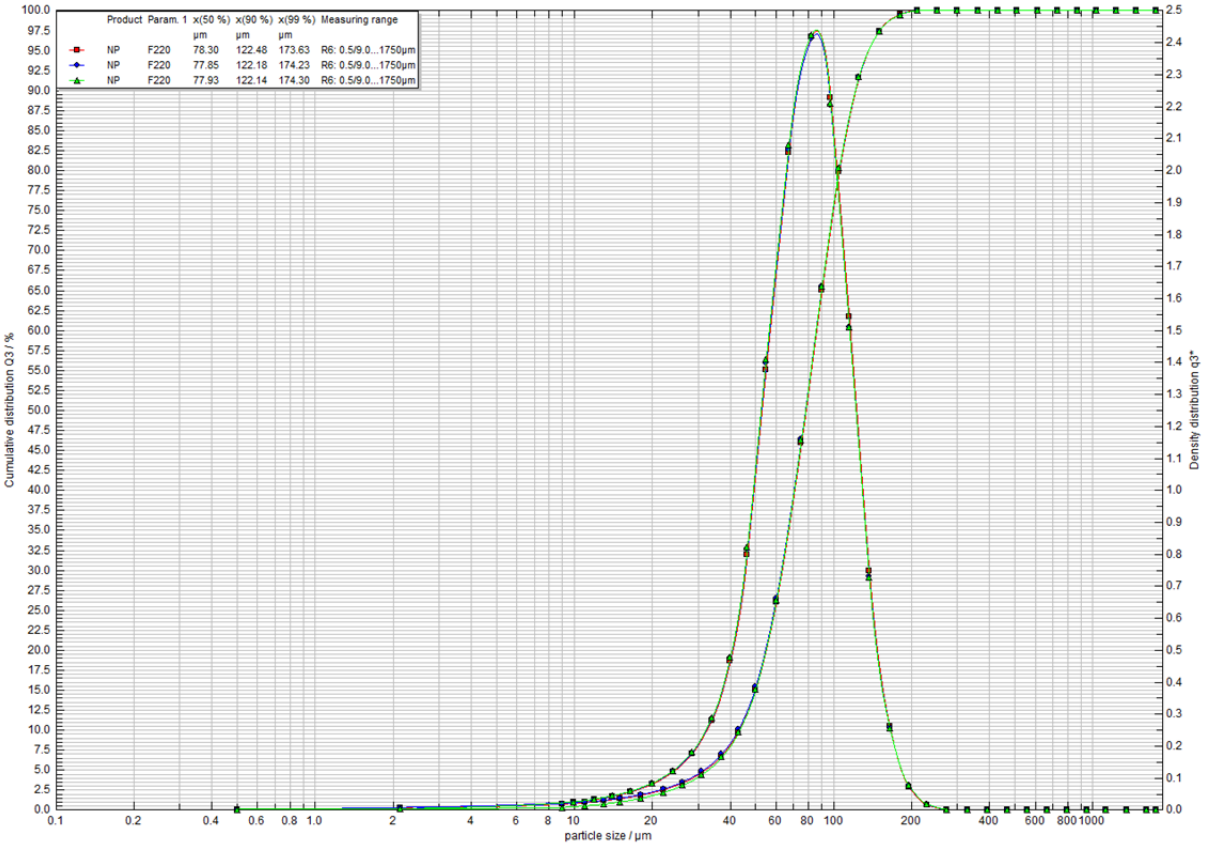

Supplement 9: *Distribution of particle sizes – SiC F220*

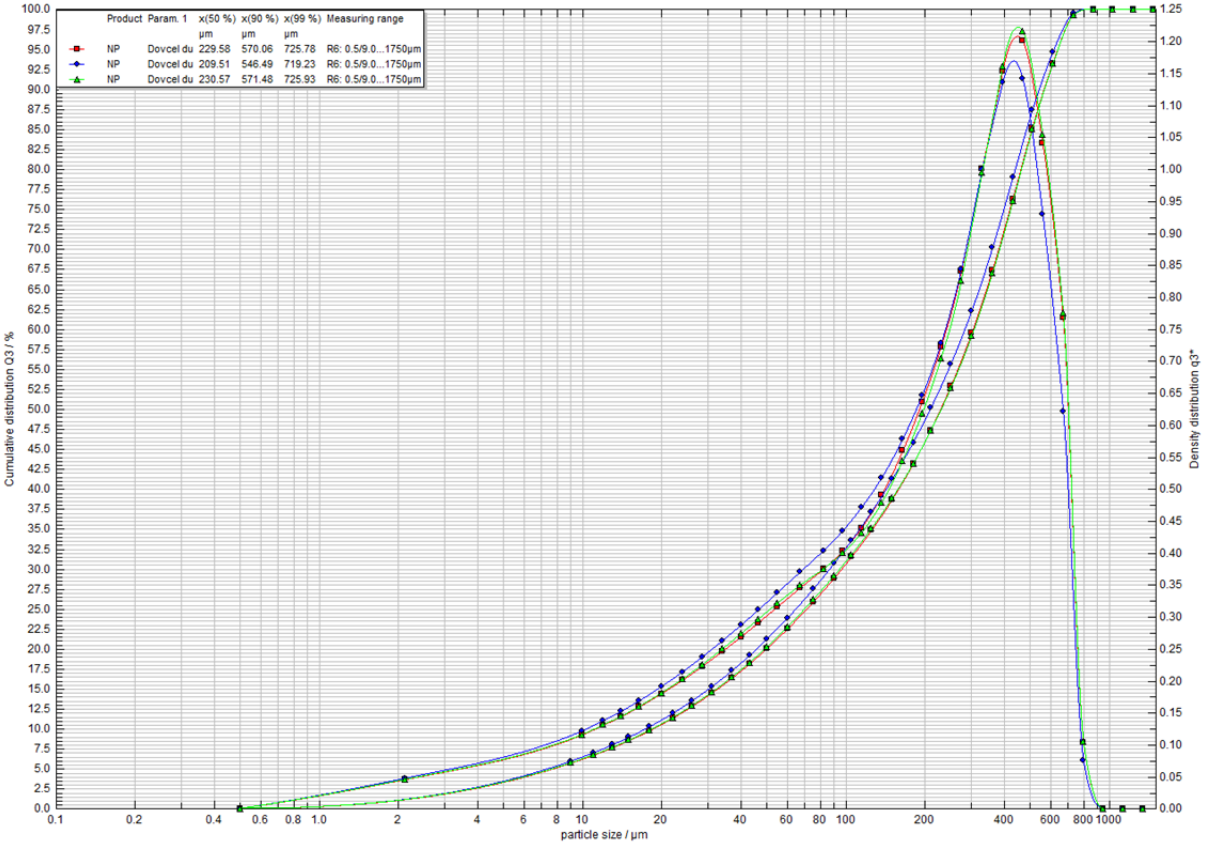

Supplement 10: *Distribution of particle sizes – milled porcelain*

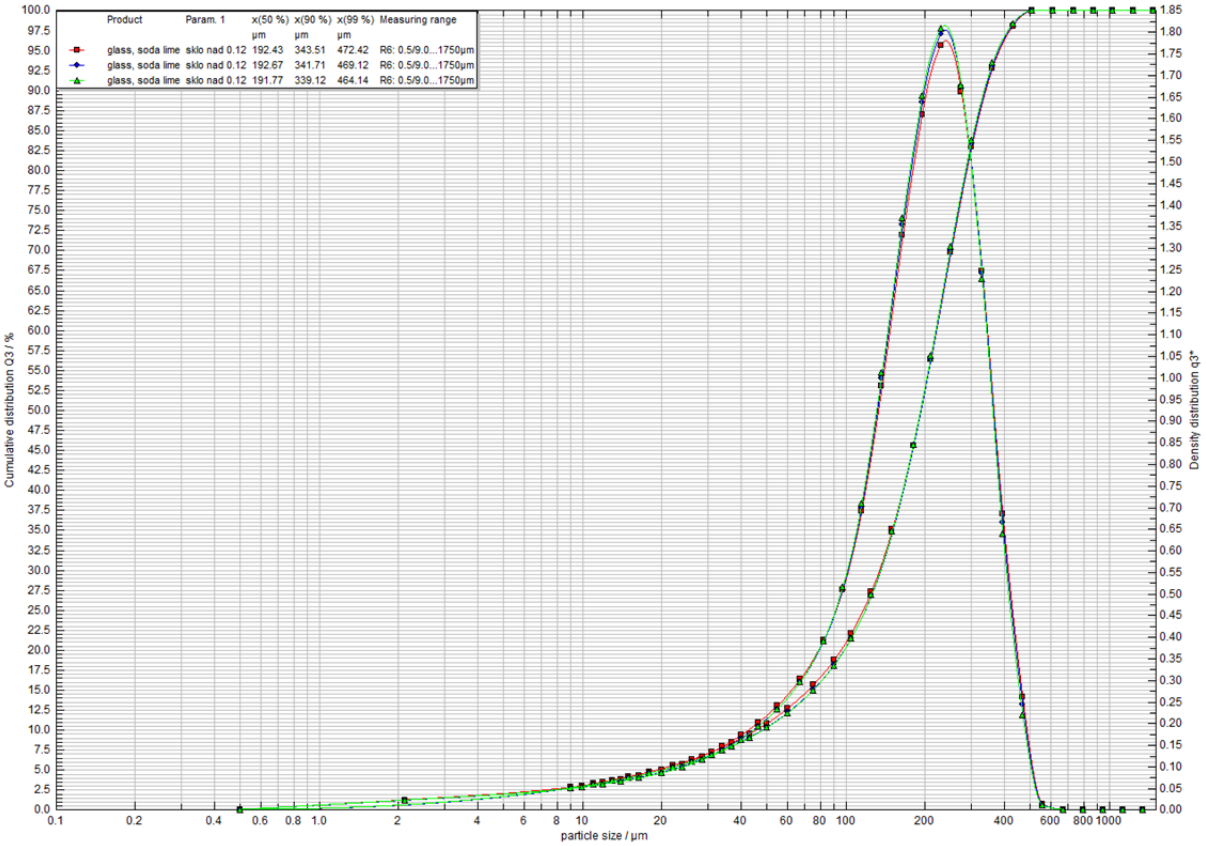

Supplement 11: *Distribution of particle sizes – milled glass 0.12 – 0.24 mm*

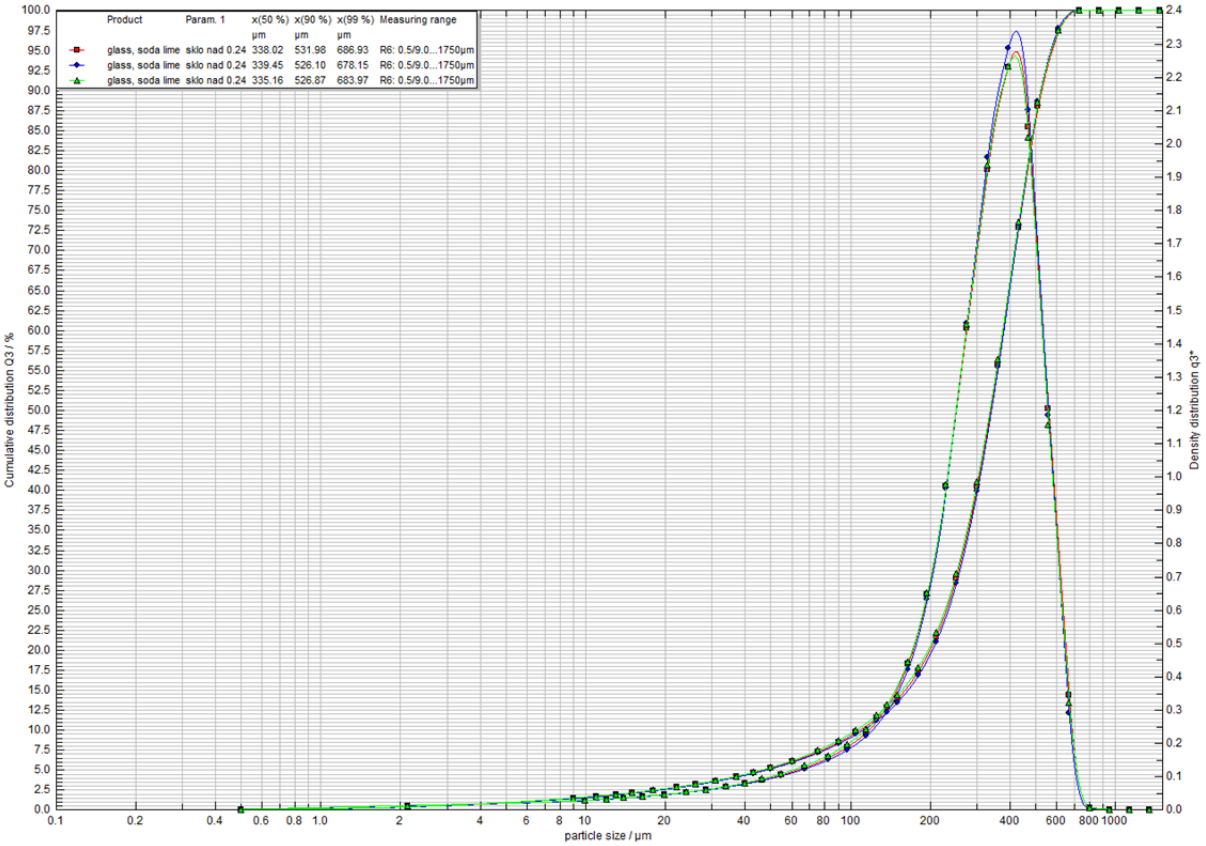

Supplement 12: *Distribution of particle sizes – milled glass 0.24 – 0.40 mm*

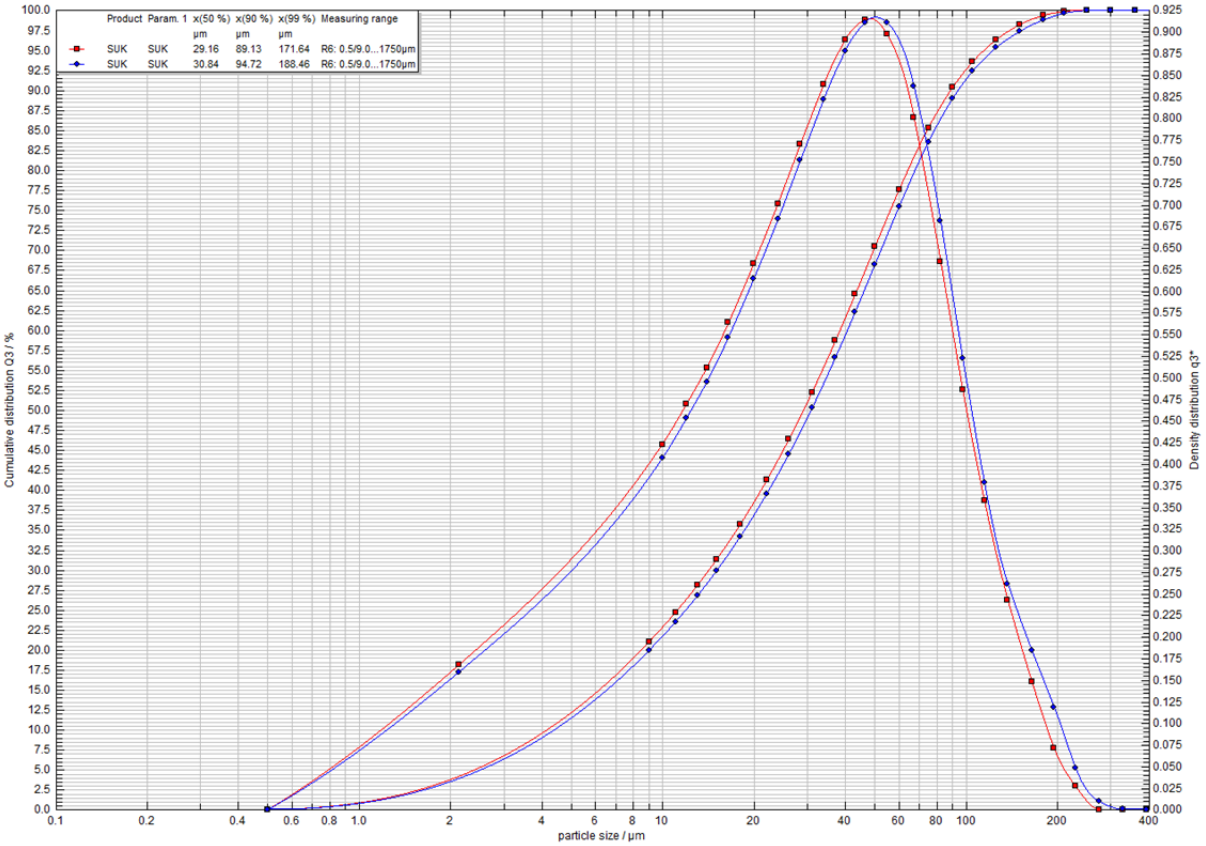

Supplement 13: *Distribution of particle sizes – FGQ*

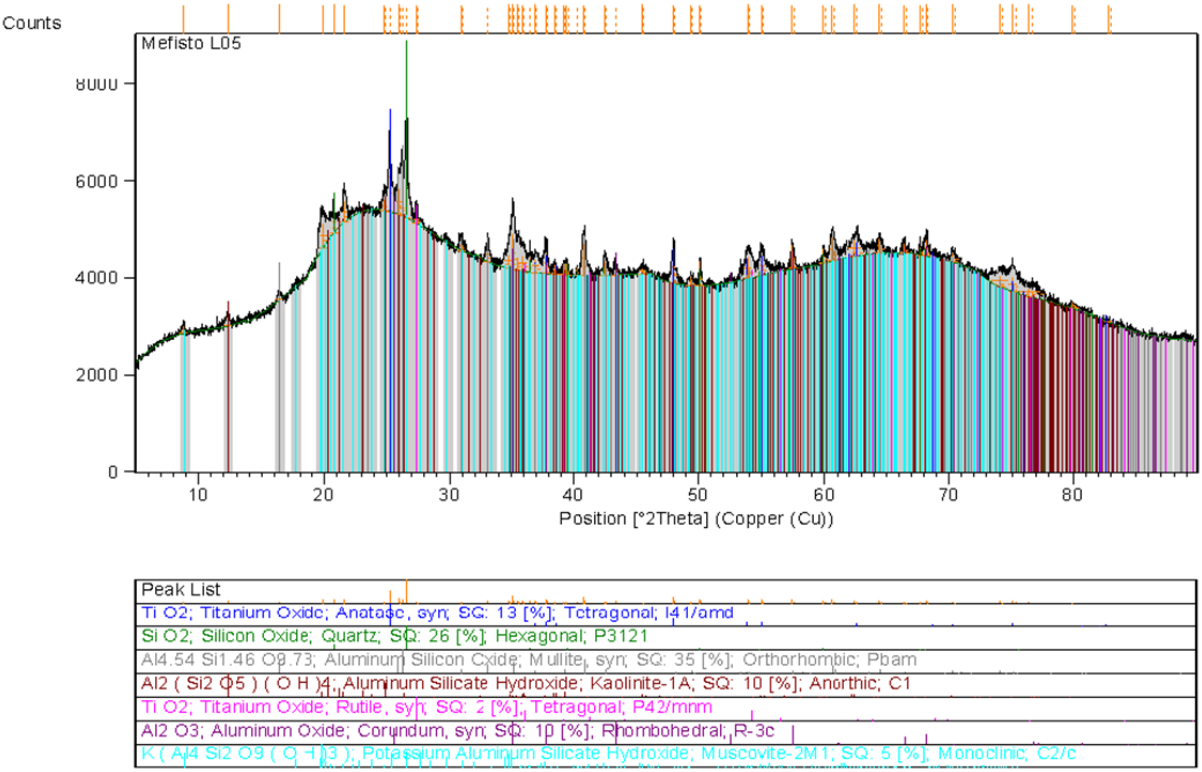

Supplement 14: *XRD spectrum – Metakaolin Mefisto L05*

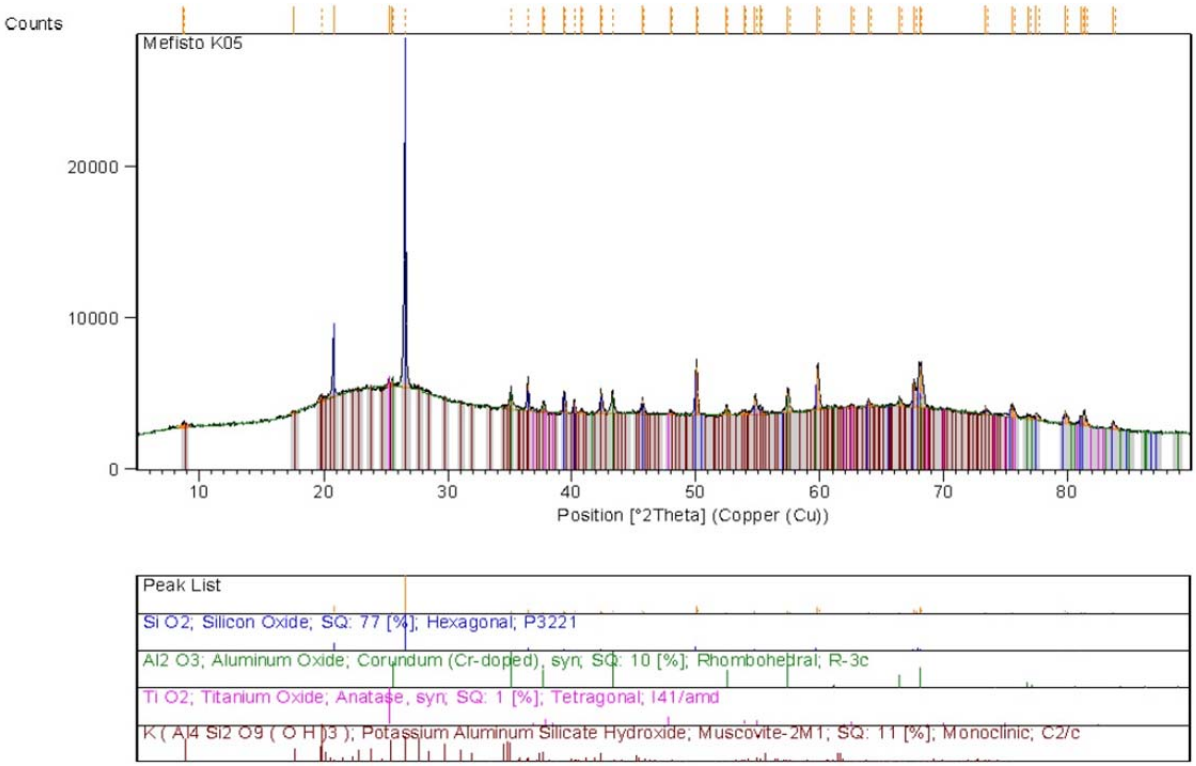

Supplement 15: *XRD spectrum – Metakaolin Mefisto K05*

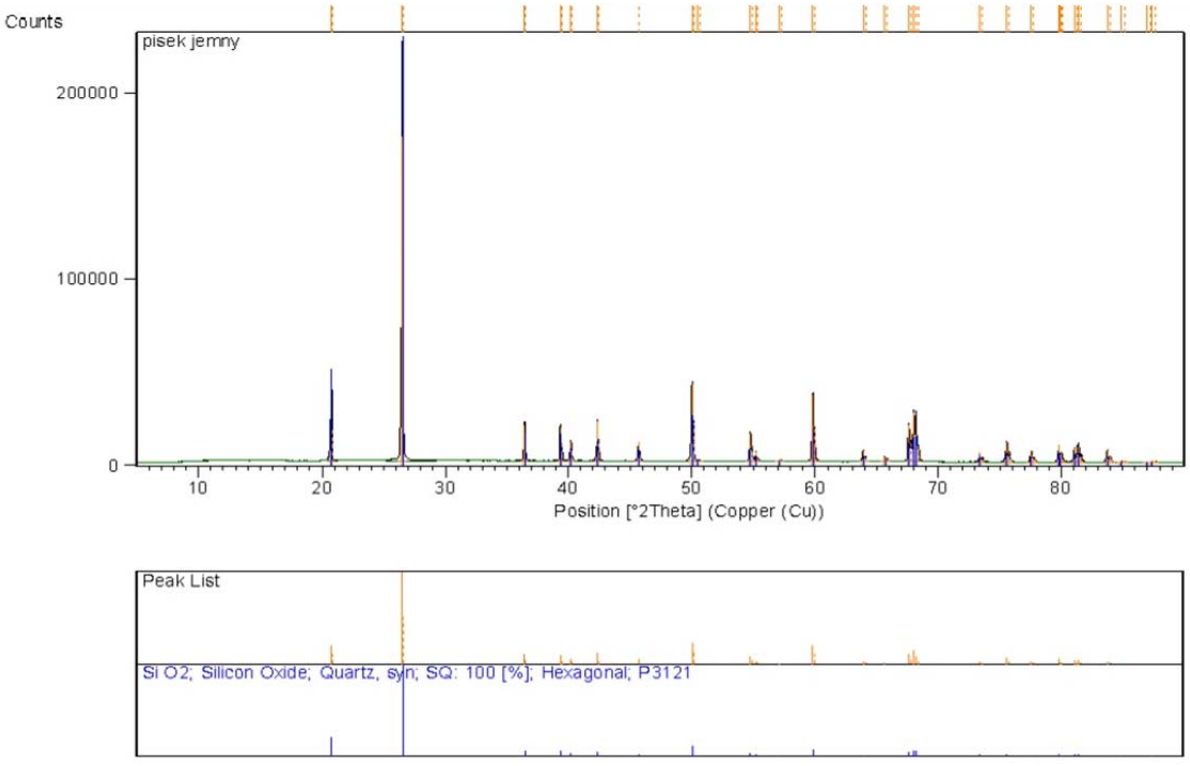

Supplement 16: *XRD spectrum – standard sand fine (ČSN 1)*

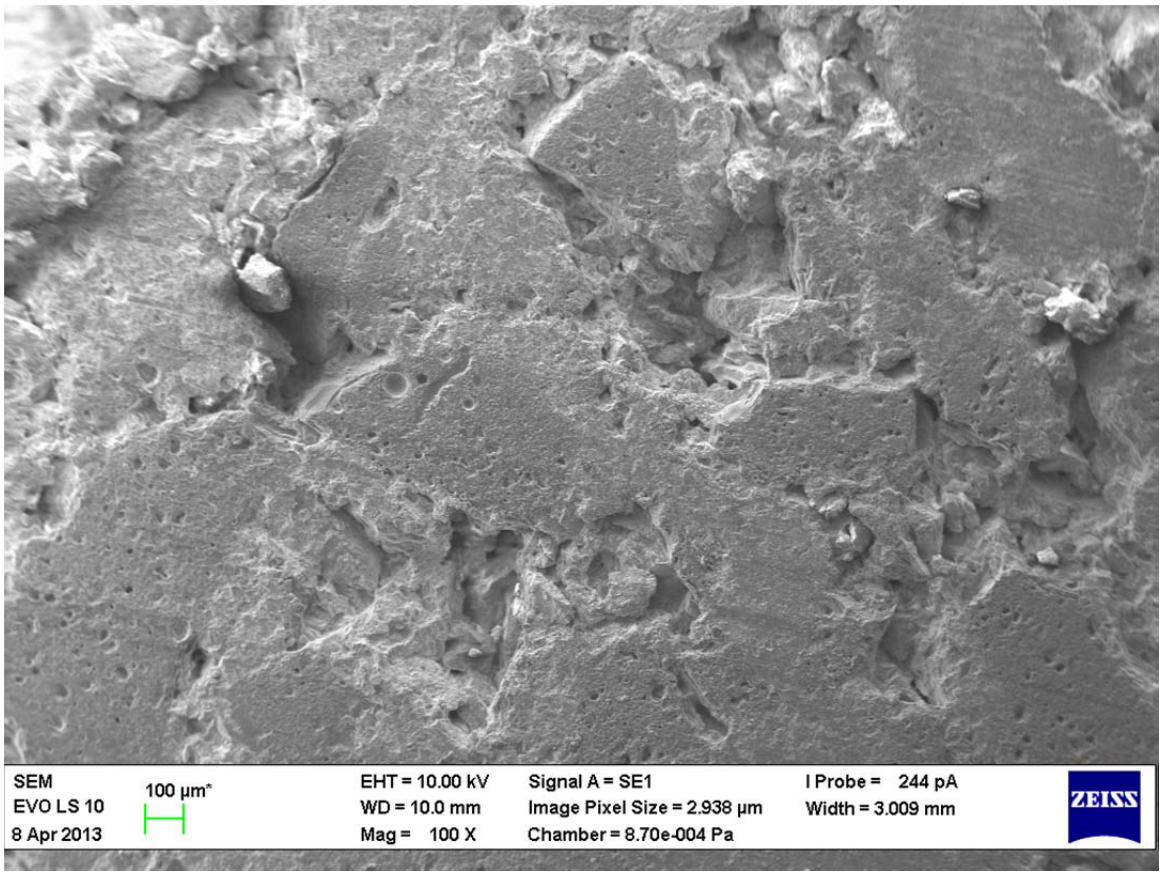

Supplement 17: *Structure of PC-Por-40. Magnification: X100 (SEM)*

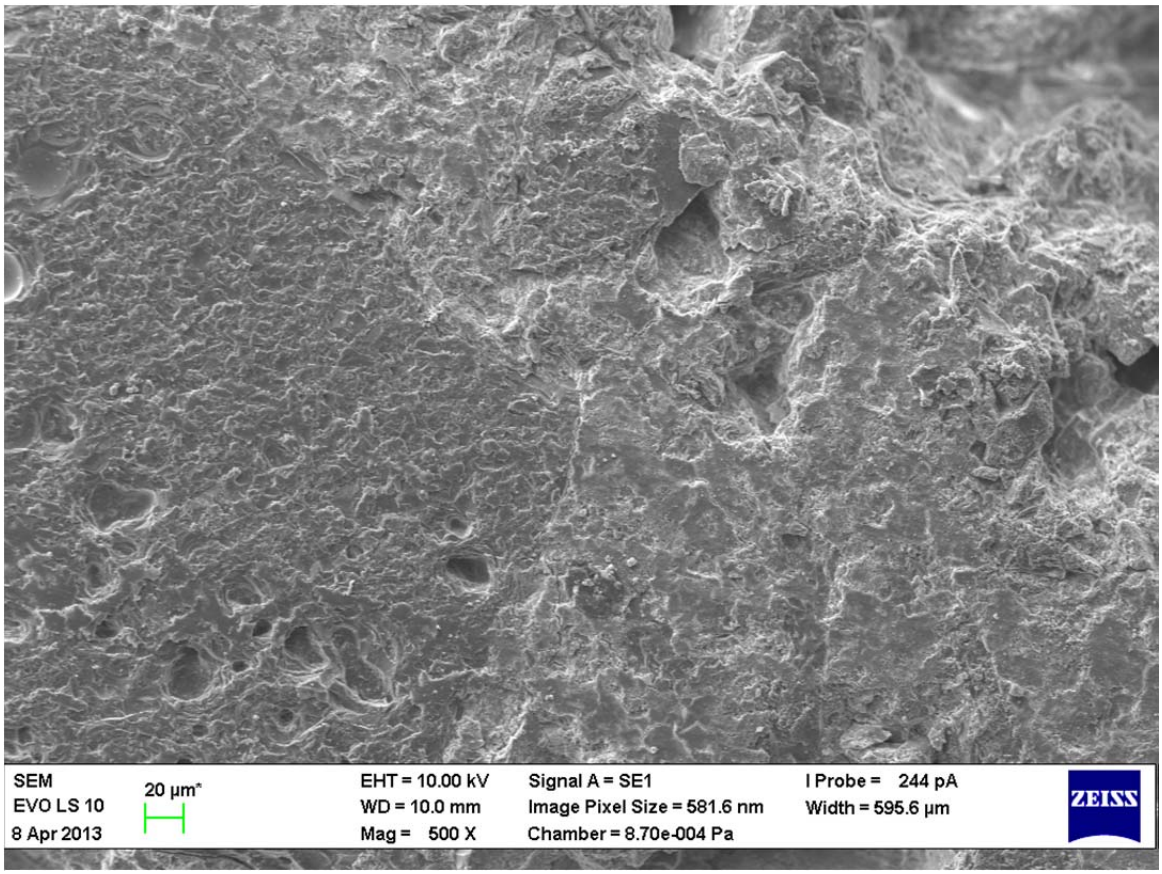

Supplement 18: *Structure of PC-Por-40. Magnification: X500 (SEM)*

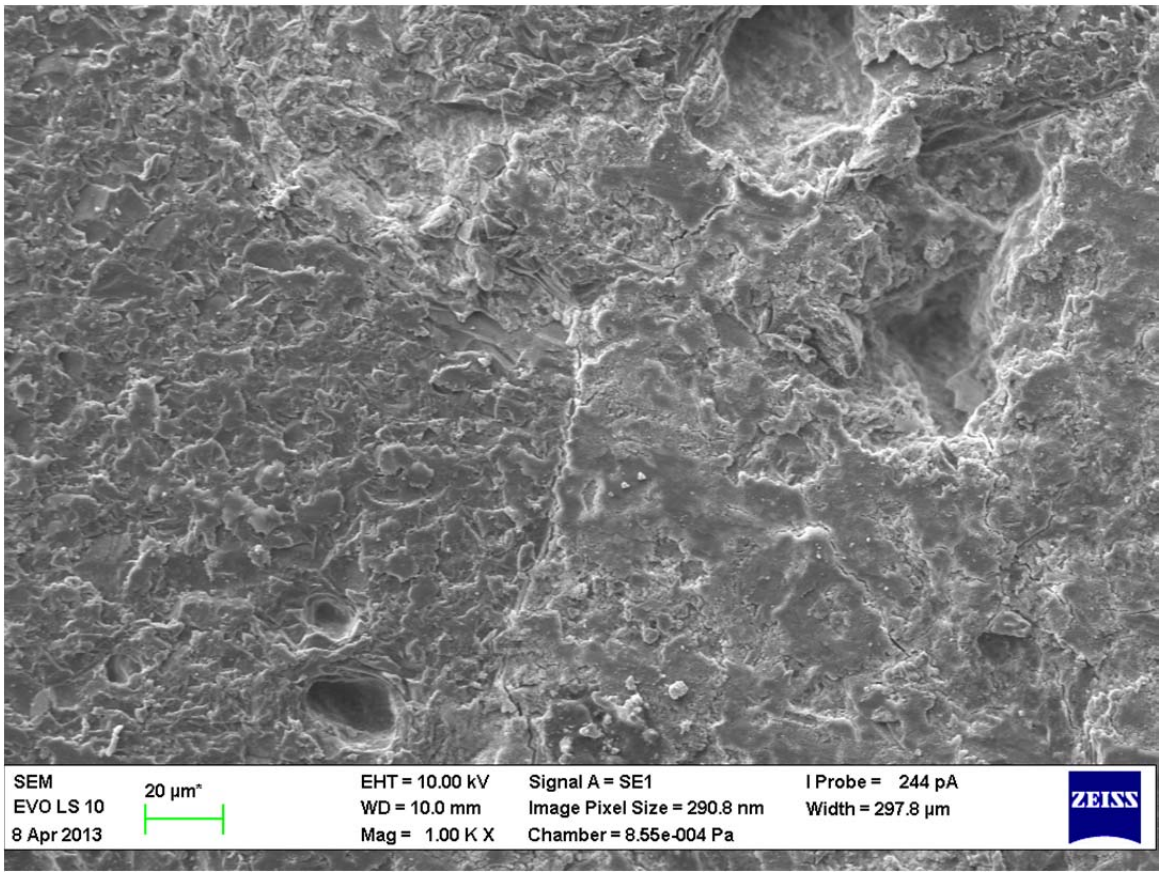

Supplement 19: *Structure of PC-Por-40. Magnification: X1000 (SEM)*

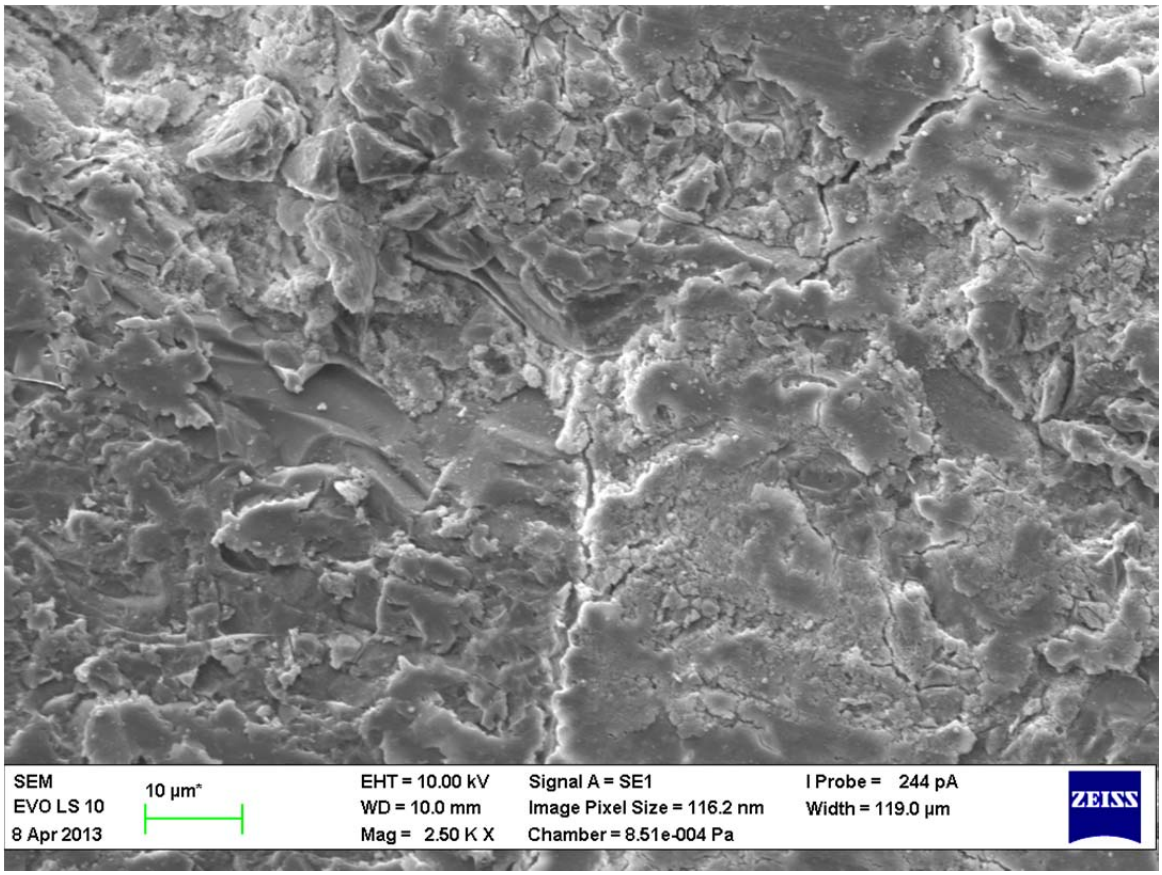

Supplement 20: *Structure of PC-Por-40. Magnification: X2500 (SEM)*

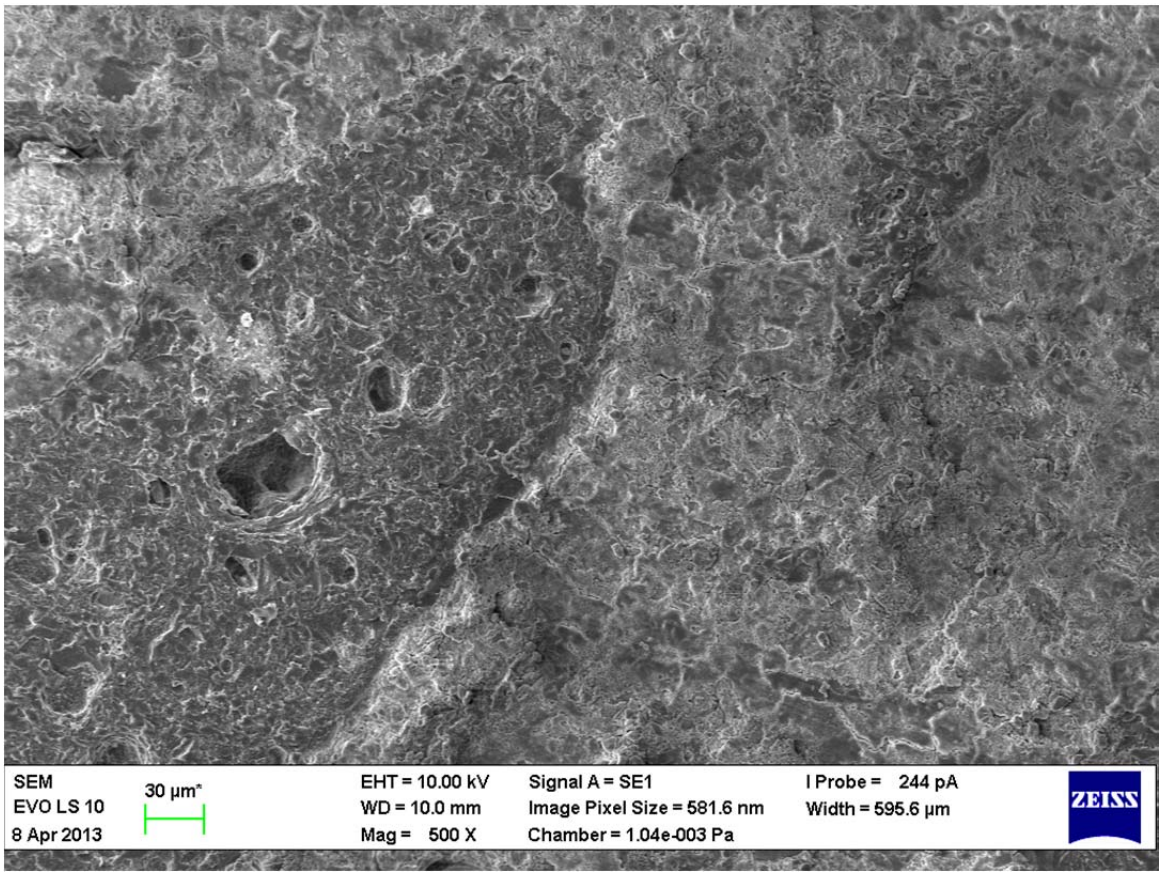

Supplement 21: *Structure of PC-Por-60. Magnification: X500 (SEM)*

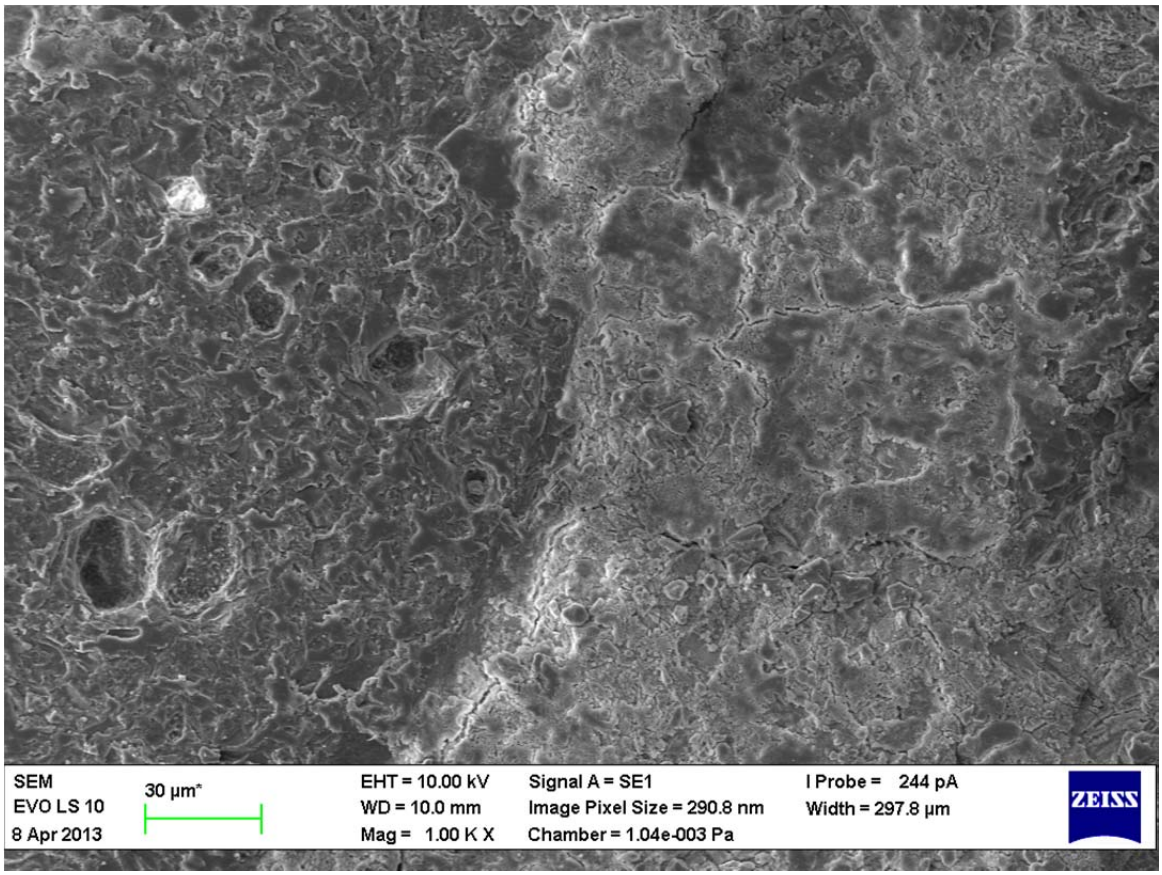

Supplement 22: *Structure of PC-Por-60. Magnification: X1000 (SEM)*

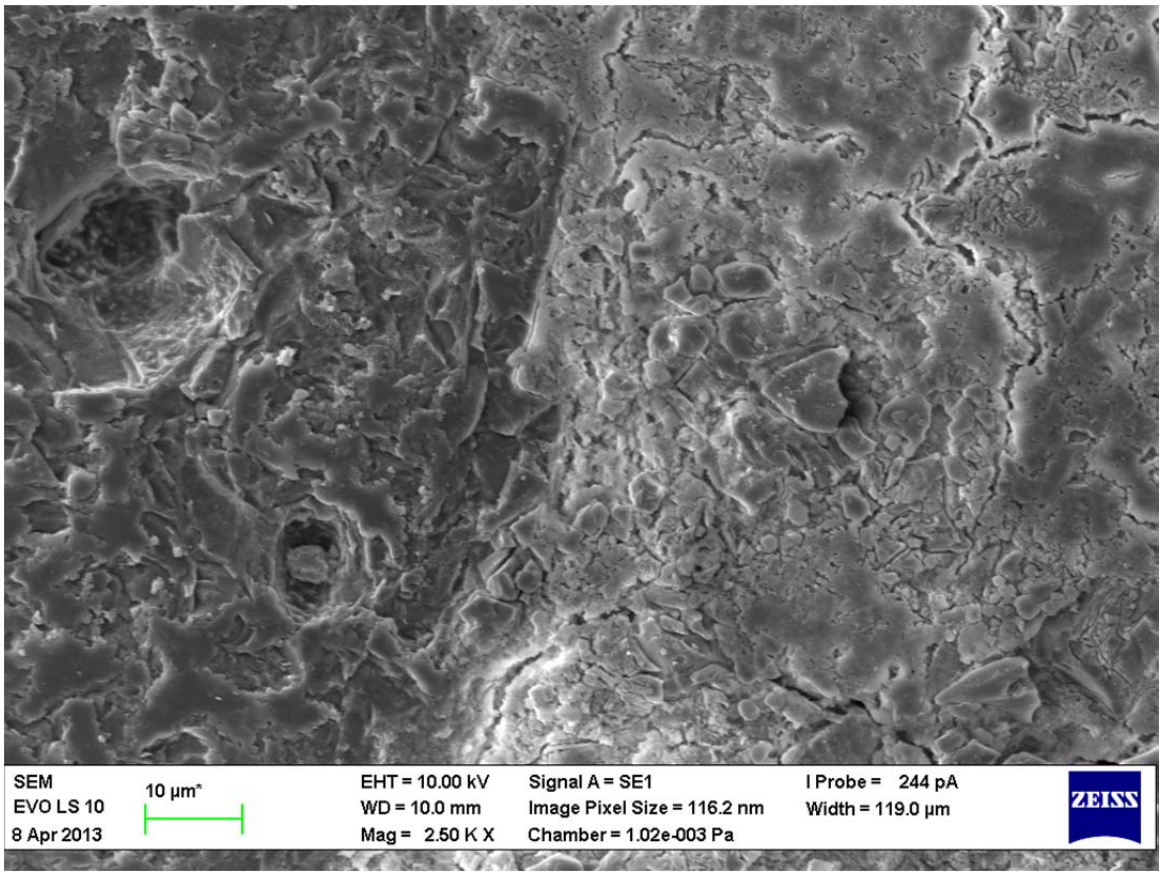

Supplement 23: *Structure of PC-Por-60. Magnification: X2500 (SEM)*

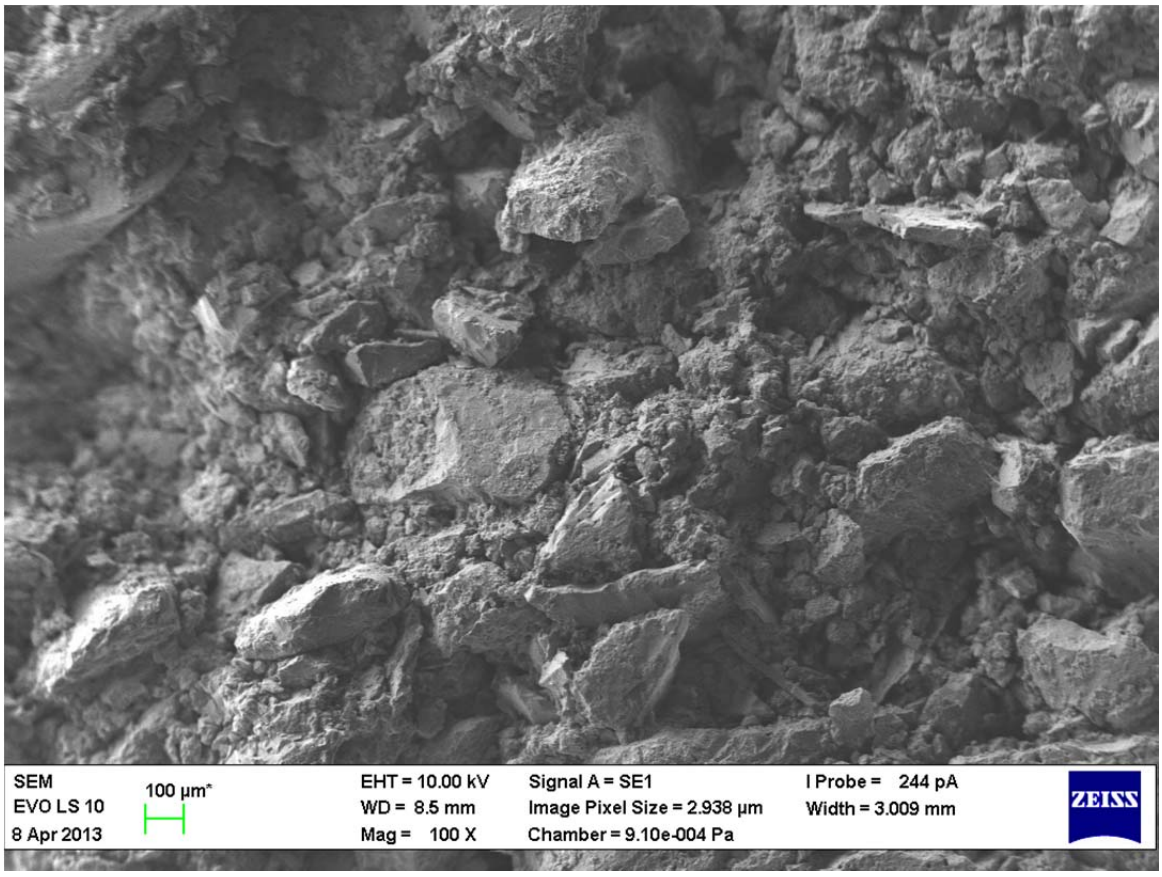

Supplement 24: *Structure of AC-Por-40. Magnification: X100 (SEM)*

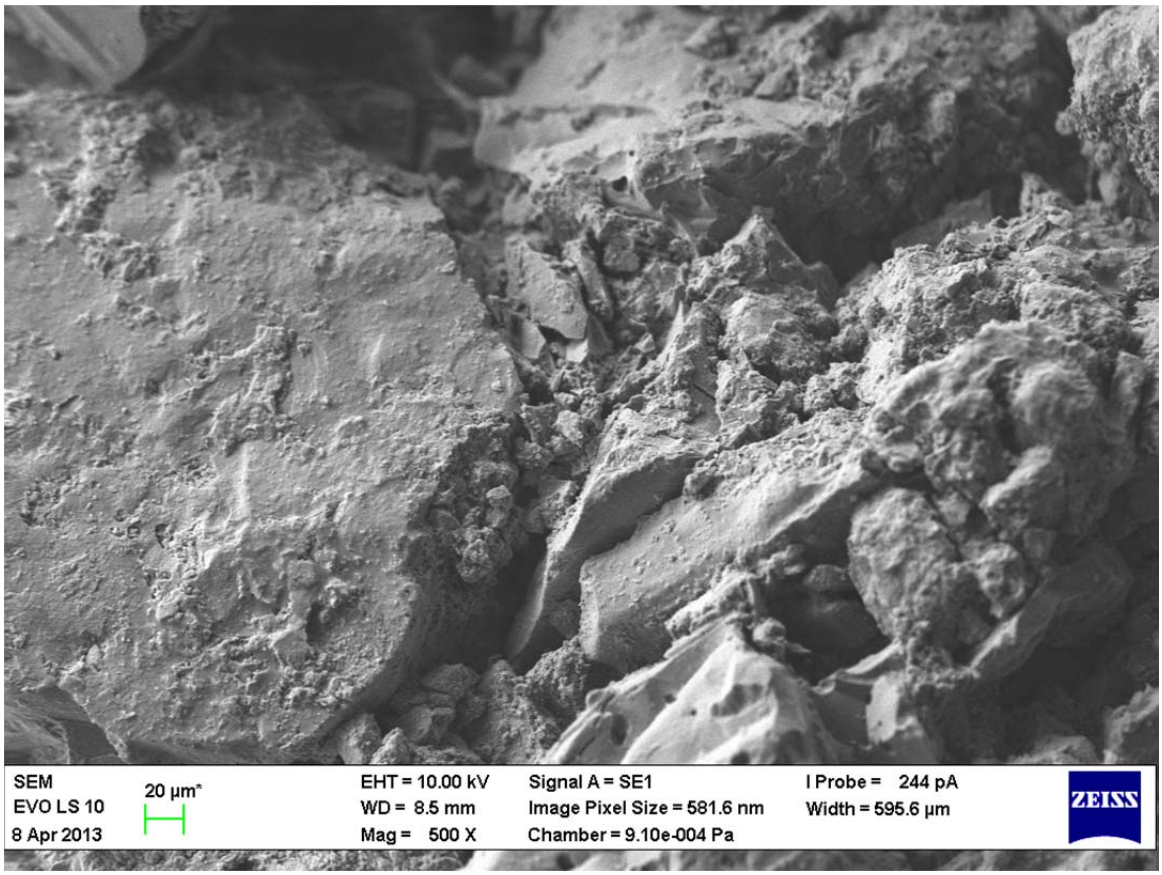

Supplement 25: *Structure of AC-Por-40. Magnification: X500 (SEM)*

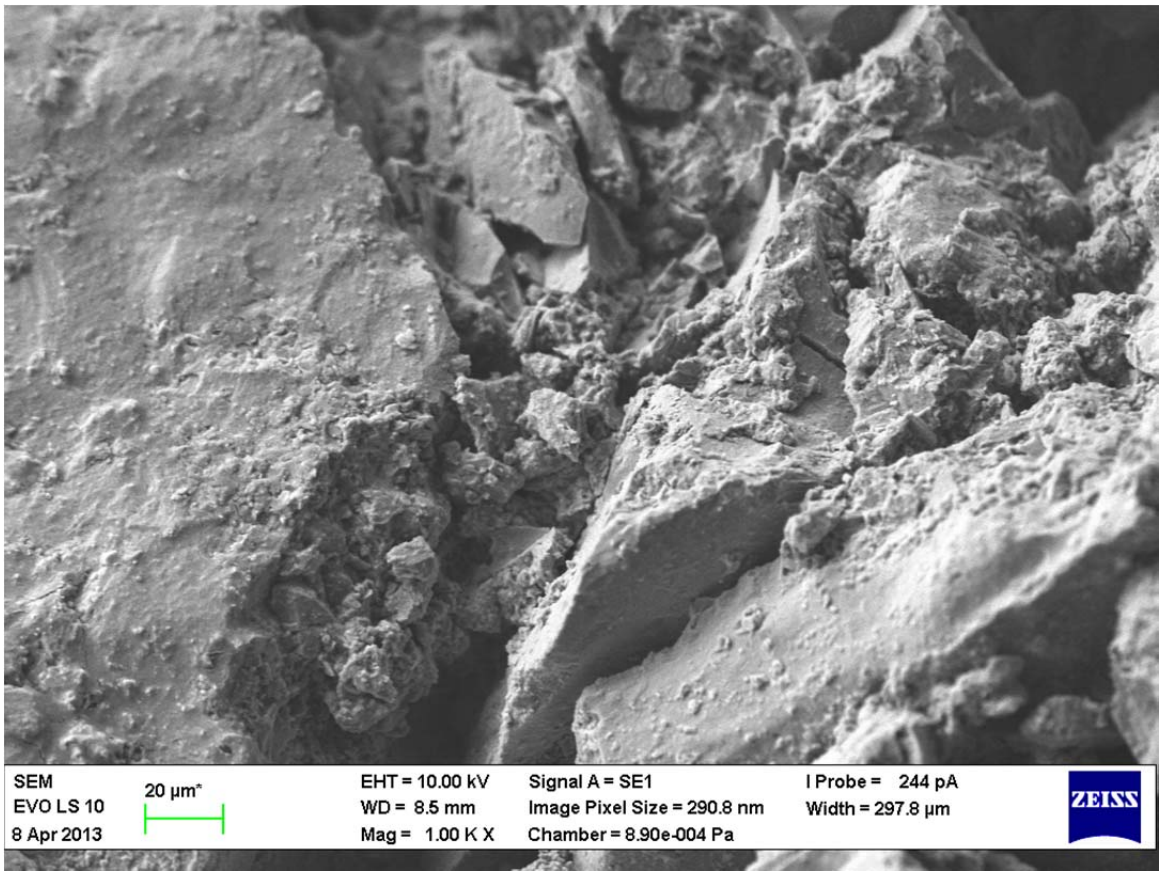

Supplement 26: *Structure of AC-Por-40. Magnification: X1000 (SEM)*

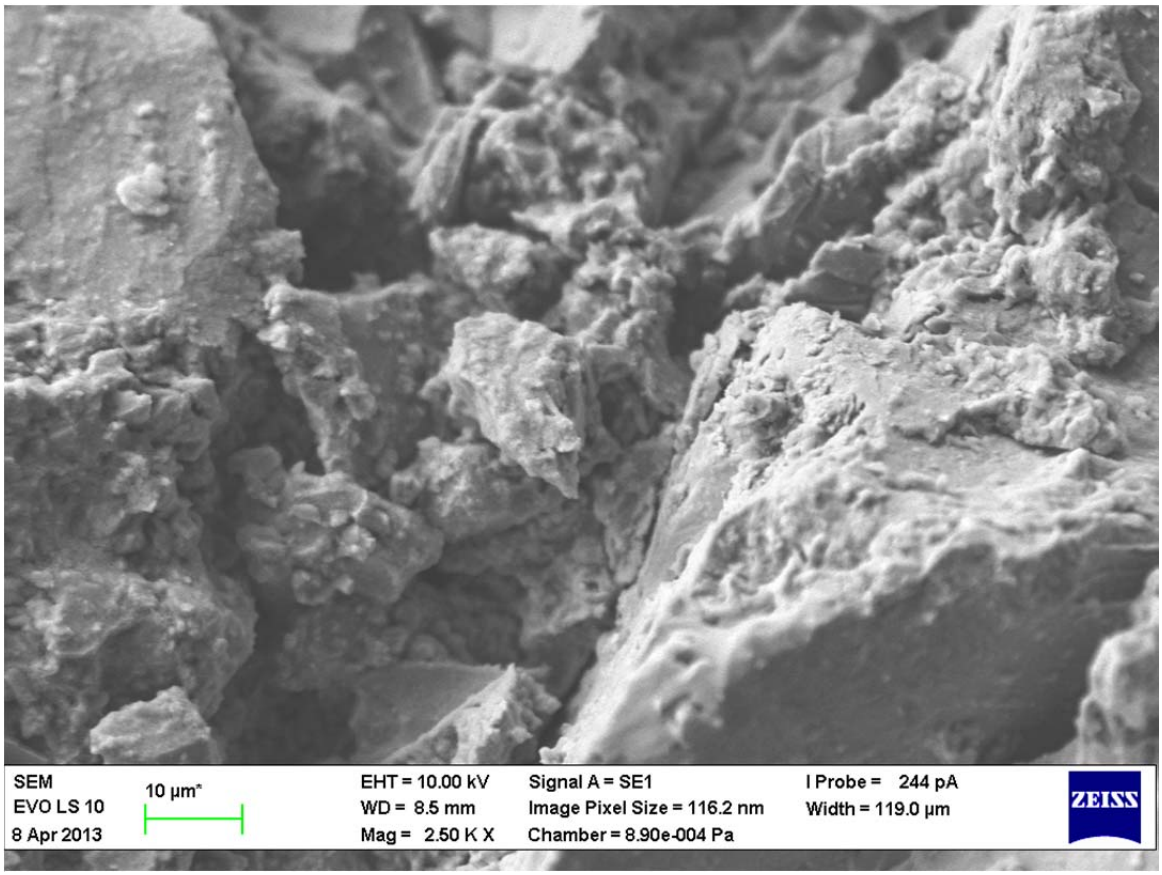

Supplement 27: *Structure of AC-Por-40. Magnification: X2500 (SEM)*

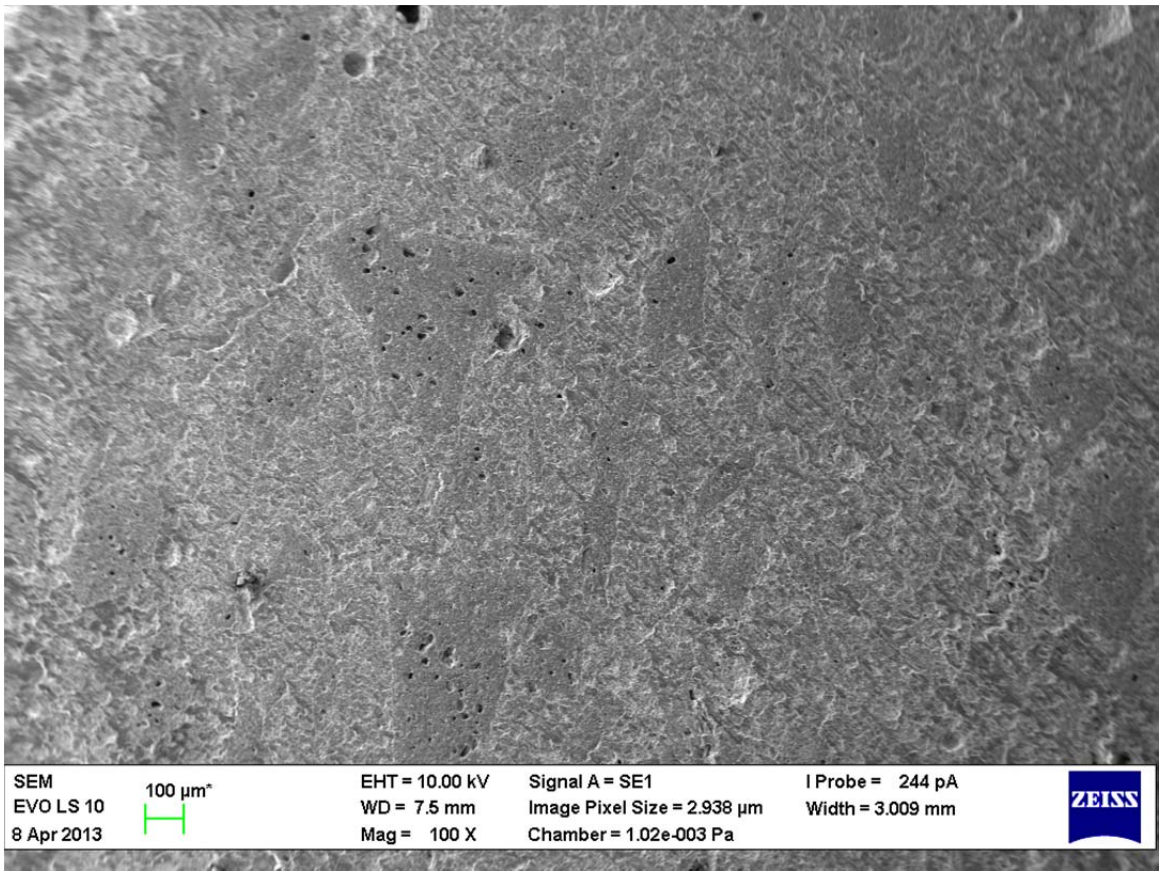

Supplement 28: *Structure of AC-Por-60. Magnification: X100 (SEM)*

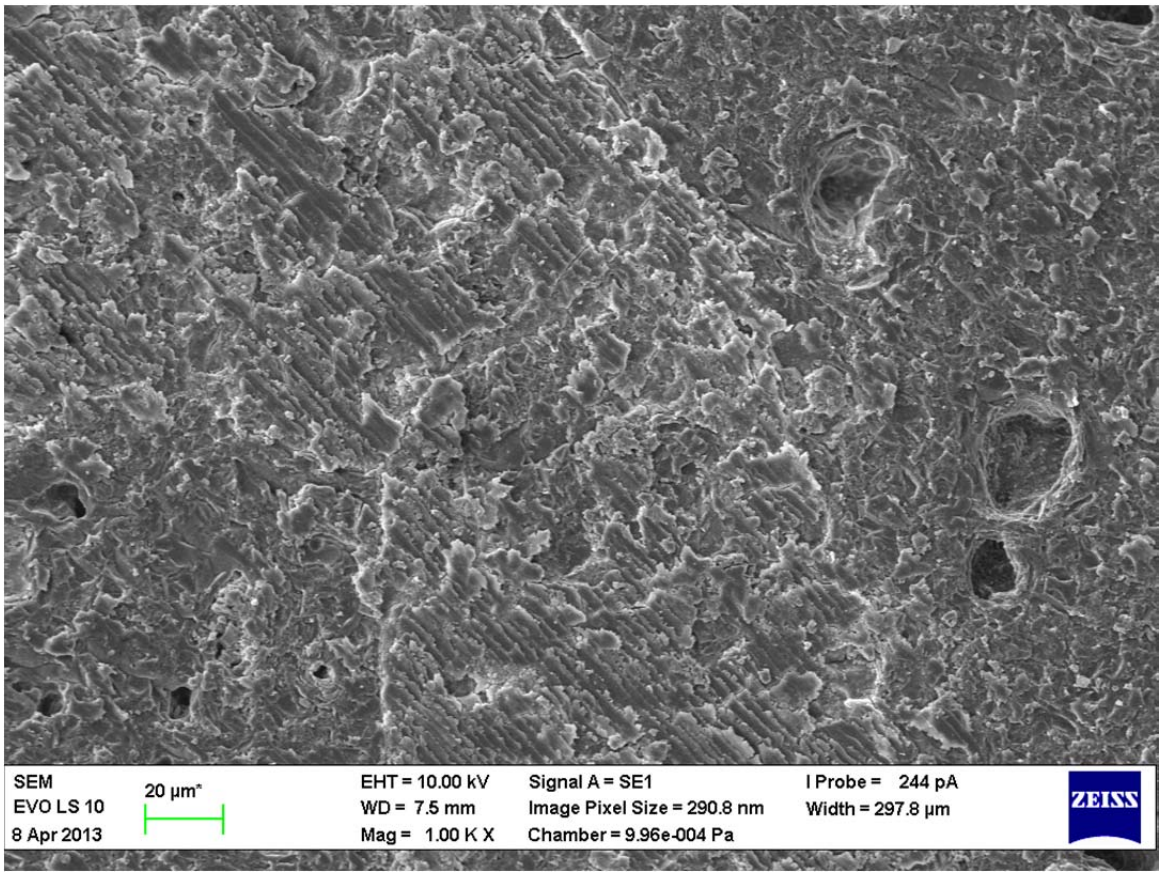

Supplement 29: *Structure of AC-Por-60. Magnification: X1000 (SEM)*

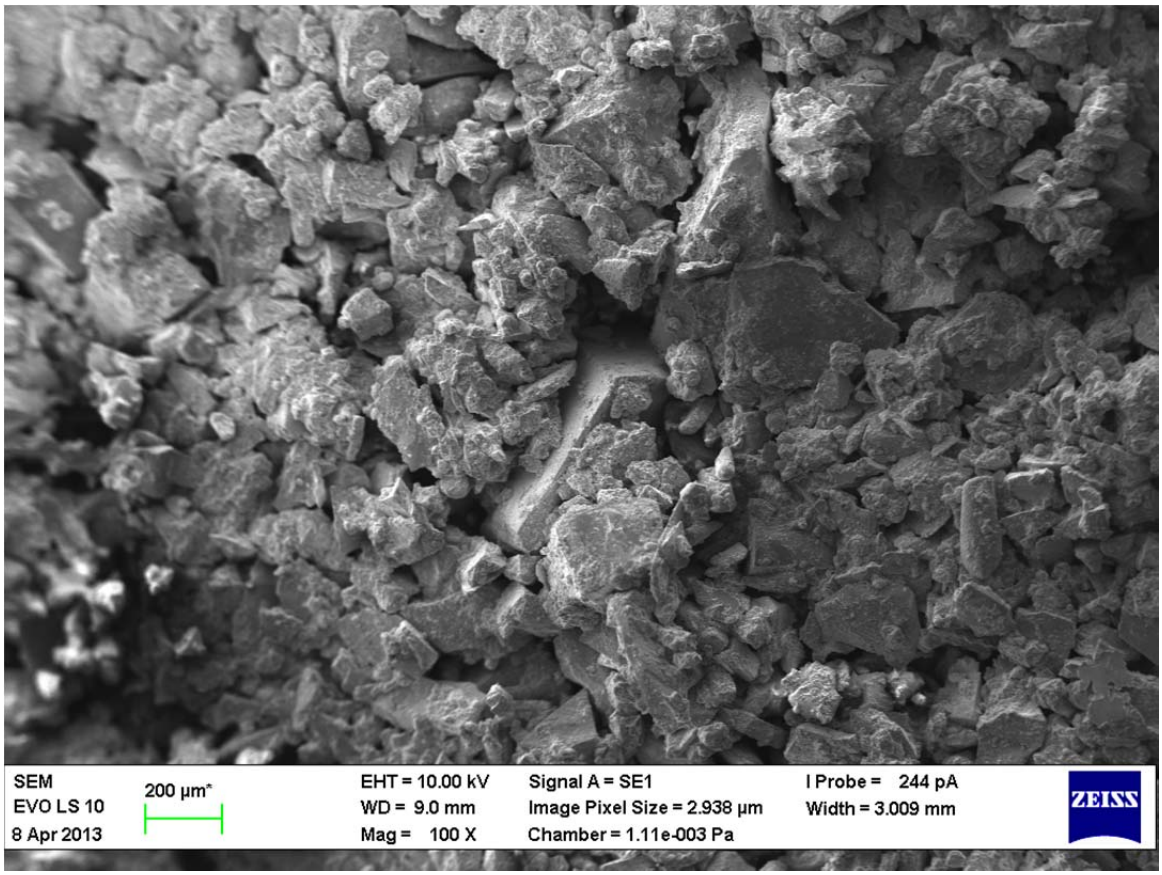

Supplement 30: *Structure of AC-150-42. Magnification: X100 (SEM)*

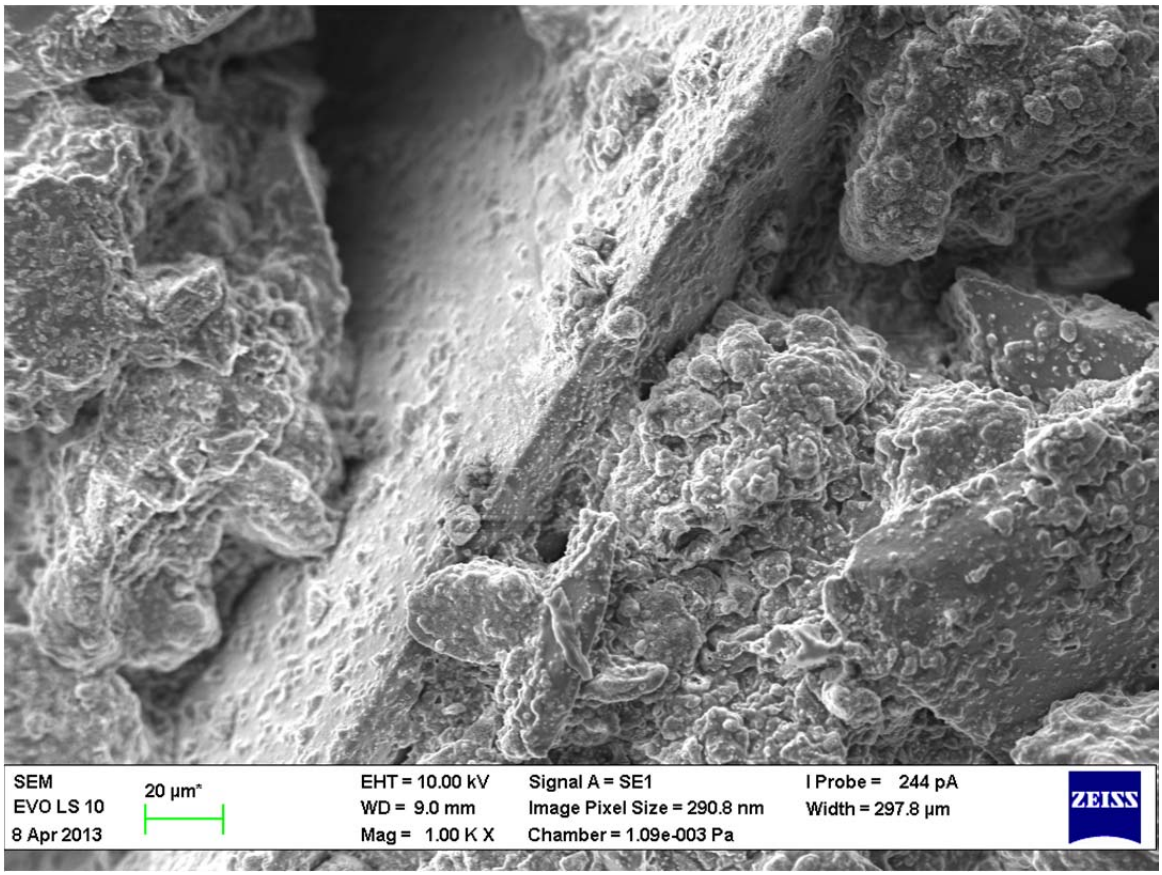

Supplement 31: *Structure of AC-150-42. Magnification: X1000 (SEM)*

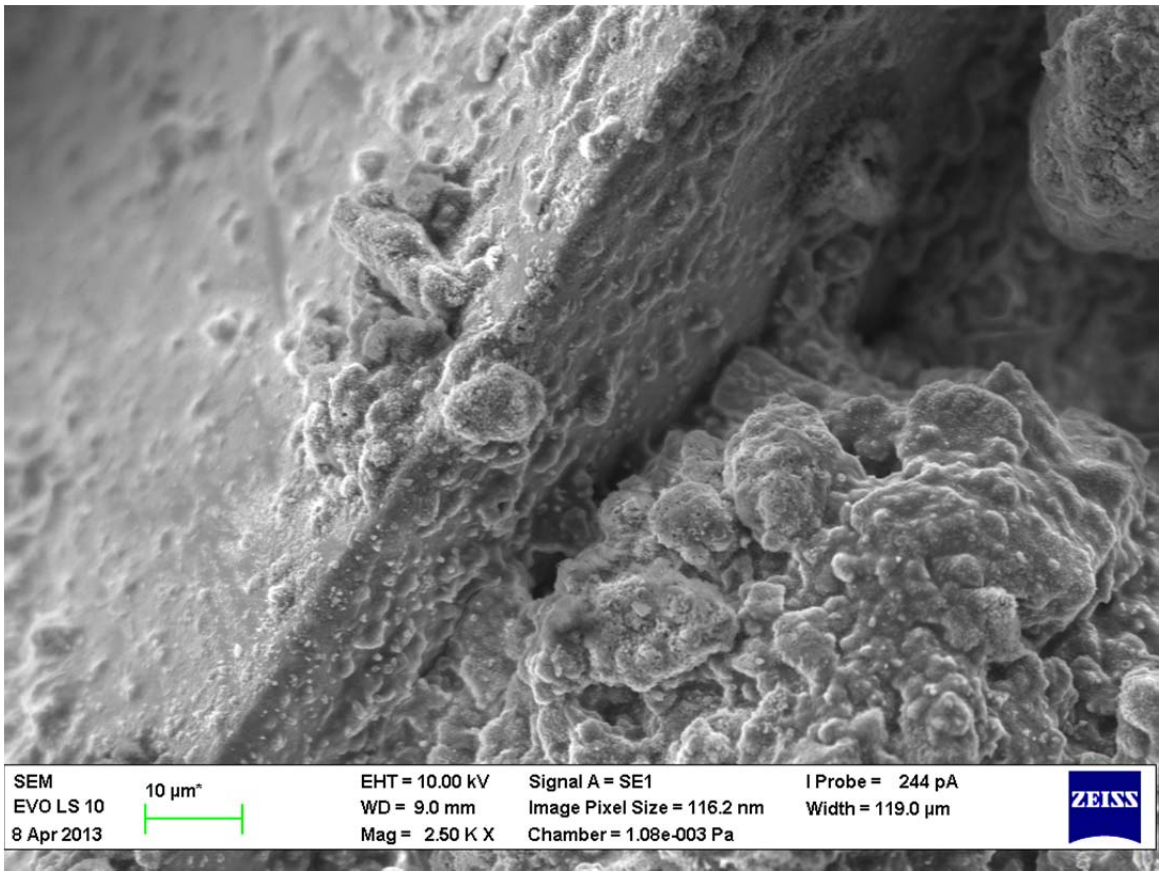

Supplement 32: *Structure of AC-150-42. Magnification: X2500 (SEM)*

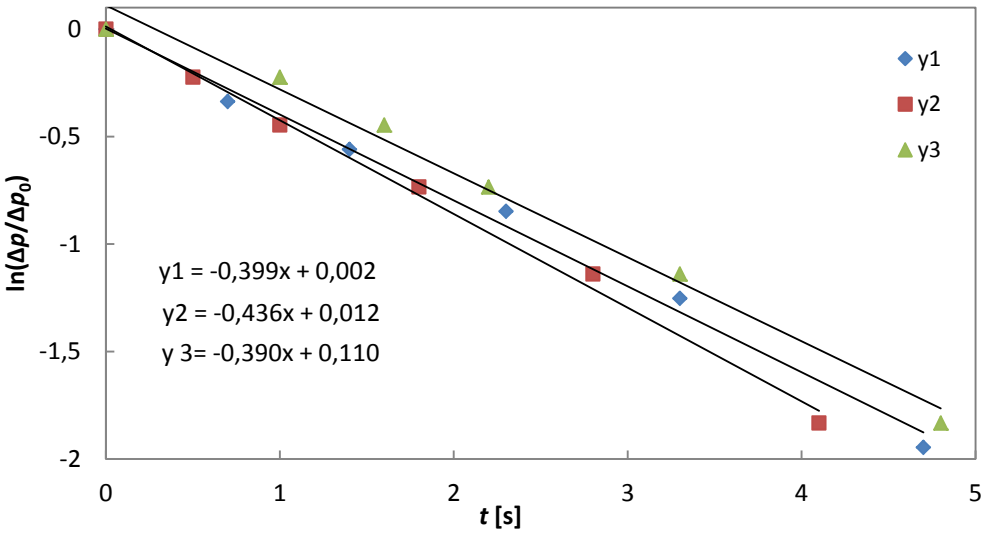

Supplement 33: *Permeation measurement plot – AC-100-32*

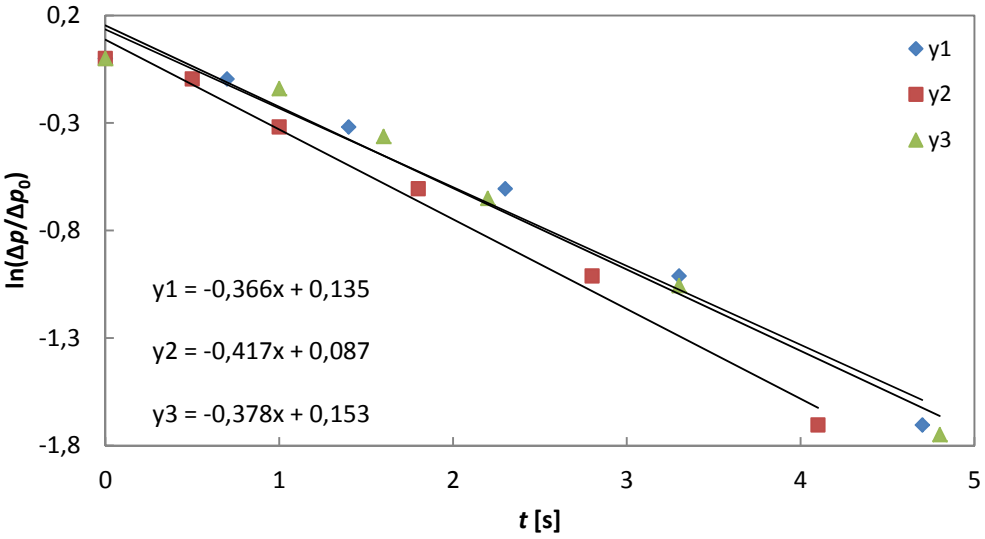

Supplement 34: *Permeation measurement plot – AC-60/40-26 (1)*

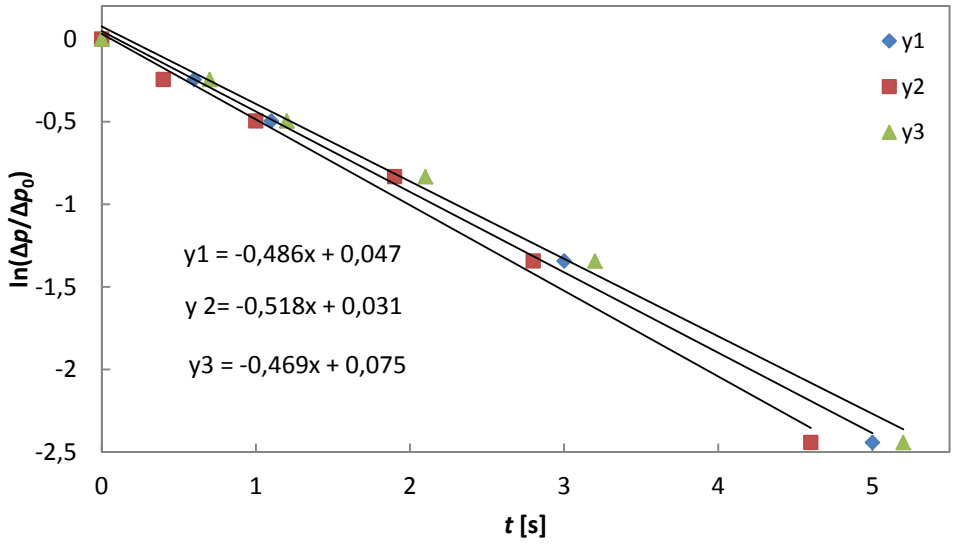

Supplement 35: *Permeation measurement plot – AC-60/40-26 (2)*

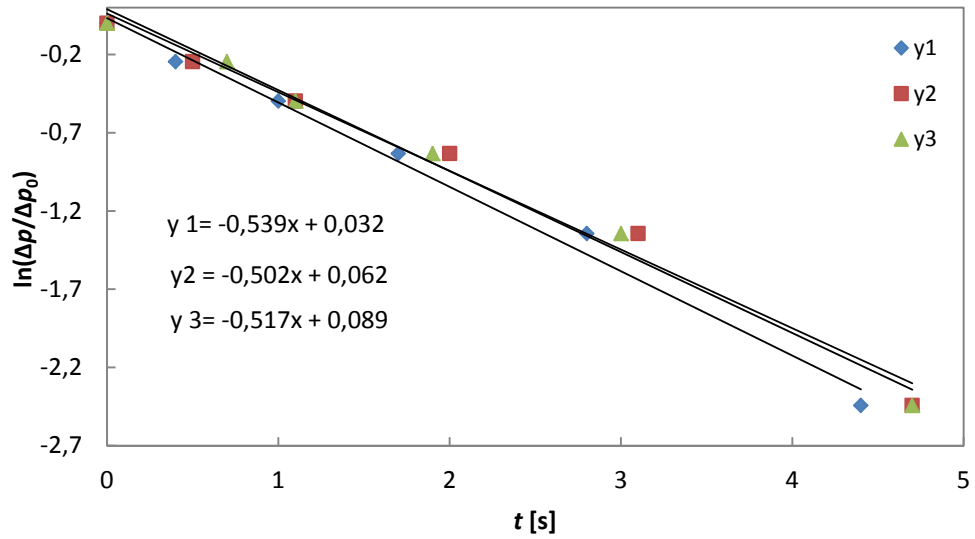

Supplement 36: *Permeation measurement plot – AC-150-42 (2)*

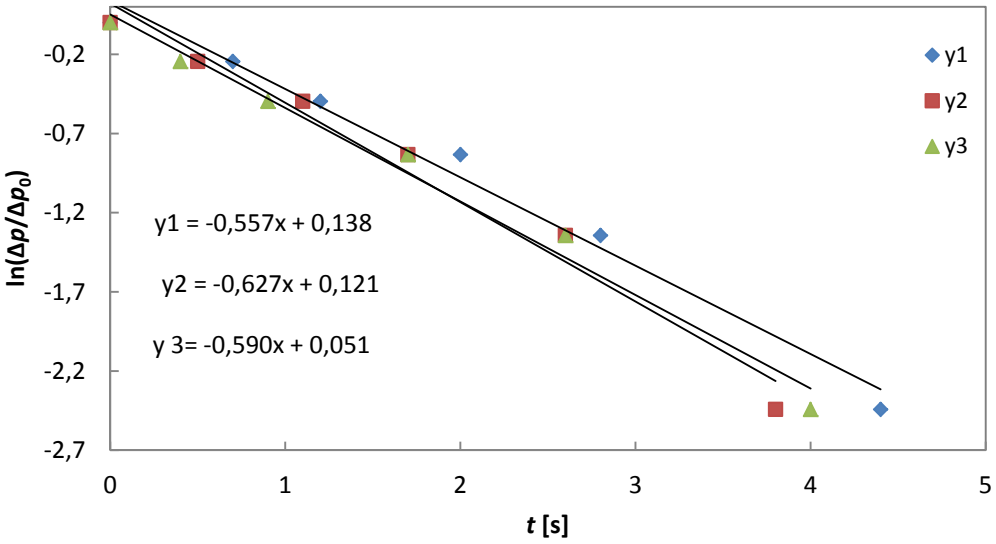

Supplement 37: *Permeation measurement plot – AC-150-42 (3)*

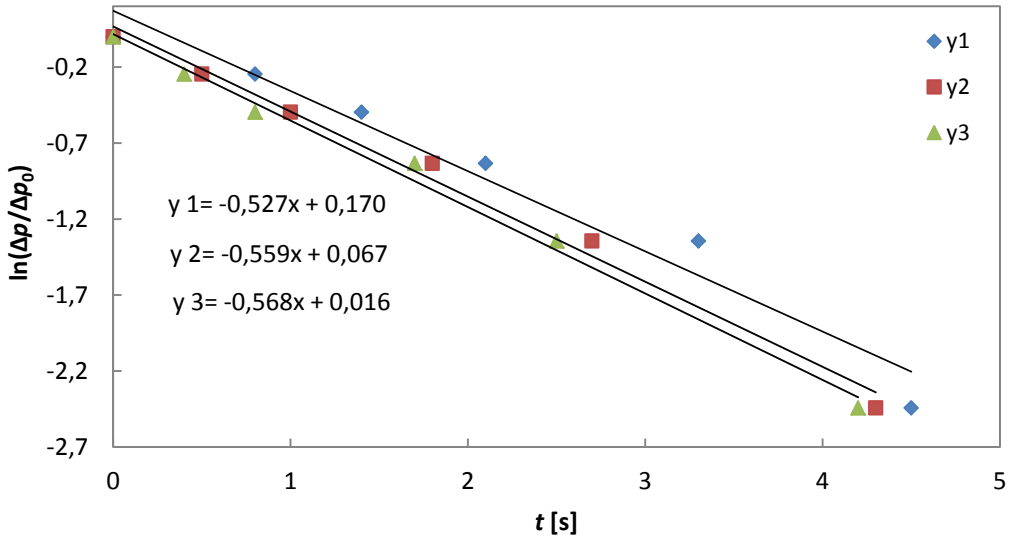

Supplement 38: *Permeation measurement plot – AC-Por-40*

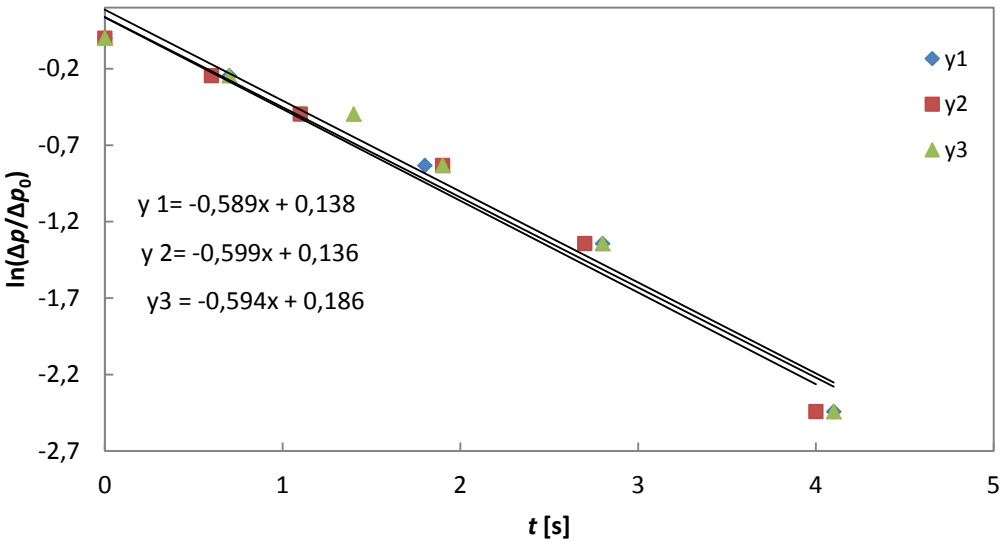

Supplement 39: *Permeation measurement plot – PC-G-0.24-32*

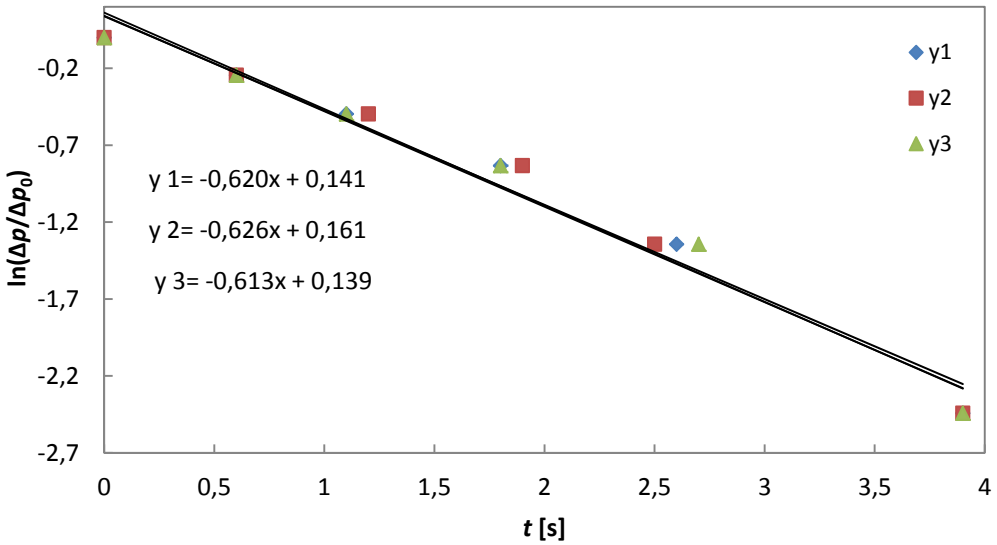

Supplement 40: *Permeation measurement plot – AC-G-0.24-32*

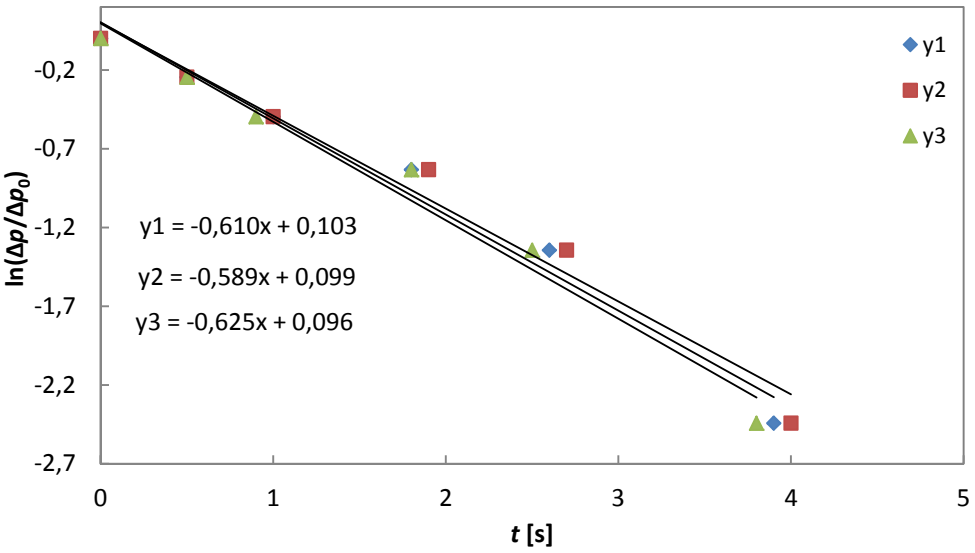

Supplement 41: *Permeation measurement plot – AC-100-32 (1)*

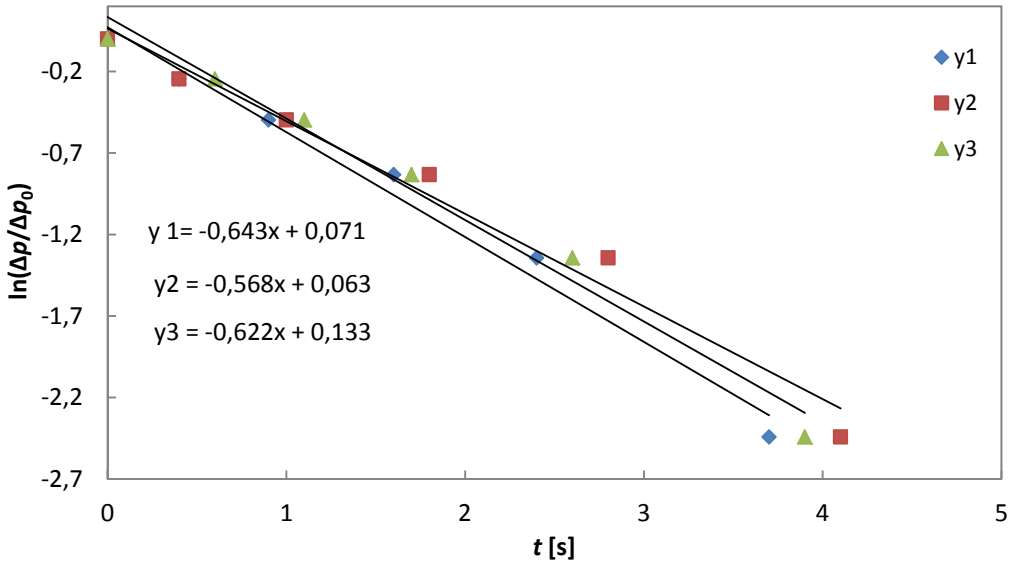

Supplement 42: *Permeation measurement plot – AC-100-32 (2)*

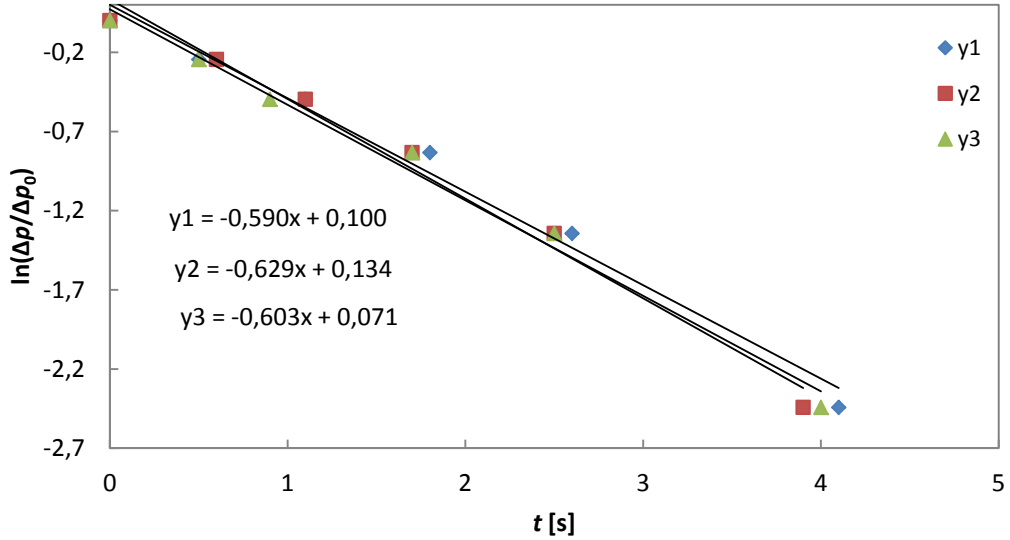

Supplement 43: *Permeation measurement plot – AC-100-32 (3)*